Universidade de Aveiro
2021

Tiago Emanuel Pereira Rodrigues

OTIMIZAÇÃO MUSCLE-IN-THE-LOOP EM TEMPO REAL PARA REABILITAÇÃO FÍSICA COM UM EXOSQUELETO ATIVO – UMA MUDANÇA DE PARADIGMA

REAL-TIME MUSCLE-IN-THE-LOOP OPTIMIZATION FOR PHYSICAL REHABILITATION WITH AN ACTIVE EXOSKELETON – A PARADIGM SHIFT

University of Aveiro
2021

Universidade de Aveiro
2021

Tiago Emanuel Pereira Rodrigues

OTIMIZAÇÃO MUSCLE-IN-THE-LOOP EM TEMPO REAL PARA REABILITAÇÃO FÍSICA COM UM EXOSQUELETO ATIVO – UMA MUDANÇA DE PARADIGMA

REAL-TIME MUSCLE-IN-THE-LOOP OPTIMIZATION FOR PHYSICAL REHABILITATION WITH AN ACTIVE EXOSKELETON – A PARADIGM SHIFT

Dissertação apresentada à Universidade de Aveiro e ao Departamento de Física da mesma instituição para cumprimento dos requisitos necessários à obtenção do grau de Mestre em Engenharia Biomédica, realizada sob a orientação científica do Professor Doutor Jorge Augusto Fernandes Ferreira, Professor Associado do Departamento de Engenharia Mecânica da Universidade de Aveiro, e do Doutor Guillaume Vincent Durandau, Investigador do *Neuromechanical Modeling and Engineering Lab* na *University of Twente*.

Dissertation presented to the University of Aveiro and to the Department of Physics of the same institution to fulfil the necessary requirements to obtain the Master of Science Degree in Biomedical Engineering, carried out under the scientific supervision of Professor Doctor Jorge Augusto Fernandes Ferreira, Associated Professor of the Department of Mechanical Engineering at the University of Aveiro, and Doctor Guillaume Vincent Durandau, Researcher of the Neuromechanical Modeling and Engineering Lab at the University of Twente.

The present work was developed under the research scope of the ERC Starting Grant INTERACT, with the Grant Agreement ID 803035.

The present work received financial support from the Erasmus+ Programme for individual international mobility under the contract reference 2020-1-PT01-KA103-077834.

To my family, for the luck and success they helped me build.

À minha família, pela sorte e sucesso que me ajudaram a construir.

O júri / The jury

Presidente / President	Prof.ª Doutora Ana Luísa Monteiro da Silva Professora Auxiliar em Regime Laboral, Departamento de Física da Universidade de Aveiro
Vogais / Commitee	Prof. Doutor Jorge Manuel Mateus Martins Professor Associado, Departamento de Engenharia Mecânica do Instituto Superior Técnico
	Prof. Doutor Jorge Augusto Fernandes Ferreira Professor Associado, Departamento de Engenharia Mecânica da Universidade de Aveiro

Acknowledgements

This master thesis presents itself as the final mark of a great and rich academic journey, with the major emphasis being on the fantastic adventure abroad in the Netherlands and, specifically, in Enschede and at the University of Twente. It would not be possible to finish this master's degree all by myself. Thereby, there are some people that I would like to formally thank, whom I will take into consideration throughout my life span.

First of all, I would like to thank Prof. Jorge Ferreira for accepting the challenge I proposed for this dissertation, for the scientific guidelines, teachings, and availability, and for all the support that he has been giving me over the past couple of years.

To Guillaume Durandau, for having welcomed me into his research group so nicely, for all the scientific and logistical guidelines, for his liveliness and friendliness while helping me with the everyday problems, and, overall, for accompanying me during my whole assignment at the University of Twente.

To Profs. João Veloso and Ana Luísa Silva, for their friendliness, logistical support, and accompaniment throughout my academic course and, especially, during the process of my dissertation.

To Prof. Rosário Correia and Christine Cordeiro, from the University of Aveiro, and Prof. Dorien Van De Belt, Ms. Tahnee Smits, and Ms. Mia Lucas, from the University of Twente, for the support, monitoring and guidance concerning the mobility process under the Erasmus+ program.

To Prof. Marco Santos, for his availability, disposition, and scientific guidance in terms of control systems and servomechanisms, which helped me to get the needed scientific basis for the development of this dissertation.

To Prof. Massimo Sartori, as Principal Investigator, and to my colleagues at the Neuromechanical Modeling and Engineering Lab and Biomechanical Engineering group at the University of Twente, for the support, funny moments, and companionship.

To my childhood, basic and secondary education professors and educational assistants, for helping me keep my feet on the ground while dreaming high and for helping to mould the person I am today.

To the professors at the University of Aveiro that I met throughout the last five years, who contributed strongly to my growth, motivation, and passion for my course, namely Prof. Ana Breda, Prof. João Rodrigues, Prof. Luís Cadillon, Prof. Catarina Almeida, Prof. Ricardo Dias, Prof. Svitlana Kopyl, Prof. António Completo, and Prof. António Ramos.

To my friends and course colleagues who embarked with me in the early years of the Integrated Master´s Degree in Biomedical Engineering at the University of Aveiro, for all the companionship, support, courage, and dedication in all the projects for the dissemination and enhancement of our course in Portugal and the world.

To my mates of all the groups, associations, and federations I made part, namely XPTO, ADAFA, CFFA 2018, NEEF-AAUAv, ANEEB, COENEEB 2020, and BiomediCall Future, for all the amazing challenges and adventures that we came through.

To Sofia, for all the affection, motivation, and strength that she daily shares with me, for the challenges we overcame together and for her company throughout this big, fantastic, and striking journey.

Finally, to my parents, my sister, and my amazing family, for all their tireless support, sacrifices, advices, and inspiration. It is thanks to them that I am able to present this dissertation and it is to them that I dedicate all my work and dedication.

A sincere thanks to all.

Agradecimentos

Esta tese de mestrado apresenta-se como a marca final de uma enorme e rica jornada académica, com maior ênfase na grande aventura nos Países Baixos e, especialmente, em Enschede e na *University of Twente*. Nunca seria possível concluir este mestrado sozinho. Assim, gostaria de agradecer formalmente algumas pessoas, que levarei sempre em consideração ao longo da minha vida.

Em primeiro lugar, gostaria de agradecer ao Prof. Jorge Ferreira por aceitar o desafio que propus para esta dissertação, pelas orientações científicas, ensinamentos, disponibilidade e pelo acompanhamento que me foi dando nos vários projetos ao longo dos últimos dois anos.

Ao Guillaume Durandau, por me acolher tão bem no seu grupo de investigação, por todas as orientações científicas e logísticas, pela sua alegria e companheirismo ao ajudar-me nos problemas diários e, em geral, pelo acompanhamento ao longo do meu percurso na Universidade de Twente.

Ao Prof. João Veloso e à Profª. Ana Luísa, pela simpatia, apoio logístico e acompanhamento ao longo de todo o meu percurso académico e, especialmente, durante o processo da minha dissertação.

À Prof. Rosário Correia e à Dra. Christine Cordeiro, da Universidade de Aveiro, e à Prof. Dorien Van De Belt, à Tahnee Smits e à Mia Lucas, da *University of Twente,* pelo apoio, acompanhamento e orientações relativamente ao processo de mobilidade ao abrigo do programa Erasmus+.

Ao Prof. Marco Santos, pela disponibilidade, disposição e orientações científicas a nível de sistemas de controlo e servomecanismos, que me permitiram adquirir as bases necessárias ao desenvolvimento desta dissertação.

Ao Prof. Massimo Sartori, como Investigador Principal, e aos meus companheiros do *Neuromechanical Modeling and Engineering Lab* na *University of Twente* e do *Biomechanical Engeneering group*, pelo apoio, momentos de descontração e companheirismo.

Aos(às) professores(as) e auxiliares de educação da minha infância e ensino básico e secundário, por ajudarem a manter os pés no chão, mas a sonhar alto, e moldar a pessoa que sou hoje.

Aos professores que fui encontrando ao longo dos últimos cinco anos e que contribuíram fortemente para o meu crescimento, motivação e paixão pelo meu curso, nomeadamente a Profª. Ana Breda, o Prof. João Rodrigues, o Prof. Luís Cadillon, a Profª. Catarina Almeida, o Prof. Ricardo Dias, a Profª. Svitlana Kopyl, Prof. António Completo e o Prof. António Ramos.

Aos meus amigos e colegas de curso, que embarcaram comigo nos primeiros anos do Mestrado Integrado em Engenharia Biomédica na Universidade de Aveiro, por todo o companheirismo, apoio, coragem e dedicação em todos os projetos para a divulgação e valorização do nosso curso em Portugal e no mundo.

Aos meus companheiros de todos os grupos, associações e federações de que fiz parte, nomeadamente do XPTO, ADAFA, CFFA 2018, NEEF-AAUAv, ANEEB, COENEEB 2020 e BiomediCall Future, pela pelos desafios e aventuras extraordinários por que passamos.

À Sofia, por todo o carinho, motivação e força que partilha diariamente comigo, pelos desafios que superámos juntos e pela companhia ao longo de todo este grande, fantástico e turbilhonante percurso.

Finalmente, aos meus pais e à minha família, por todo o apoio incansável, sacrifícios, conselhos e inspiração. É graças a eles que me é possível apresentar esta dissertação e é a eles que dedico todo o meu trabalho e dedicação.

A todos, um sincero obrigado.

Palavras-chave

Biomecânica, EMG, Neuromecânica, Optimização, Reabilitação Física, Robótica para Vestir

Resumo

Auxiliar a locomoção humana com uma ortose robótica ainda é bastante desafiante, em grande parte devido à complexidade do sistema neuromusculoesquelético, à dinâmica variável no tempo que acompanha a adaptação motora e à singularidade da resposta de cada indivíduo à assistência dada pelo robô. Até hoje, está por cumprir a promessa inicial destes dispositivos, principalmente devido ao facto de não serem perfeitamente adequados para a reabilitação de pacientes neuropatológicos. Um dos principais desafios que dificultam esse objetivo foca-se ainda na interface e na co-dependência entre o ser humano e a máquina. Hoje em dia, a maioria dos exoesqueletos comerciais reproduz padrões de marcha predefinidos, enquanto que os exoesqueletos em investigação estão só agora a mudar para controladores com base em perfis de binário otimizados. Na maioria dos casos, a dinâmica do sistema musculoesquelético humano ainda é ignorada e não tem em consideração as condições ideais para induzir uma modulação positiva da atividade neuromuscular. Isso ocorre porque ambas as estratégias de reabilitação ainda são enfatizadas no nível macro de toda a articulação, em vez de se concentrar na dinâmica e atividade dos músculos, que são os elementos anatómicos que realmente precisam de ser reabilitados. Estratégias para manter o ser humano em loop nos comandos que controlam o exoesqueleto em tempo real podem ajudar a superar estes desafios.

O principal objetivo desta dissertação é fazer uma mudança de paradigma na abordagem em como a assistência que é dada a um sujeito por um exosqueleto é modelada e controlada durante a reabilitação física. Portanto, no contexto do presente trabalho, pretendeu-se projetar, conceder, implementar e validar um modelo de otimização muscle-in-the-loop em tempo real para encontrar a melhor relação de suporte capaz de induzir as condições ideais de reabilitação para um grupo específico de músculos fragilizados, tendo um impacto mínimo nos outros músculos saudáveis.

O modelo de otimização desenvolvido foi implementado na forma de um *plugin* e foi integrado numa interface baseada num modelo neuromecânico para o controlo de um exoesqueleto bilateral de tornozelo. Testes experimentais piloto avaliaram a viabilidade e a eficácia do modelo. Os resultados dos testes mais significativos demonstraram reduções de EMG de até 61 ± 3 % no Soleus e 41 ± 10 % no Gastrocnemius Lateral. Adicionalmente, os resultados demonstraram também a eficiência em reabilitação da redução específica no EMG devido à otimização tendo em conta a fadiga muscular após cada teste.

Finalmente, dois estudos preliminares paralelos emergiram dos testes piloto, que analisaram a adaptação muscular após uma nova condição assistiva ter sido definida ao longo do tempo e o efeito do posicionamento lateral dos atuadores do exoesqueleto nos músculos da perna.

Keywords **Biomechanics, EMG, Neuromechanics, Optimization, Physical Rehabilitation, Wearable Robotics**

Abstract

Assisting human locomotion with a wearable robotic orthosis is still quite challenging, largely due to the complexity of the neuromusculoskeletal system, the time-varying dynamics that accompany motor adaptation, and the uniqueness of every individual's response to the assistance given by the robot. To this day, these devices have not met their well-known promise yet, mostly due to the fact that they are not perfectly suitable for the rehabilitation of neuropathologic patients. One of the main challenges hampering this goal still relies on the interface and co-dependency between the human and the machine. Nowadays, most commercial exoskeletons replay pre-defined gait patterns, whereas research exoskeletons are switching to controllers based on optimized torque profiles. In most cases, the dynamics of the human musculoskeletal system are still ignored and do not take into account the optimal conditions for inducing a positive modulation of neuromuscular activity. This is because both rehabilitation strategies are still emphasized on the macro level of the whole joint instead of focusing on the muscles' dynamics and activity, which are the actual anatomical elements that may need to be rehabilitated. Strategies to keep the human in the loop of the exoskeleton's control laws in real-time may help to overcome these challenges.

The main purpose of the present dissertation is to make a paradigm shift in the approach on how the assistance that is given to a subject by an exoskeleton is modelled and controlled during physical rehabilitation. Therefore, in the scope of the present work, it was intended to design, concede, implement, and validate a real-time muscle-in-the-loop optimization model to find the best assistive support ratio that would induce optimal rehabilitation conditions to a specific group of impaired muscles while having a minimum impact on the other healthy muscles.

The developed optimization model was implemented in the form of a plugin and was integrated on a neuromechanical model-based interface for driving a bilateral ankle exoskeleton. Experimental pilot tests evaluated the feasibility and effectiveness of the model. Results of the most significant pilots achieved EMG reductions up to 61 ± 3 % in Soleus and 41 ± 10 % in Gastrocnemius Lateralis. Moreover, results also demonstrated the efficiency of the optimization's specific reduction on rehabilitation by looking into the muscular fatigue after each experiment. Finally, two parallel preliminary studies emerged from the pilots, which looked at muscle adaptation, after a new assistive condition had been applied, over time and at the effect of the lateral positioning of the exoskeleton's actuators on the leg muscles.

Index of Contents

List of Figures

Supplementary Content and Online Repository

The reading of present document should be followed with the supplementary content supplied, where additional background and secondary information is provided as follows:

Additionally, the repository also includes folders with the original figures and diagrams of this dissertation, the implemented code, and the graphical experimental results with the original resolution. The online repository can be accessed from: https://dx.doi.org/10.5281/zenodo.5494470

This supplementary content can be cited as: *Rodrigues, T., Ferreira, J., Sartori, M., Durandau, G.; (2021), "Supplementary Content of Real-Time Muscle-In-The-Loop Optimization for Physical Rehabilitation with an Active Exoskeleton - A Paradigm Shift", Zenodo, DOI: 10.5281/zenodo.5494470*.

List of Symbols

$d\theta$	Displacement of the joint
$f(L^M)$	Force-length relationship
$f(V^M)$	Force-velocity relationship
τ	Joint Torque
$F^{Max}(t)$	Maximum isometric force
$\overline{EMG}$	Mean of the post-processed EMG signal
$\overline{EMG}^{(REF)}$	Mean of the post-processed reference EMG signal of each muscle
F^{MTU}	MTU force at instant *t*
dl	MTU length displacement
L^M	Muscle's length
C_{SOL}	Muscle-specific Contribution Weight of Soleus
C_s	Muscle-specific Contribution Weight of the muscle *i*
δ	Muscle-specific Target Reduction Factor
F^{mt}	Musculotendon force
L^{mt}	Musculotendon length
$E(t)$	Normalized muscle activation at instant *t*.
$f_p(L^M)$	Passive force-length relationship
α	Pennation angle
SR_{GL}	Support Ratio of Gastrocnemius Lateralis
SR_{GM}	Support Ratio of Gastrocnemius Medialis
SR_{SOL}	Support Ratio of Soleus
SR_{TA}	Support Ratio of Tibialis Anterior
F^T	Tendon force
L^T	Tendon's length
r	Three-dimensional moment arms
L^{MT}	Total length of the muscle-tendon unit

List of Abbreviations

Ach	Acetylcholine
ADP	Adenosine Diphosphate
ADS	Automation Device Specification
API	Application Programming Interface
BSS	Blind-Source Separation
BW	Body Weight
CE	Contractile Element
CEINMS	Calibrated EMG-Informed Neuromusculoskeletal Modelling Toolbox
CEINMS-RT	Real-time Calibrated EMG-Informed Neuromusculoskeletal Modelling Toolbox
CMA-ES	Covariance Matrix Adaptation Evolutionary Strategy
CNS	Central Nervous System
DOF	Degrees of Freedom
ECG	Electrocardiography
EMD	Electromechanical Delay
EMG	Electromyography
EtherCAT	Ethernet for Control Automation Technology
FD	Forward Dynamics
FIO_2	Fraction of Inspired Oxygen
GL	Gastrocnemius Lateralis muscle
GM	Gastrocnemius Medialis muscle
GRF	Ground Reaction Forces
GTO	Golgi Tendon Organ
HD	High Density
HMI	Human-Machine Interface
ID	Inverse Dynamics
IK	Inverse Kinematics
IMU	Inertial Measurement Units
MA	Moment Arm
MN	Motor Neuron
MRI	Magnetic Resonance Imaging
MTF	Muscle-Tendon Force
MTU	Muscle-Tendon Units
MUAP	Motor Unit Action Potential
MVC	Maximal Voluntary Contraction
NMS	Neuromusculoskeletal
PEE	Parallel Elastic Element
Pi	Inorganic Phosphate group
PNS	Peripheral Nervous System
ROM	Range of Motion
SA	Corana's Simulated Annealing
SC	Spinal Cord
SCI	Spinal Cord Injury
SEA	Series Elastic Actuators
SEE	Series Elastic Element
SOL	Soleus muscle
SR	Support Ratio
UDP	User-Defined Problem
WE2	Symbitron Wearable Exoskeleton 2
WHO	World Health Organization
WRO	Wearable Robotic Orthosis
XML	Extensible Markup Language
XSD	XML Schema Definition

Chapter 1. Introduction

1.1. Motivation

Population ageing is one of the most critical challenges in the near future, characterized by a low birth rate and a long-life expectation, especially in industrialized societies. In 40 years from now, nearly 35% of the European population will be over 60 years old, resulting in the urgency to provide solutions that allow our ageing society to remain active, creative, productive, and, above all, independent [1]. Furthermore, cerebrovascular accidents (stroke) is the sudden death of brain cells due to lack of oxygen when the brains' blood flow is lost by blockage or rupture of an artery to the brain. According to the World Health Organization (WHO), in 2016, this disease was the second global cause of death [2]. Despite the fact that stroke occurrence is declining in many countries, 15 million people worldwide annually suffer from a stroke. Of these, 5 million people die and, of the survival group, only a few regain the full functionality whereas the rest will have to live with some kind of disability [3]. On the other hand, between 250.000 and 500.000 people worldwide suffer from Spinal Cord Injury (SCI), a neurological lesion that might result in severe motor weakening [4].

The impact of rehabilitation is still limited in these cases and the success of rehabilitation procedures is mainly dependent on the skill of the responsible medical expert [5]. In fact, effective rehabilitation requires long, intense, costly, and task-based therapy sessions, leading people with physical disabilities to not receive optimal healthcare, limiting the quality of their everyday lives [3,5].

In contrast, a wearable orthosis can augment the physical abilities of human able-bodies to enhance their performance in health, industrial, sport, civil or military environments while being able to, simultaneously, acquire vital data, such as heart rate, body temperature, blood pressure, or movement parameters [1]. Taking a big role in increasing the quality of life of healthy or disabled people, assistive wearable robotic devices are conceived as a functional extension of the human's organism through a certain symbolic human-machine relationship and might help to mitigate the impact of neuromusculoskeletal (NMS) injuries on one's quality of life [5].

1.2. The Paradigm

The ability of locomotion directly relates to a subject's quality of life. Neurological lesions such as those underlying stroke and spinal cord injury often result in severe motor impairments (i.e., paresis, spasticity, abnormal joint couplings) that compromise an individual's motor capacity and health throughout the life span. These NMS injuries' impact on the quality of life could be mitigated by wearable robotic orthosis (WRO), which allow better and intensive training than classic rehabilitation and demand less muscular effort from physiotherapists. Assistive wearable robotic devices are already in use for several years, yet, despite advances in mechatronics and bioelectrical signal processing, these devices still suffer from several limitations, mainly for what concerns to the high-level controlling strategies. Moreover, walking with an exoskeleton can be arduous due to the added weight, kinematic constraints, and resistive force owing to imperfect torque controllers [6].

In fact, this type of devices still has a long way to go in terms of research when it comes to their application in neurorehabilitation, mostly due to the underdevelopment of the assistive robotic devices' human-machine interfaces (HMI), which still cannot offer voluntary control from its user neither positively adapt to the muscles' specific dynamics. An HMI represents the connection between the machine and the human, who literally wears it, through kinematics, kinetics, bio-signals data and the assistance provided to them by the device.

Considering an effective application of WRO in this sort of physical and neurologic rehabilitation, there are three major challenges that are still hampering the most wanted paradigm shift. The first one relies in the inability of current systems to enable the patient to voluntarily control the robotic device while inducing a positive modulation of their neuromuscular activity. The second is

still incomplete understanding of how lesions of the central nervous system (CNS) impact the musculoskeletal system function, therefore impeding the optimization of the support provided by the WRO to better follow the patients' motor intentions. Finally, the third challenge, which will be the main focus of this dissertation, lies in the fact that the available WRO still operates on a joint level, by concentrating all the rehabilitation purpose on the assistive torque that is provided to a joint, acting on all the anatomical structures that compose them, when most of the times the rehabilitation process should have a positive impact on a specific group of muscles that might have been perturbated due to a disorder or accidental occurrence. Therefore, this rehabilitation strategy may not be able to provide optimal conditions for the muscle-oriented rehabilitation, facilitating the activity-driven neuroplastic changes that are required for this muscle-specific recovery, and still have a negative impact on other healthy muscular groups.

1.3. Approach, Objectives, and Prospects

As an alternative to current interfaces, a new class of methods using biomechanical modelling with optimization methods can be studied, which might consider individual patients' neuromuscular alterations, fundamental for enhancing the motor function of neurologically impaired patients. Additionally, to enable a more beneficial and personalized human-machine physical interaction, it is important to have a closed-loop scheme on a muscular level, so it takes into account the optimal neuroplasticity conditions and the dynamic changes of the user's biomechanical variables. These muscle-specific profiles can be further optimized by gathering human-in-the-loop methods [7,8] and NMS modelling [9,10] so it can give a better understanding of the NMS mechanics involved in the human body, enable the discovering of which muscle or group of muscles have been causing abnormal gait patterns, help to optimize the specific assistance level, and, consequently, improve the outcomes of a muscle-specific treatment.

Durandau *et al*. [6] developed an HMI based on an EMG-driven musculoskeletal model to modulate all transformations from muscle excitation onset, i.e. EMGs, to mechanical moment production around multiple lower-limb degrees-of-freedom (DOF), and applied them on different robotic orthosis and exoskeletons. This neuromechanical model-based approach accounted for the form and function of the human NMS system in neurologically impaired patients, therefore opening horizons for the first model-based HMI that enables neurologically impaired patients to voluntarily control multiple DOF in complex robotic exoskeletons.

In this scope, the present dissertation aims to enhance and optimize the real-time modelling framework developed by Durandau *et al.* by expanding the capabilities of a high-level wearable robotic's controller so it becomes able to adjust its behaviour online in order to provide optimal rehabilitation conditions on a muscular level. In particular, it is intended to (i) design, develop, and implement a muscle-specific optimization model, (ii) test and evaluate its feasibility for real-time driving and validate it with experimental data using an active exoskeleton, (iii) confirm that the optimization is able to reduce the muscular effort of one specific muscle while having a minimal impact on the other agonist and antagonist muscles, and (iv) discuss possible future improvements to the used methodologies.

The present work will mark the firsts steps and the first attempt, to the best of the author's knowledge, of changing the rehabilitation emphasis to a real muscular level. To achieve this paradigm-shift, the following hypothesis have emerged:

1) Is the optimization model able to run on the EMG-driven HMI developed by Durandau *et al.* and send the computed assistive torque to the WE2 exoskeleton in real-time?
2) Can the optimized assistive torque reduce the effort of a specific muscle while having a minimal impact on the other muscles that act on the ankle joint?
3) For each Support Ratio candidate, is it possible to evaluate its optimality within 1, 3, or 5 gait cycles?

1.4. Structure and Outline of the Dissertation

Concerning the stated objectives, this report is organized into 6 chapters. This first chapter presents and synthesizes the motivation, the goals, and the context of the work. The remaining chapters are organized as follows:

- *Chapter 2. Context Background:* Gives a brief description and a bibliographic review of the important subjects addressed in this dissertation, namely the state-of-the-art on Wearable Robotics, its context, methodologies and applications, and an overview of the ankle joint anatomy and physiology and neurological lesions and motor disabilities;
- *Chapter 3. Giving Motor Assistance with an Exoskeleton*: Intends to explore the tools to be used along with this dissertation and the current state of the art of an EMG-driven human-machine interface for motor assistance and rehabilitation;
- *Chapter 4. Muscle-in-the-loop Optimization:* Presents the study strategy and the procedures for the enhancement and optimization of the EMG-driven human-machine interface;
- *Chapter 5. Validation Experimental Studies:* Describes the materials, methods and procedure employed in the experimental validation tests, the results and a final discussion;
- *Chapter 6. Conclusion*: Gives an overview of the developed work and how it achieved the stated goals and describes future directions on the continuity of the developed work.

Chapter 2. Context Background

In this chapter, it is aimed to conceptualize important subjects that are necessary for the development of this dissertation. In the first section, it is reported the general concept of Wearable Robotics and the different approaches and applications of Robotic Orthosis. Additionally, a description of the different sensors and control strategies is also given. In the second section, the anatomy and physiology of the ankle joint, specifically its skeletal and muscular structure, joint ligaments, and biomechanics are described. Finally, in the last section, an overview of the neuro-mechanical interfacing and neurological lesions is given.

2.1. State-of-art of Wearable Robotic Orthosis

2.1.1. Wearable Robotics

In the actual scenario of an ageing and industrializing population, it is plausible that people will become progressively more reliant on technology to meet their desire to live independently, actively, and satisfactory [1]. Among all the assistive devices springing up, WROs can be used to either augment, train, or supplement human motor function. These devices can provide forces to a body joint in parallel, for example, exoskeletons, exosuits, or body-worn collaborative robots, or in series, such as the case of bionic prostheses.

A WRO is generally anthropomorphic, prepared to be comfortably worn by a person. Given the close interaction with the user, the robot should be lightweight and take into account the user's joints range of motion (ROM) and degrees of freedom (DOF), its morphology, and kinematics in the order that it can provide a proper physical human-robot interface. Besides, the actuation and control of the robot should allow the user to implement their own movement without hindrance while receiving a certain assistance safely [11,12].

Many wearable robotics systems can be found in the current state-of-art, presenting an enormous variability in mechatronic design, control, and human-robot interfaces due to its targeted end and expected usage. However, all systems are mainly composed of mechanical structures, actuators, multisensory systems, controllers, and power sources, as shown in Figure 1 [13].

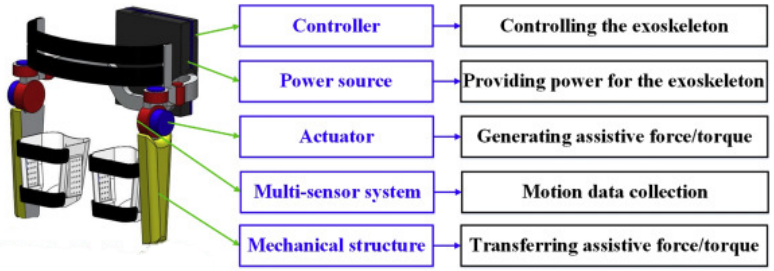

Figure 1. Essential components of an exoskeleton. The essential components include the mechanical structure for transferring assistive force/torque, an actuator for generating assistive torque, a multisensory system for motion data collection, a controller for controlling the exoskeleton, and a power-source for providing power to the exoskeleton (image from [13]).

2.1.2. Classification and Applications

WROs are mainly developed for four specific targeted ends: musculoskeletal rehabilitation, motor assistance, human strength augmentation, and industrial support.

Human Musculoskeletal Rehabilitation

Elderly people with weakened muscle strength may not be able to move as properly as before and may also lose their stability during daily movements as walk, stand up, or sweep the floor. Loss of motor control may occur due to many medical conditions, leading to the privation of quality of life [14].

Moreover, neurological injuries such as cerebral paralysis, stroke, infectious diseases, result in significant muscle weakness and impaired motor control. Orthopaedic rehabilitation generally involves performing specific movements to provoke motor recovery and ultimately improve their musculoskeletal strength and motor control whereas minimizing functional deficits [14].

In traditional rehabilitation therapies, intensive labour should be involved, and physical therapists should provide the patients with planed repetitive training that is usually inefficient [14,15]. Wearable robots developed for rehabilitation can provide intensive, repetitive, and adaptative motions for patient's training, and hence relieve therapists from the heavy work in physical therapy. In this situation, physiotherapists can concentrate their effort on analysing the patients' motor performance in order to provide more effective rehabilitation. Besides, with the usage of robotic orthosis, the motor recovery of the patients can be quantitatively assessed through sensors capable of monitoring the interaction forces and torques, as well as extra vital data, such as Electrocardiography (ECG) or EMG. This state-of-art resource of assisted rehabilitation is also cost-effective when compared to traditional labour rehabilitation [14,16].

The robotic orthosis LOPES (LOwer-extremity Powered ExoSkeleton), presented in Figure 2, was developed by H. Van Der Kooij and his team at the University of Twente (Netherlands) with the goal of building a device for gait training and assessment of motor function in stroke survivors. With 8 actuated DOF, LOPES combine a freely translatable and 2-D-actuated pelvis segment with a leg exoskeleton containing three actuated rotational joints: two at the hip and one at the knee. The joints are impedance controlled to allow bidirectional mechanical interaction between the robot and the training subject, being indeed capable of high assistance while keeping a low output impedance, thanks to its Series Elastic Actuator (SEA) strategy. Evaluation measurements showed that the device allows both "patient-in-charge" and "robot-in-charge" modes, in which the robot is controlled either to follow or to guide a patient, respectively. EMG measurements on eight important leg muscles demonstrated that free walking in the device strongly resembles free treadmill walking, which is an indication that the device can offer task-specific gait training [17,18].

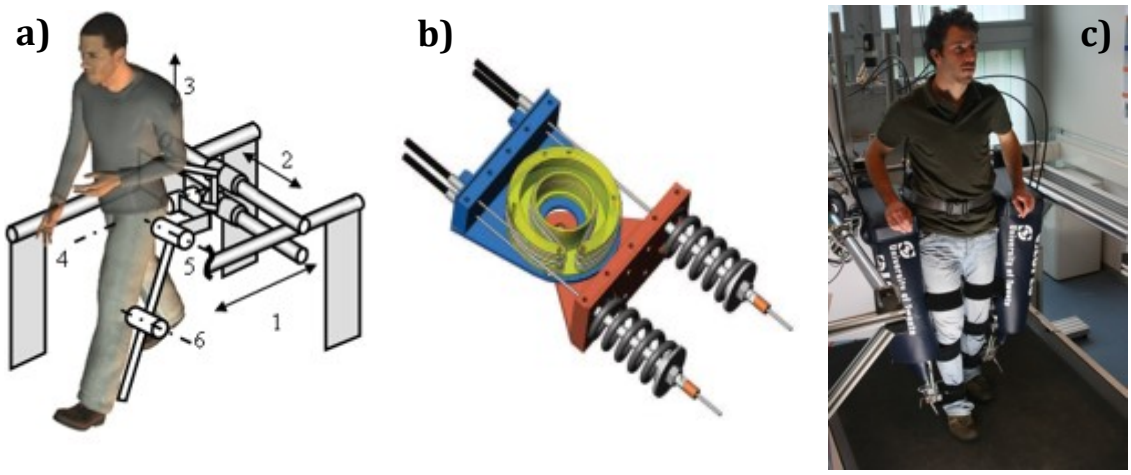

Figure 2. First Prototype of the Robotic Orthosis LOPES: a) Schematic overview of DOFs; b) Schematic overview of bowden cable-driven SEA; c) Subject's leg strapped to LOPES exoskeleton (image from [17]).

The Lokomat® orthosis (Figure 3) was developed by Hocoma company (Zurich, Switzerland) with the aim of automating treadmill training rehabilitation of locomotion for SCI and stroke patients. This system provides functional walking training for patients with mobility dysfunctions in their lower limbs. The whole system is composed of a robotic gait orthosis, a bodyweight support system, and a treadmill. The patient exercises in a virtual reality environment with constant audio and visual feedback, allowing the system to adapt its task-specific performance. The orthosis has 4 DOFs in total, and the hip and knee joints are actuated by linear drives to provide assistive torque in the sagittal

plane. Force sensors mounted between the actuators and orthosis measure the hip and knee joint torques [19–21].

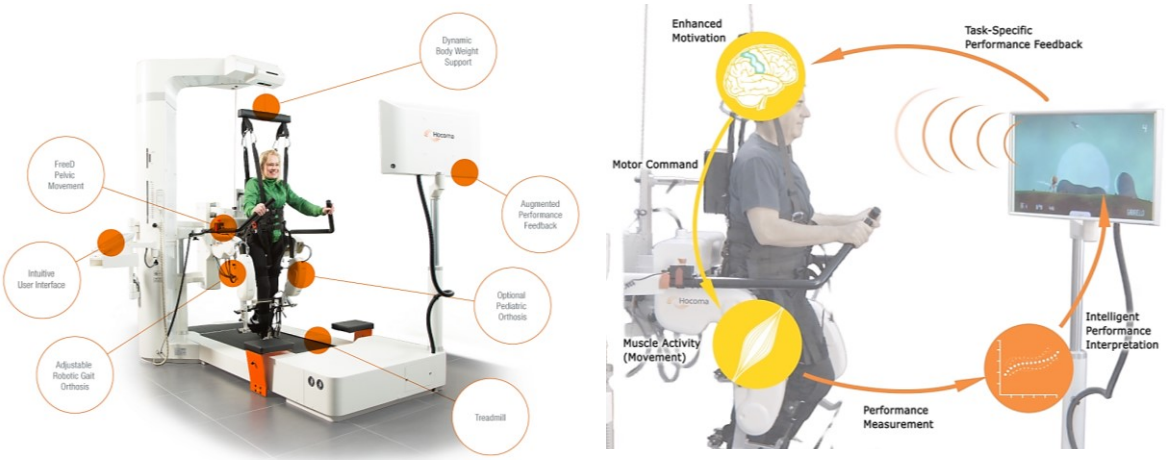

Figure 3. Lokomat® system for robot-assisted therapy with the exploitation of neuroplasticity (image from [19]).

The Armeo®Power, also developed by Hocoma company (Zurich, Switzerland), is an upper-limb rehabilitation exoskeleton that allows early treatment of motor disabilities and provides intelligent arm support in a large 3-dimensional workspace, therefore, enabling patients to perform intensive, repetitive, and goal-oriented exercises. With 6 actuated DOF, this device could efficiently induce new connections and facilitate plasticity phenomena potentiation. Similarly to Lokomat®, the patient exercises in a virtual reality environment, where an extensive library of game-like Augmented Performance Feedback exercises have been designed to train core movement patterns that are commonly used in activities of daily living [22–24].

Human Motor Assistance

Wearable Orthosis developed for human motor assistance are primarily used to help partially or total paralyzed patients who have lost or never had mobility on their limbs. A WRO can provide external torques at the human joints' rotational points to replace the patients' deficient motor function, and therefore give patients greater strength to regain the ability to perform essential daily life motions such as standing up, walking, or wash their hands [25].

Figure 4. Wearable robots for human motor assistance: a) The ReWalk™ Personal 6.0 system (image from [26]); b) Powered knee prosthesis developed by Reboocon Bionics (image from [29]).

The ReWalk™ Personal 6.0 Exoskeleton (Figure 4. a)), a WRO developed by ReWalk Robotics™ (Massachusetts, USA), was the first exoskeleton to receive FDA - U.S. Food and Drug Administration -

clearance for personal use in the United States. It provides powered hip and knee motion to enable individuals with spinal cord injury (SCI) to stand upright, walk, turn, and climb and descend stairs. The user controls the movement using subtle changes in their centre of gravity. A forward tilt of the upper body is sensed by the system, which initiates the first step. Repeated body shifting generates a sequence of steps that mimics a functional natural gait of the legs [14,26]. Clinical studies show that paralyzed patients can practically stand upright and walk with increased independence and their life quality is largely improved. The results also demonstrate that patients experienced a reduction in secondary social and psychological complications resulting from life in a wheelchair, such as depression and neuropathic pain [27,28].

The powered knee prosthesis (Figure 4. b)) developed by the startup Reboocon Bionics, is an ultra-lightweight motorized knee prosthesis. Although it is not CE marked yet, there are research projects with the main goal of developing advanced control algorithms to re-enable natural walking for amputees and collect clinical evidence to show the effectiveness of using this device [29].

Human Strength Augmentation

WRO developed for human strength augmentation can enhance human strength and endurance during various activities and enable individuals to perform tasks that they cannot easily perform by themselves. Providing soldiers, disaster relief workers, wildfire fighters, and other emergency personnel, these systems provide the ability to carry heavy loads such as food, rescue equipment, first aid supplies, communications gear, and weaponry [30].

The BLEEX (Berkeley Lower Extremity) Exoskeleton (Figure 5. a)), was developed by A. B. Zoss's group at the University of California Berkeley (USA) to help soldiers to carry heavy loads. It has seven DOF per leg: three DOF at the hip joint, one DOF at the knee joint, and three DOF at the ankle joint. Among these DOFs, hip flexion/extension, hip abduction/adduction, knee flexion/extension, and ankle dorsiflexion/plantarflexion are actuated by linear hydraulic actuators. The remaining DOFs are passively actuated by steel springs and elastomers. It has been reported that BLEEX wearers can walk at an average speed of 1.3 m/s while carrying a 75 kg payload [30].

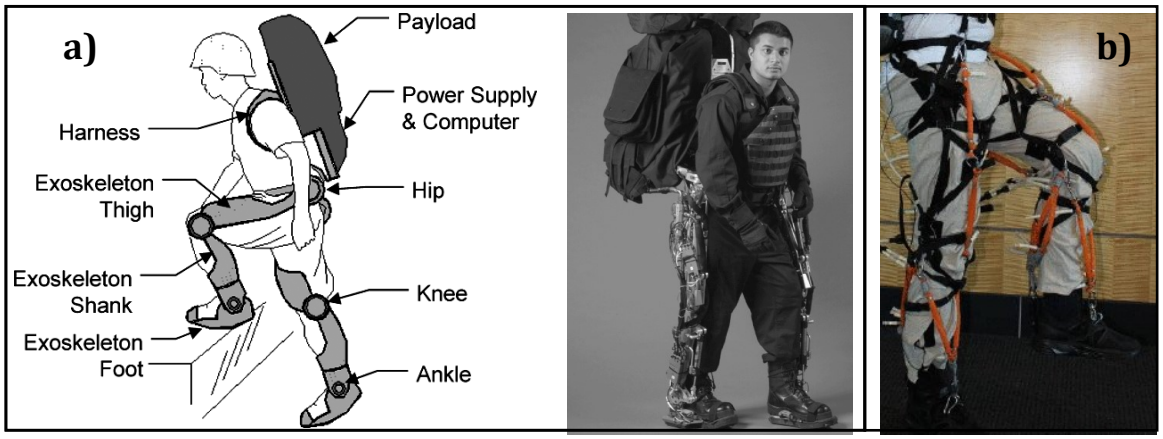

Figure 5. Wearable robots for human strength augmentation: a) LEEX (Berkeley Lower Extremity) Exoskeleton (image from [37]); b) Soft lower extremity robotic exosuit by Wehner *et al*. (image from [31]).

Wehner *et al*. had developed a soft lower extremity robotic exosuit (Figure 5. B)) at Harvard University (USA) to augment normal muscle functions in healthy individuals. Compared to previous exoskeletons, the device is ultra-lightweight, resulting in low mechanical impedance and inertia. The exosuit has custom pneumatic actuators that can assist the hip, knee, and ankle. The actuators attach to the exosuit through a network of soft, inextensible webbing triangulated to attachment points utilizing a novel virtual anchor technique. This approach was designed to transfer forces to locations on the body that can best accept a load. This system demonstrates to be able to comfortably transmit joint torques to the user while not restricting mobility and has the potential to reduce the wearer's metabolic cost during walking [31,32].

Robotic Orthosis in Industrial Scenarios

In industrial scenarios, the use of WRO in a production line allows employees to adopt a healthy posture, thus avoiding injuries resulting from repetitive performed actions, and consequently reducing physical wear and increasing production speed [33].

PARM (Power-Assisted Robot Arm – Figure 6) was developed by Kadota *et al.* (Tokyo Institute of Technology, Yokohama, Japan) and it uses pneumatic artificial rubber muscles to mimic the motion of biarticular muscles and, then, assist the wrist and elbow joint. This WRO control's system is based on the pressure value from a balloon sensor and it is used to achieve accurate power-assist motion of lifting an object. The EMG signals of the brachioradialis and the biceps brachii for a subject who lifted a 10-kg object from the floor and then set the object back down on the floor were studied and the experimental results for the cases with and without assistance indicate that the magnitude of the EMG signals decreased while wearing the power-assist unit; thus verifying the effectiveness of the system [34,35].

Figure 6. PARM (Power-Assisted Robot Arm) exoskeleton (image from [34]).

2.1.3. Data Acquisition and Analysis

To control a WRO on providing intelligent, effective, and comfortable assistance to the wearer, it is essential to acquire different types of motion and vital data of the human-WRO system during movement. Measured data can be used to recognize the wearer's intention, analyze its motion status, and gait pattern, and evaluate the motion performance. With multiple sensor systems in hardware and sensor fusion algorithms in the software, WRO's controllers can acquire and process data for motion control purposes. Generally, there are four types of biomedical data, which are measure with different types of sensors, associated with human motion: kinematic data, such as body posture and joint angles; kinetic data such as human joint torque, ground reaction forces, and interaction force between wearer and WRO; bioelectric data, such as EMG, ECG or brain signals; and metabolic data, such as Fraction of Inspired Oxygen (FIO_2), ventilation, and energy expenditure [14,36].

Kinematic Data

Kinematics is the field that analyzes motion patterns that allow assessing a comparative, biomechanical performance of healthy and injured subjects by obtaining positions and orientations of relevant bones and single body segments [37]. Many methods of kinematic analysis have been developed, such as skin markers, roentgen stereophotogrammetry, magnetic resonance imaging (MRI), computer simulation, *in vivo* fluoroscopy, and angular sensors [38]. Most commonly, in real-time analysis, angular sensors such as encoders and potentiometers are used to measure the joint angles and angular velocity of WROs, which are basic information for orthosis control [13].

Kinetic Data

Since the early '80s, joint kinematics, specifically joint moments, powers, and forces, have been used as an additional tool in the assessment of normal and pathological gait. Identifying specific joint

kinetic patterns and their relationship to associated clinical measures, such as joint ROM, is an important component to the understanding of the mechanisms of gait patterns [39].

Joint kinetics provides an opportunity to better appreciate the role of trunk positioning and the relationship between joints and limbs during gait. For example, the evaluation of the relationship of power generation on the involved versus the non-involved side of persons with hemiplegia suggests that the non-involved limb shows greater than normal power generation to compensate for the weaker non-involved limb. Understanding this general mechanism of gait in unhealthy persons helps the clinician recognize pathology specific concerns and may eventually guide treatment protocols [39].

For WROs powered by SEAs, compliant elements such as springs are generally implemented into the actuators. The compliant elements can reduce the WRO's mechanical impedance. Absolute encoder and strain gauges can be used to measure the deformation of the spring and, with the information of the spring stiffness, the actuators' output torque can be calculated. Other sensors such as the current sensor, Hall effect sensor, force-sensing resistor sensor, and torque sensor are used. These sensors are used to measure the information of electric current, which can be used to calculate the generated torque. Furthermore, force-sensing resistor sensors are used to measure the human-orthosis interaction forces, and the wearer's motion intention can be recognized by measuring the pressure information on the thigh by the sensors [13].

Bioelectric Data

In recent systems, human bioelectric signals such as EMG and ECG signals, which are related to the muscular and cardiac activities on human locomotion have been used. Bioelectric signals measured in real-time from the wearer directly indicate a human patient's motion intention and then actuate according to the requested assistance. On the other hand, EMG signal–based control has also been used to control the WROs by establishing a link between the actuated torques and the phases of a gait cycle and can be further used to evaluate motion performance [13]. However, there are some inherent limitations to overcome. For example, the calibration of bioelectric sensors takes substantial time, and neighbouring sensor nodes and noise easily interfere with the collected bioelectric signals [14].

Metabolic Data

To date, the standard for performance evaluation of WROs has not been established. Most researchers measure the wearer's metabolic cost of specific tasks and use it as the metric to evaluate the system's performance. Therefore, the individual's oxygen and carbon dioxide flow are measured to evaluate the metabolic cost and conclude about the system's performance and efficiency [13].

2.1.4. Control Strategies

The amount of research on developing WRO has been growing in recent years, however, the best control design remains unclear. From the point of view of human physiologic locomotion, its control can be divided into reflexes (feedback, e.g. force, displacement and velocity reflexes) and central pattern generators (CPGs, *i.e.* feedforward) generated by the central nervous system and the reflex responses resulting from muscle dynamics [40].

A WRO is attached to the wearer and integrates human intelligence and capacity with robotic technologies. From the control aspect, the wearer and WRO must form a closed loop as a human-WRO cooperation system, as represented in Figure 7 [14].

In the WRO system part, reference torque or reference joint trajectory is obtained according to a specific assistive pre-defined function. The reference inputs go through the motion controller to produce control signals that drive the actuators. Then, the generated mechanical torque of the actuator is used to drive the wearer and the WRO itself. As a result, the interaction torque is applied to the wearer's joints as the external assistance of the desired motion. In the human-WRO cooperation system, the function of the human body part is different among its application. In the application of human strength augmentation, the wearer takes charge of the motion planning, and the WRO is expected to follow the wearer's trajectory. By contrast, as for the WRO used for gait rehabilitation and

human locomotion assistance, joint torque generated by the wearer's muscle is, generally, much smaller (even null for completely paralyzed patients). Therefore, the wearer's mobility is strongly assisted by the exoskeleton with interaction torque [14].

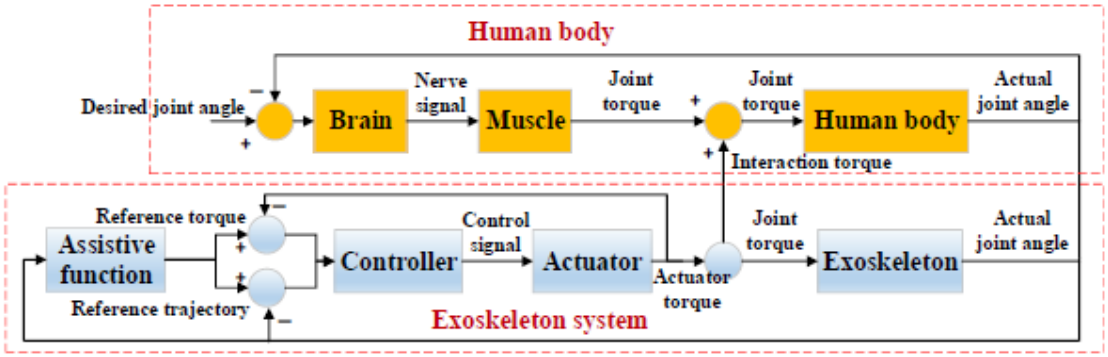

Figure 7. Schematic of the Human-Exoskeleton cooperation control system (image from [14]).

The control strategies rehabilitation WRO can be generally divided into two main classic categories: trajectory tracking and assist as needed. In trajectory tracking control, the predefined trajectories of the joints, usually collected from healthy individuals, are used as the control targets. On the other hand, an "assist as needed" strategy suggests that the assistive devices only supply as much effort as a patient needs to accomplish training tasks by assessing their performance in real-time and intelligently adjusting its support according to the patients' physical conditions and efforts during rehabilitation. Hybrid position and force control is one type of exoskeleton control strategy that takes into consideration the joint trajectories and interaction forces between the wearer and WRO. Impedance control is another popular method, which its basic idea is to regulate the dynamic relation between the assistive device and the wearer by relating the position error (e.g., joint angles) to the interaction force/torque through a mechanical impedance of adjustable parameters. This mechanical impedance is the output impedance of the WRO, which is usually modelled as a mass-damper-spring system. High output impedance will increase the assistance to guide the patient's limbs onto the reference trajectory. If the patient shows greater effort in the training, the desired output impedance will similarly be lower to allow the patient to deviate more from the reference trajectory. Furthermore, trajectory tracking control is the most widely used control strategy for human locomotion assistance. With this control strategy, the joint angles of the WRO and its wearer are precisely controlled to follow a target trajectory. The WRO controller must minimize the deviation between the target and feedback joint angles. To adopt trajectory tracking control, reference trajectories of all the active joints of the WRO should be set in advance. Finally, hybrid position and force control are the most widely used control strategy for the application of human strength augmentation such as transporting or lifting heavy loads tasks. In a gait cycle, the WRO's stance segment must be controlled with a position controller while its swing segment must be controlled with a force controller [14].

In different applications, the wearers have different physical conditions, and hence different control strategies should be adopted by the WRO. Even for the same application, different control strategies may be appropriate in different phases of its usage. In rehabilitation, for example, in an initial stage, the trajectory tracking control strategy is suitable when the wearers do not have much strength in their limbs. However, after a period of training, the patients may have an improved physical condition, and "assist as needed" control strategies should be adopted to provide more effective training with the patients' active participation [14].

For what concerns to research, during these late years, the control strategies in assistive wearable robots did not advance as much as their mechatronic counterpart (*i.e.*, motor, power, etc.) or as the electrode design and recording techniques (i.e., bio-signal recording, nerve interface, etc.). For exoskeletons, a major paradigm shift on mechatronic design happened, for example, with advances like

series-elastic actuation, which offers better torque and stiffness control [41], whereas, regarding recording techniques, new electrode designs and bioelectrical signal processing like high-density surface electromyography (HD EMG) or active EMG electrodes allowed a better understanding of motor control by the estimation of motor neuron activities and facilitated the EMG signal processing [42]. An instance of this paradigm can be seen in the current state of the art approaches. HMIs in commercially available robotic exoskeletons for neurorehabilitation (e.g., Rewalk™ [26], Lokomat ® [19], and LOPES [17]) largely rely on position and impedance control. In these approaches, the robotic exoskeleton creates joint trajectories or force fields along with predefined kinematic profiles and gait patterns previously extracted from healthy subjects. However, this does not fully engage the patient, hampering the emergence of positive neuroplasticity, with limited rehabilitation outcomes concerning conventional therapy. The ability to operate a control model in real-time is important in the context of human-machine interfacing for wearable assistive devices, as it would enable predicting the intended movement even before the actual manifest in the human body, allowing, namely, to support individuals with reduced motor abilities but detectable electrophysiological activity.

Over the past few years, novel EMG-driven models have been developed in order to truly make a connection between the user's will and the assistance given by the robotic exoskeleton [10,43,44]. EMG-driven forward dynamic musculoskeletal models are still under deep research and allow to simulate all transformations from muscle excitation onset, *i.e.*, EMGs, to mechanical moment production around multiple limb DOFs. These approaches therefore account for the form and function of the human neuromusculoskeletal system in healthy and neurologically impaired patients and enable them to voluntarily control multiple DOF in complex robotic exoskeletons. Additionally, models from [7,8,45,46] further intended to optimize the human-exoskeleton performance by measuring metabolic variables with a respiratory system. Their main goal is to dynamically adjust the controlling laws during the use of an exoskeleton so it would minimize the subject effort and, consequently, its energetic costs.

2.2. The Human Foot and the Ankle Joint

The foot is a complex anatomical and biomechanical structure. It acts to transfer forces between the lower limb and the ground, allowing stable ambulation and stance. During the gait cycle (see Supplementary Content 2.), the foot functions as a flexible shock-absorber, deforming to uneven surfaces before undergoing a series of biomechanical changes which allow it to act as a rigid lever to exert force. The dense concentration of structures required for normal foot function makes the foot and ankle a treacherous area [47,48].

2.2.1. Skeletal Structure

The foot is composed of 26 bones (see Supplementary Content 3.1.). The tarsal bones of the ankle are arranged in proximal and distal groups, which allow the load-bearing role of the ankle. The largest tarsal bone is the calcaneus, which forms the heel. The remaining bones of the foot are divided into metatarsal bones and phalanges [49].

The ankle joint complex is composed of three main joints which are responsible for the important role in the ankle's biomechanical function. They are the tibiotarsal or talocrural joint, well-known as the ankle joint, formed by the tibia, fibula and talus, the subtalar joint that comprises the talus and calcaneus bones, and finally the transverse tarsal joints [46]. The talocrural joint is a syndesmosis and includes two articulations: a medial joint between the tibia and talus and a lateral joint between the fibula and talus, both enclosed in one joint capsule [49]. These three main joints allow most of the motion of the foot and the remaining ones only allow small motions, and do not involve frequent medical consideration [50].

The distal end of the tibia, the malleolus, and the fibula overhang the talus on each side like a cap and prevent most side-to-side motion [47]. The malleolus consists of an articular facet that contacts the lateral side of the talus and a convex, medial surface articulates with the concave, lateral

surface of the tibia. The ankle joint is stabilized by this articulation during dorsiflexion and plantarflexion [51]. Therefore, it is possible to affirm that the ankle is characterized as a hinge-type joint, this is because it admits only one axis of rotation (uniaxial) of a convex component that articulates on a concave surface, as demonstrated in Figure 8.

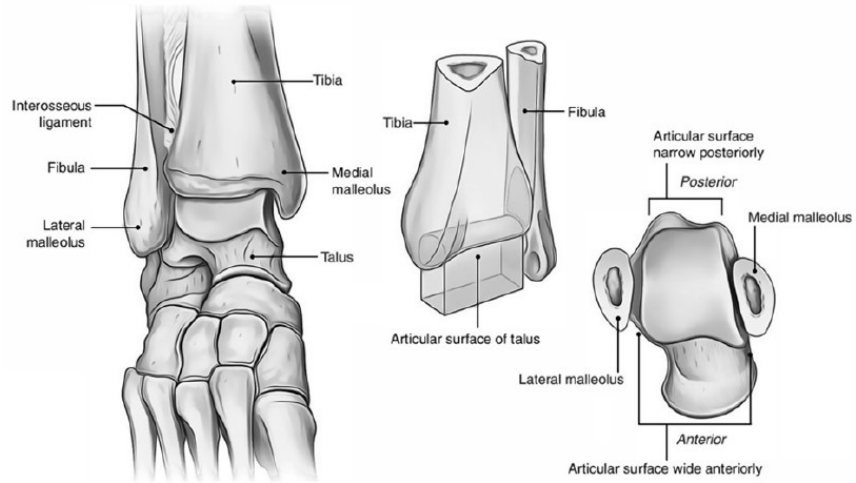

Figure 8. Representation of the axis of rotation of the ankle. (Image credits: António Ramos, 2020, Biomechanical Devices, University of Aveiro)

2.2.2. Joint Ligaments

On reviewing the anatomy of the ankle joint complex, it is impressive the number of groups of ligaments and the large number of smaller ligaments that make up each of these groups (see Supplementary Content 3.2.). Nevertheless, in general, the ligaments around the joint can be divided, depending on their anatomic position, into three groups which include: (1) anterior and posterior tibiofibular ligaments, which bind the tibia to the fibula; (2) a multipart medial (deltoid) ligament, which binds the tibia to the foot on the medial side; and (3) a multipart lateral collateral ligament, which binds the fibula to the foot on the lateral side. The calcaneal (Achilles) tendon extends from the calf muscles to the calcaneus. It plantarflexes the foot and limits dorsiflexion. Plantar flexion is limited by extensor tendons on the anterior side of the ankle and by the anterior part of the joint capsule [52,53].

2.2.3. Muscular Structure

The muscles of the ankle (see Supplementary Content 3.3.), like its skeletal architecture, are essential to its function. There are a number of muscles that dorsiflex, plantarflex, evert, and invert the foot at the ankle. Together, these muscles can also act to stabilize the joints they cross during locomotion. The muscles acting at the ankle and foot can attach as high on the leg as the femoral condyles and as low as the distal tibia and fibula. The muscles attach distally at multiple locations, from the most posterior calcaneus to as far forward as the phalanges [54].

The muscles acting on the foot can be divided into three major groups, namely anterior (extensor), posterior (flexor) and lateral (fibular) compartments [49]. The anterior and lateral muscles of the ankle provide the joint for various movements and functions. These muscles can be recruited for plantar flexion if they pass behind the lateral malleolus or for dorsiflexion if they cross in front of the talocrural joint (ankle joint). Those that cross in front also provide some extension (lifting) of the toes, those with medial distal attachments aid in the inversion of the foot, and those with lateral distal attachments contribute to eversion. Dorsiflexion of the foot via the anterior and lateral musculature is an important movement function. This type of movement occurs if the foot is the least stable end of the lever system, as in walking, running, or any other movement requiring the forefoot to be elevated. It is the opposition of plantar flexion via the posterior muscles. In posture maintenance, where the foot is the most stable end of the system, the anterior muscles pull the shin forward [55]. On the other hand,

the posterior muscles of the lower leg are the largest and most powerful of the three groups of muscles present (posterior, anterior, and lateral). Their primary function is plantar flexion, with each muscle having additional movement roles [54].

The most important muscular groups acting on the ankle joint are detailed in Table 1.

Table 1. Principal muscular groups acting on the foot [49]

Name	Action	Skeletal Attachments	Innervation
Anterior (Extensor) Compartment			
Fibularis (Peroneus) Tertius	Dorsiflexes and everts foot during walking; helps toes clear the ground during forward swing of leg	• Medial surface of lower one-third of fibula; interosseous membrane • Metatarsal V	Deep fibular (peroneal) nerve
Extensor Digitorum Longus	Extends toes; dorsiflexes foot; tautens plantar aponeurosis	• Lateral condyle of tibia; shaft of fibula; interosseous membrane • Middle and distal phalanges II-V	Deep fibular (peroneal) nerve
Extensor Hallucis Longus	Extends great toe; dorsiflexes foot	• Anterior surface of middle of fibula; interosseous membrane • Distal phalanx I	Deep fibular (peroneal) nerve
Tibialis Anterior	Dorsiflexes and inverts foot; resists backward tipping of body (balance); helps support medial longitudinal arch of foot	• Lateral condyle and lateral margin of proximal half of tibia; interosseous membrane • Medial cuneiform; metatarsal I	Deep fibular (peroneal) nerve
Posterior (Flexor) Compartment - Superficial Group			
Gastrocnemius (Lateralis and Medialis)	Plantar flexes foot; flexes knee; active in walking, running, and jumping	• Condyles and popliteal surface of femur; lateral supracondylar line; capsule of knee joint • Calcaneus	Tibial nerve
Soleus	Plantar flexes foot; steadies leg on ankle during standing	• Posterior surface of head and proximal one-fourth of fibula; middle one-third of tibia; interosseous membrane • Calcaneus	Tibial nerve
Posterior (Flexor) Compartment			
Fibularis (Peroneus) Brevis	Maintains concavity of sole during toe-off and tiptoeing; may evert foot and limit inversion and help steady leg on foot	• Lateral surface of distal two-thirds of fibula • Base of metatarsal V	Superficial fibular (peroneal) nerve
Fibularis (Peroneus) Longus	Maintains concavity of sole during toe-off and tiptoeing; everts and plantar flexes foot	• Head and lateral surface of proximal two-thirds of fibula • Medial cuneiform; metatarsal I	Superficial fibular (peroneal) nerve

2.2.4. Biomechanics

Biomechanics is the field that studies the mechanics of biological systems and seeks its influence on the construction of structures, bridges, or moving objects. Its understanding is fundamental for the correct measurement of, for example, forces applied to joints, bones, muscles, speeds, and amplitudes of displacement as well as the forces that the ground applies on the human body structure [56].

Ankle Joint Motion

For the study of the ankle's biomechanics, it is necessary to know the anatomical reference planes and axes of the foot. When a segment of the body moves, it rotates around an imaginary axis of rotation that passes through a joint to which it is attached. In the case of the foot, while the mediolateral axis is perpendicular to the sagittal plane, the longitudinal axis is perpendicular to the transverse plane and the anteroposterior axis is perpendicular to the frontal plane. Therefore, the rotation in the sagittal, transverse and frontal planes occurs around the mediolateral, longitudinal and anteroposterior axes, respectively, as shown in Figure 9 [53].

Most of the human movements are "general motions" that combine linear (translation) with angular (rotational) movements. When the human body is in the anatomical reference position, all body segments are considered to be orientated at zero degrees. In this sense, the rotation of a body

segment away from anatomical reference position is named according to the direction of motion and is quantitatively defined by measuring the angle between the position of the body segment and the anatomical reference plane [57].

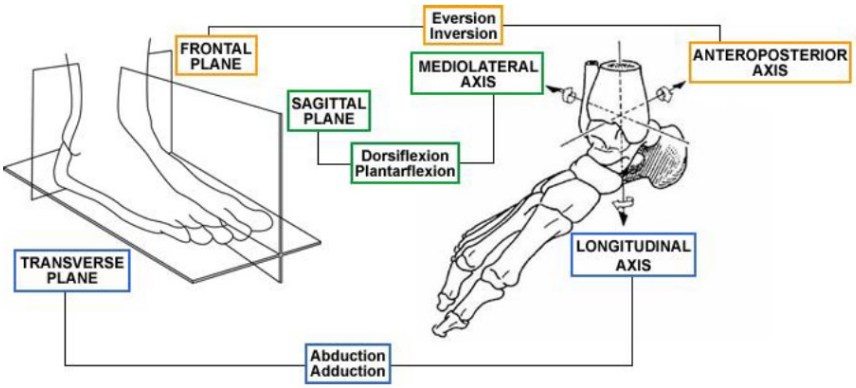

Figure 9. At left, the anatomical reference position of the foot and the three anatomical reference planes – sagittal, transverse and frontal. At right, the three anatomical reference axes applied to the ankle joint (image from [53]).

Concerning the motion of the foot, although its movement is defined through the sagittal, frontal and transverse planes, the movement does not occur in isolation within the established planes but takes advantage of the coordinated movement of the three ankle joints that allow the anterior part of the foot to move around a given oblique axis of rotation of the inner part of the foot. This is due to the fact that the subtalar and mainly the talocrural joints admit oblique angles of rotation [48]. Nevertheless, these tri-plane motions can be described as a combination of simultaneous motion in the three reference planes (Sagittal, Transverse, and Frontal planes). Thereafter, dorsi/plantarflexion motions occur around the mediolateral axis in the sagittal plane, abduction/adduction motions occur around the longitudinal axis in the transverse plane, and eversion/inversion motions occur around the anteroposterior axis in the frontal plane [53,57]. The possible motions of the foot are summarized in Figure 10. i).

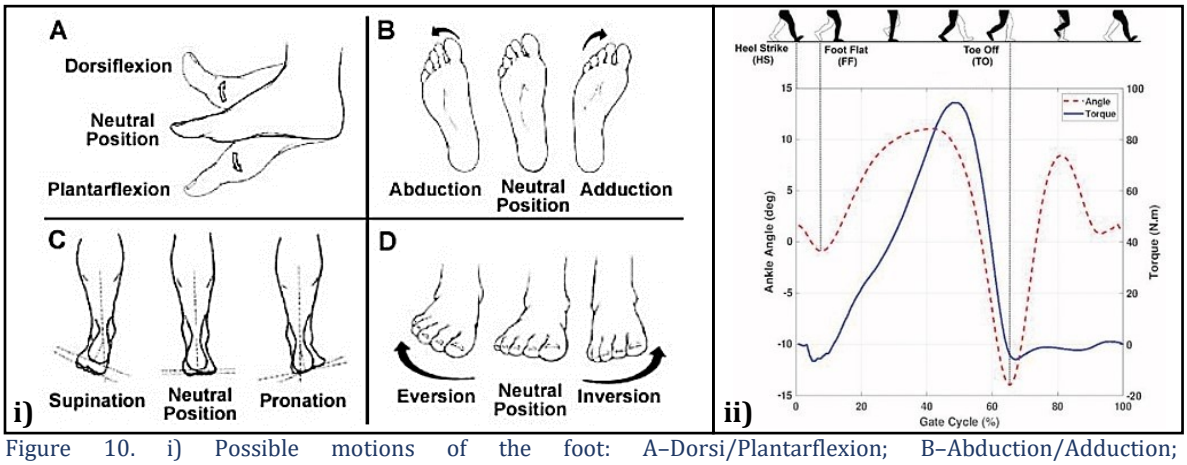

Figure 10. i) Possible motions of the foot: A–Dorsi/Plantarflexion; B–Abduction/Adduction; C-Pronation/Supination; D–Eversion/Inversion (image from [53]); ii) The human ankle angle and torque during gait cycle (adapted from [62]).

Ankle Axis and Range of Motion

For practical purposes, foot motion can be divided into two distinct types: non-weight-bearing (passive condition) and weight-bearing (active condition). The difference is that in weight-bearing motion there are forces related with the body weight and muscle contraction acting to stabilize the joints while the patient is standing, whereas in non-weight-bearing the patient is seated and lets the foot and ankle to move freely with the help of a clinician [53].

Nowadays there are still some doubts regarding the axis of rotation of the ankle joint due to its complex dynamic nature. However, Mann [58] stated that the ankle joint was uniaxial in the frontal plane there was an angle of 80º formed by the ankle joint axis, a line passing through the tips of the malleoli, and the centre of the tibial longitudinal axis, while in the transverse plane the axis was defined according to an angle of 84º from the midline axis of the foot (see Supplementary Content 3.4.). Although it is sometimes possible to consider the ankle joint as an almost purely uniplanar hinge joint, it was already stated that it might not be an accurate approach in some cases [59,60]. In fact, the fit between the distal fibula and tibia with the talus allows the movements of dorsiflexion and plantarflexion in the sagittal plane, which is the main plane of motion in the ankle joint, but the ankle joint also rotates in the transverse plane, about 5/6° around the longitudinal axis, allowing the movements of abduction and adduction and also in the frontal plane (despite the smaller degree of rotation), allowing the movements of inversion and eversion [48,53,60].

In the primary axis of rotation of the ankle joint, the amplitude of motion fluctuates between 20° to 60° with approximately 30° required for walking, 37° for ascending stairs and 56° for descending stairs. In particular, the values found in the literature for the normal range of motion in the sagittal plane range from 23º to 56º of plantarflexion and from 13º to 33º of dorsiflexion. Nevertheless, during the stance phase of gait (see Supplementary Content 2.) the range of motion is usually limited on average to a maximum of 15º for plantarflexion and 10º for dorsiflexion, as shown in Figure 10. ii), although healthy older individuals have demonstrated a decreased plantarflexion, whereas individuals with a diseased ankle have exhibited a decreased dorsiflexion [60,61].

Forces, Moments, and Power at the Ankle Joint

Forces transmitted across the ankle joint are a combination of external and internal forces. The external forces are the forces produced by the body contact with the ground, namely ground reaction forces (GRF), which can be measured experimentally during gait using a force platform. On the other hand, the internal forces are produced by muscles and ligaments and so its determination *in vivo* is still difficult and the only way to do it is using computational methods [50]. Some biomechanical models have been developed to calculate internal forces in the joints of the foot, but these internal forces are nowadays still not completely understood [9,50,53].

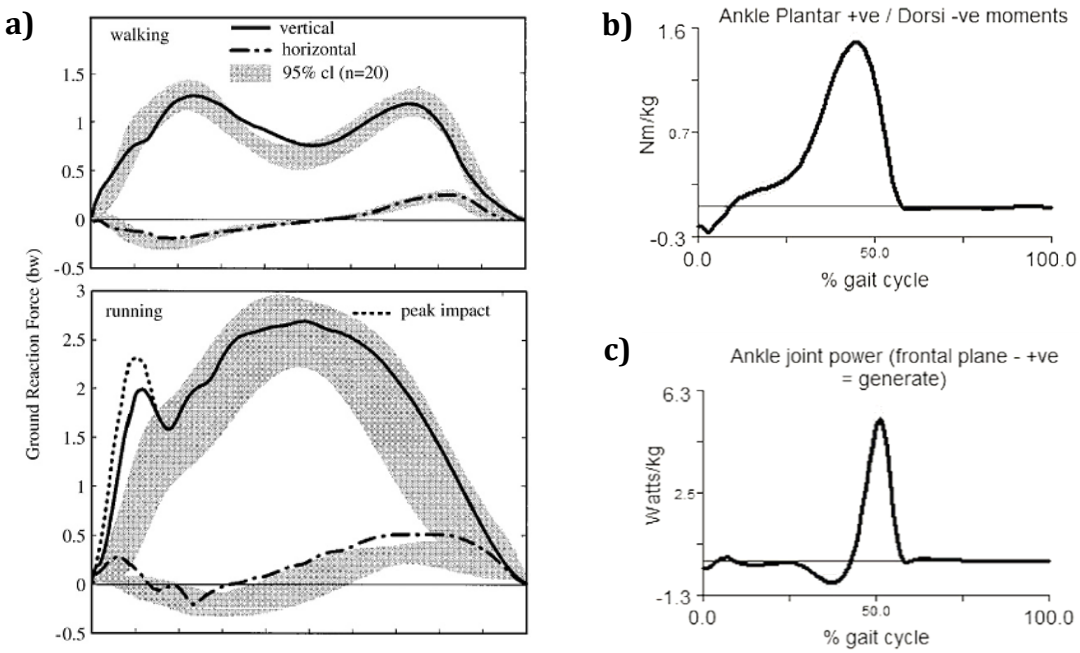

Figure 11. a) Calcaneal loading during a running and walking cycle. Ground reaction forces are expressed normalized to body weight - bw (image from [51]); b) Sagittal plane ankle moments (adapted from [63]); c) Sagittal plane ankle power (adapted from [63]).

The ankle joint complex bears a force of approximately 3 up to 5 times body weight (BW) during stance in normal walking, and up to 13 times BW during activities such as running [51,57,64]. The vertical ground reaction force applied to the foot during running is bimodal, with an initial impact peak followed almost immediately by a propulsive peak, as the foot pushes off against the ground, as demonstrated in Figure 11. a) [57]. The ankle moment (Figure 11. b)) obtained by Brockett *et. al* [63] demonstrates a dorsiflexion moment at heel strike as the dorsiflexors eccentrically contract to control the rotation of the foot onto the ground and prevent the foot from slapping the ground. During the second phase, there is a plantar-flexor moment as the ankle dorsiflexors contract eccentrically to allow forward progression of the shank over the foot. During the third phase, the plantar-flexion moment continues with the plantar flexors contracting concentrically towards toe-off. As walking speed increases, ankle kinetic patterns remain similar in profile but with greater magnitudes [51,63]. Ankle power (Figure 11. c)) varies when the major muscles acting on the ankle joint complex are either absorbing or generating power during gait. The negative values correspond with power absorption from the plantar flexors eccentrically contracting during the heel and ankle rocker phases. The maximum joint power of the ankle joint complex is generated at approximately 50% of the gait cycle during the forefoot rocker phase corresponding with the power generation of the plantar-flexors required for the lower limb to propel the body forward towards toe-off [61,63].

2.3. Neuro-mechanical Interface and Neurological Lesions

The nervous system is responsible for maintaining internal coordination through electrical and chemical signalling from cell to cell [65]. Regarding this communication, the nervous system is able to control and coordinate the body's movement throughout the Muscle-Tendon Units (MTUs). However, in the occurrence of a neurological lesion, such as those underlying stroke and spinal cord injury, it often carries a severe motor impairment that compromises the subject's motor capacity and health.

2.3.1. Neural Interfacing and Physiology

The nervous system's function relies on two subdivisions: the central nervous system (CNS), which consists of the brain and spinal cord (SC), protected by the cranium and vertebrae respectively, and the peripheral nervous system (PNS), composed of nerves (bundle of axons wrapped in fibrous tissue) and ganglia (where the cellular bodies are located) [65].

The nervous system is composed of cells whose function allows their organization into two categories: neurons (or nerve cells) and neuroglia (or glia) (Figure 12). Neurons are responsible for conducting and processing information. As for glia, it is responsible for protecting and supporting neurons, modulate signalling function, and serving additional functions, such as contributing to repair in case the nervous system is damaged when recovery is possible by promoting neuron regrowth, and preventing regeneration in case it would be harmful [65,66].

Neurons are cells specialized for long-distance electrical signalling through action potentials and intercellular communication through synapses. Their characteristic morphology comprises an axon and an arborization of dendrites, which are the primary targets for synaptic input. Synapses can either be chemical or electrical: the former is the most abundant in the mature nervous system, and the latter is predominantly found in the developing CNS [66]. These cells can be grouped into three classes: sensory neurons (afferent neurons), interneurons, and motor neurons (efferent neurons). The first ones detect stimuli and transmit the information to the CNS. The interneurons are within the CNS and are responsible for receiving the signals from the sensory neurons, process them, retrieve information, and determine how the body responds to a stimulus. As for the motor neurons, these transmit the signals from the CNS to the effectors, *i.e.,* muscle or gland cells [65].

Arising from the brainstem and extending from the first cervical vertebra until the first lumbar vertebra or slightly beyond, the SC is a "cylinder" of nervous tissue that gives rise to 31 pairs of spinal nerves. As far as spinal nerves are concerned, there are 8 cervical of them (C1-C8), 12 thoracics

(T1-T12), 5 lumbar (L1-L5), 5 sacral (S1-S5) and one coccygeal (Co) [65,66]. Looking at a transverse section of the SC, it exhibits an H-shaped grey matter core (composed of the somas, dendrites, and synapses of the neurons) surrounded by white matter (that consists of the axons) [65]. Sensory signals enter the SC through the dorsal root into the dorsal horn, following the ascending tracts. Then, the efferent signal follows the descending tracts and exit the SC through ventral roots. The ventral horn contains the cell bodies of the Motor Neurons (MN) that send axons via the ventral roots of the spinal nerves (Figure 13) [66,67]. Motor signals are usually initiated in the upper MN in the cerebral cortex and travel to a lower MN in the SC. The lower MN leaves the CNS through a nerve to the muscle [65].

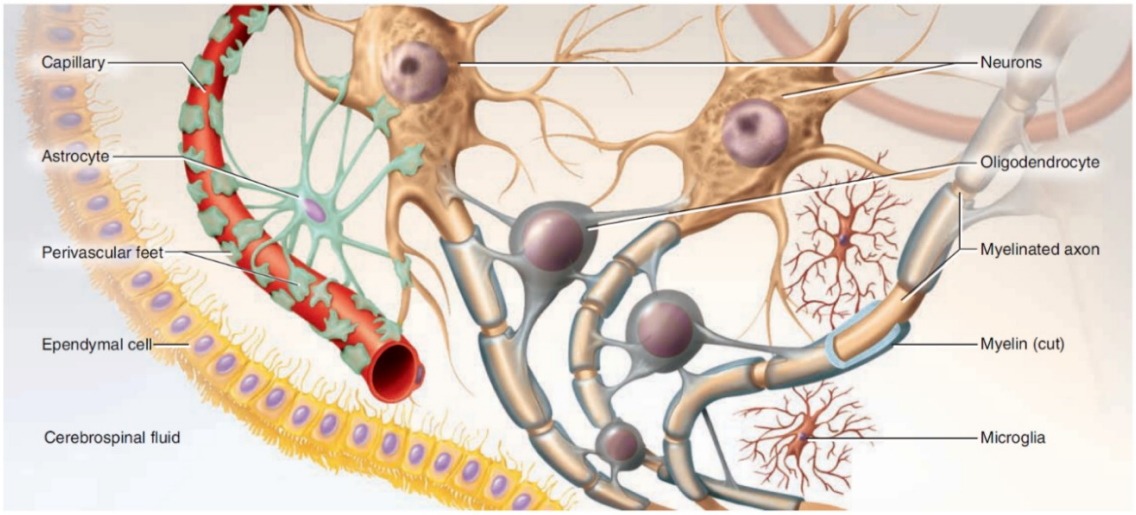

Figure 12. Neurons and Neuroglia of the Central Nervous System (image from [65]).

In case of injury, the anatomical integrity of the SC is compromised, which poses a severe problem as it has a limited capacity to regenerate itself [67]. Thus, these injuries usually result in sensory and motor loss, and the resulting sequelae depend on the location of the injury, as shown in Figure 13.

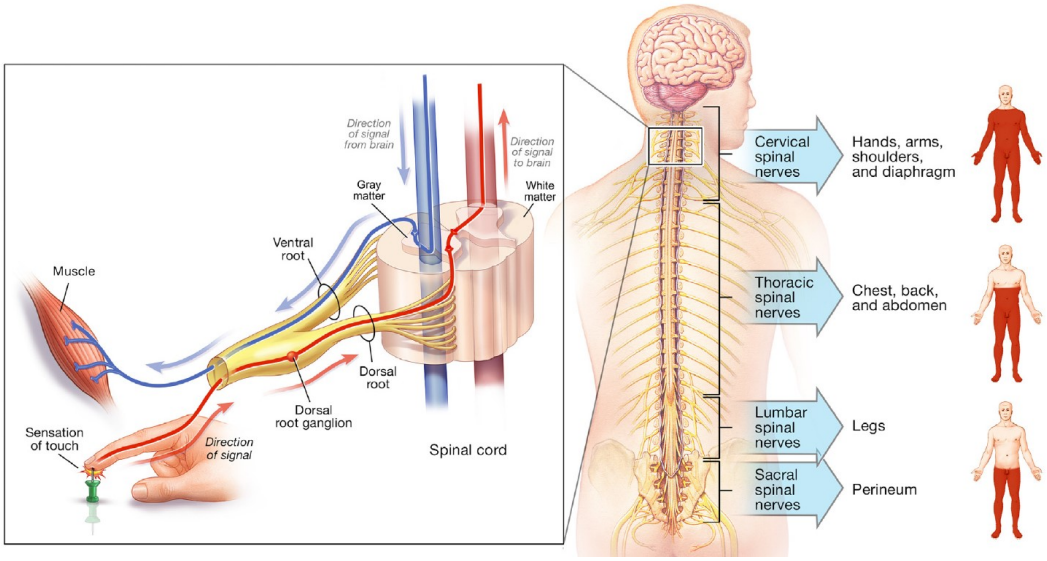

Figure 13. Signal pathways and areas with sensory and motor sequelae are represented in red. (image from [67]).

2.3.2. Muscle-Tendon Unit Physiology

The neural system sends neural signals to the MTUs (see Supplementary Content 4.) by firing alpha motor neurons. These are the main force/torque generator in the human body and are composed of a tendon, which is attached to the skeletal system on one side, and the muscle on the

other side. Tendons are mainly made of collagen and act as a spring in the muscle-tendon system. Muscles, on the other hand, can actively produce force by twitching under the effect of motor unit action potential (MUAP) that is the main command signal of the muscle-tendon system. The muscle is mainly comprised of muscle fibre bundled together in the fascicle, which are activated together by the same MUAP [6,65]. Muscle fibres are composed of myofibrils, which are built of proteins (actin, myosin and titin) that, organized into myofilaments, can slide along each other under the effect of MUAP and thus creating muscle contraction [65,68].

For the CNS to be aware of the MTU state, the MTU is composed of multiple proprioception mechanisms. For example, the muscle spindle type II will activate (or fire) depending on the stretch level of the muscle fibre giving information about the length of the muscle. Muscle spindle type I will activate depending on the rate of change in contraction giving information about the muscle velocity. Golgi tendon organ (GTO) named after Italian physician Camillo Golgi, is situated as the intersection between the muscle and the tendon. The GTO will activate when compressed by the muscle fibre thus encoding muscle force [6].

2.3.3. Neurological Lesions and Motor Diseases

The ability to walk directly relates to the quality of life. Neurological lesions such as those underlying stroke and spinal cord injury (SCI) often result in severe motor impairments (i.e., paresis, spasticity, abnormal joint couplings) that compromise an individual's motor capacity and health throughout the life span. Following a neurological lesion, secondary adaptation processes occur in the entire musculoskeletal system, i.e., alterations of muscles, ligaments and tendons properties [69].

SCI is a condition caused by any lesion to the SC [70]. It implies the loss of sensory, motor and autonomic functions and it can either result from traumatic events or non-traumatic events [71]. For traumatic events, these include road traffic injuries and falls as the primary causes, followed by violence and sports injuries medical/surgical causes [72]. Other non-traumatic events that usually are due to an underlying pathology, such as degenerative CNS disorders, tumours, congenital problems or infectious diseases can also induce lesions to the spinal cord [70]. SCI most frequently results in loss of sensibility and paralysis below the level of injury, which can either manifest as paraplegia, tetraplegia, paraparesis, or tetraparesis. Autonomic dysreflexia, loss of control of the urinary bladder and bowel, pain or burning sensation, breathing difficulties, and circulatory problems are also consequences of SCI [71].

Stroke has an acute onset and often results in a chronic and disabling condition due to physical, cognitive and emotional problems [73]. Because mobility is deemed to be instrumental to community participation for stroke survivors, limitations in walking ability is considered one of the greatest contributors to disability, loss of independence, restricted participation in society, and reduced quality of life. The goal of stroke rehabilitation programs is to restore as much independence as possible by improving physical and cognitive function. Two major functional impairments related to stroke are the loss of selective joint control and muscle weakness. From a clinical perspective, both issues must be addressed via safe, comfortable and feasible positions for the patient [6,74].

For several decades, scientific effort in rehabilitation robotics has been directed towards exoskeletons that can help enhance motor capacity in neurologically impaired individuals. However, despite the recent advances, robotic exoskeletons still achieved only modest clinical impact in neurologically impaired patients, i.e., stroke and SCI patients [75].

Chapter 3. Giving Motor Assistance with an Exoskeleton

This third chapter aims to contextualize the work of this dissertation. The first section presents the main tools and resources for modelling the musculoskeletal system. The second section gives the state of the art of the system developed by our group at the *Neuromechanical Modeling and Engineering Lab* (University of Twente, Netherlands) as well as the aborded problematic and solution directions.

3.1. Main Tools for Modelling the Musculoskeletal System

Musculoskeletal modelling has applications ranging from the study of muscle contributions to movement [9,76] to the development of novel human-machine interfaces [77,78]. There are two traditional modelling approaches to studying the biomechanics of human movement for musculoskeletal modelling: forward dynamics (FD) and inverse dynamics (ID) (Figure 14). Either approach can be used to determine joint kinetics, i.e. estimate joint moments during movements [79].

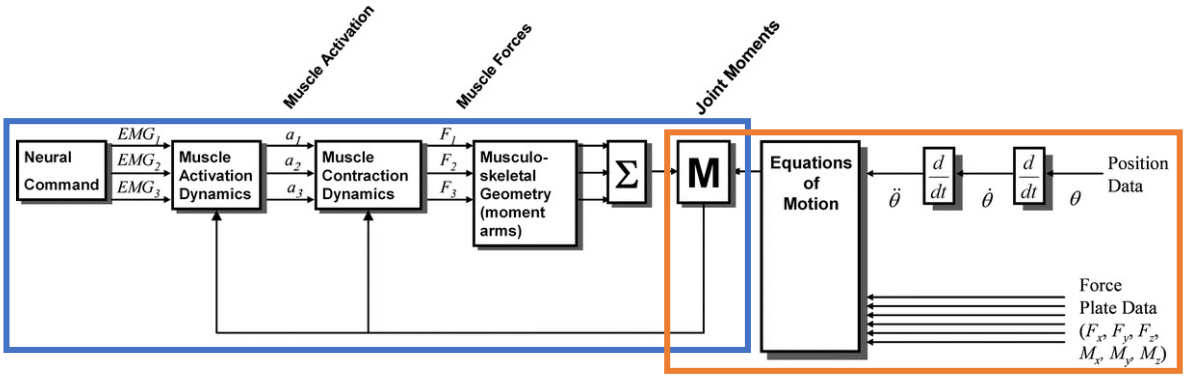

Figure 14. Approaches to estimating joint moments. Beginning at the left (blue), the forward dynamics approach starts with the neural command and then uses muscle activation dynamics, muscle contraction dynamics, and musculoskeletal geometry to estimate the joint moments. These joint moments can also be estimated using inverse dynamics (right side orange) (adapted from [79]).

For giving assistance with a lower limb exoskeleton, it is important to get knowledge of the human body internal properties and motor capacities so that the HMI and the wearable robot controller can produce the desired motions.

For the estimation of joint torques for an exoskeleton, the current standard is based on inverse dynamics, which computes torques using joint positions and GRF, however, it suffers from a list of drawbacks, which will be discussed later [80]. Another solution to compute joint torque would be to use machine learning but this approach suffers from extrapolation issues outside of the training data [81]. Nevertheless, owing to these limitations, EMG-driven modelling has been presented as a feasible FD solution for computing joint torque as it offers full portability since only EMG and joint position are needed, and offers accurate joint torque computation [82].

3.1.1. Inverse Dynamics

In inverse dynamics (Figure 14. right side), the torque's prediction begins by measuring position and the external forces acting on the body. For example, in gait analysis, the position of tracking targets attached to the subjects' limbs are recorded using a marker-camera-based video system and the external forces are recorded using a force platform. The tracking targets on adjacent limb segments are used to calculate the relative position and orientation of the segments, and from those, joint angles are then calculated, and these data are differentiated to obtain velocities and accelerations. The accelerations and the information about other forces exerted on the body (e.g., the recordings from a force plate) can be input to the equations of motion to compute the corresponding

joint reaction forces and moments. If the musculoskeletal geometry is included, muscle forces could then, in theory, be estimated from the joint moments.

Musculoskeletal models based on ID and inverse kinematics (IK) are currently operated offline in multibody software packages such as OpenSim [80] or AnyBody [83], where generic and openly available models can be scaled according to subject-specific anthropometric data. Recent studies proposed online solutions, facilitating translation to clinical scenarios [84]. However, this approach presents limitations if used to study muscle contributions to specific daily tasks [79].

One of the main issues of this method is that a force plate is needed to record GRF, which is not practicable when using a wearable robot. This is mostly due to the size of the force plates (only one step for each force plate) and their non-portability. Another issue is that the user must be able to produce enough force to create movements that can be detected by ID, which can be challenging for some patients [81].

3.1.2. Electromyography as a Neural Interface for Forward Dynamics

EMG is a technique to record the electrical signal of the muscles, allowing the indirect measure of their excitations. Therefore, measured EMG can be used as input of a forward dynamics model (Figure 14. left side), to emulate human movement mechanics while accounting for differences in muscle recruitment strategy between different users. These signals represent the summation of all MUAP and can be recorded using surface electrodes placed directly on the skin or via intramuscular electrodes using needles electrodes introduced in the muscle [85].

Surface electrodes are currently the most popular form of recording EMG owing to the fact that other methods such as needle electrodes are invasive and not comfortable to use [86]. In order to apply the recorded EMG signals in NMS modelling, it is usual to make use of its envelopes, being therefore important to use some signal processing, such as high pass filtering, normalization, low pass filtering, and normalization against maximal voluntary contraction [6]. However, besides its benefits, surface EMG measurements present some limitations, namely cross-talk, movement artefacts, the inability to access deep muscles and the weak association between EMG amplitude and motor unit action potentials [87].

Additionally, a NMS model can also be directly driven by MUAP from non-invasive high density (HD) EMG recordings [88], which uses multiple electrodes in a matrix configuration to record EMG on the whole muscle and access high-dimensional data-streams of muscle fibres' electrical activity [89]. The HD-EMG signal can be then manipulated and decomposed to extract the discharges of excitation of the innervating spinal motor neurons, thus establish a connection between the muscle model and spinal motor neurons [90,91].

3.1.3. Neuromusculoskeletal Modelling

To date, locomotion modelling studies have been performed to investigate the adaptation mechanism through sensory-motor integration in the spinal cord by integrating models at the skeletal, muscle, and neural levels [43,91–93]. The knowledge of the force developed by muscles during dynamic activity could be of primary interest for adapting the assistive torque applied by an exoskeleton online. Experimental muscle force measurements are extremely difficult and constraining since the gold-standard method relies on surgical procedures to implement internal sensors [108]. Due to the very slight possibility of in vivo measurements, muscle force estimation remains a major challenge for clinical practice. In order to implement a computational model describing muscle behaviour, the dynamics of muscle tissue play a vital role in the acquisition of physiologically valid muscle force values, and therefore in the construction of such model. Spatially, to simulate the active behaviour of muscles in body motion, an explicit model of the contractile structures must be implemented to estimate the muscle forces, thus relating muscle activation values $a(t)$ with muscle force F^{mt} [68].

First of all, the EMG signals must be converted into neural activation, *a(t)*, for each MTU. This can be done using a 2nd order twitch model (Eq. 3.1) and a nonlinear transfer function (Eq. 3.2):

$$u_j(t) = \alpha \cdot e_j(t-d) - \beta_1 \cdot u_j(t-1) - \beta_2 \cdot u_j(t-2) \quad \text{(Eq. 3.1)}$$

$$a_j(t) = \frac{e^{A \cdot u_j} - 1}{e^A - 1} \quad \text{(Eq. 3.2)}$$

where $u_j(t)$ is the postprocessed EMG, $e_j(t)$ the filtered EMG, α the filtered gain coefficient, β_1 and β_2 the recursive coefficients, d the electromechanical delay (EMD), A is the nonlinear shape factor, and j the muscle index [75].

The firsts mathematical models used in generic tissue modelling were based on passive elements (such as the Maxwell and the Kelvin-Voigt models), which are able to precisely mimic the behaviour of soft tissues under compressive and tensile loads [94]. However, due to the absence of an active element, these models are incapable of representing the dynamics of muscle contractile structures [68]. Archibald Hill [95] introduced an adaptation of the Kelvin model (Figure 15), including an additional contractile element, for which he received the 1922 Nobel prize in Physiology or Medicine.

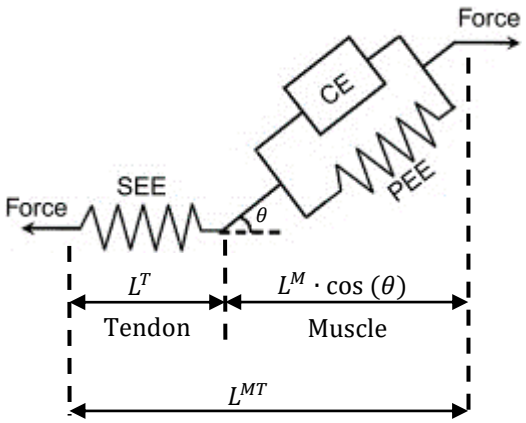

Figure 15. The most commonly used three-element Hill-type muscle model (adapted from [96]).

Hill-type muscle model

Due to this active characteristic Hill-type models are widely used in the biomechanics field to reproduce both contractile and passive behaviour of muscle tissue, since these have accessible parameters and they are computationally tractable for systems with several muscles [44,75,96]. The model is comprised of a contractile element (CE), parallel elastic element (PEE) and a series elastic element (SEE). CE is the contractile element of muscle representing the interaction between actins and myosins and is responsible for active force generation. On the other hand, SEE is the series elastic element of muscle representing the elasticity of the myofilaments, tendon, and aponeuroses. Finally, PEE is the parallel elastic element of muscle representing the connective tissue surrounding the muscle fibres. α is the pennation angle which is defined as the angle between the direction of muscle fibres and the line of action of the muscle force [96].

The MTU's force can be approximated by (Eq. 3.3):

$$F^{MTU}(t) = F^T = F^{Max} \cdot \left[f(L^M) \cdot f(V^M) \cdot a(t) + f_p(L^M)\right] \cdot \cos\left(\theta(L^M)\right) \quad \text{(Eq. 3.3)}$$

where F^{MTU} is the MTU force at instant t, F^T the tendon force (SEE), F^{Max} the maximum isometric force, $f(L^M)$ the active force-length relationship (see Figure 16), $f(V^M)$ the force-velocity relationship,

$a(t)$ the normalized muscle activation from equation 3.2. These last three values represent the contractile elements (CE). Finally, $f_p(L^M)$ is the passive force-length relationship (PEE) (see Figure 16) and $\theta(L^M)$ the pennation angle.

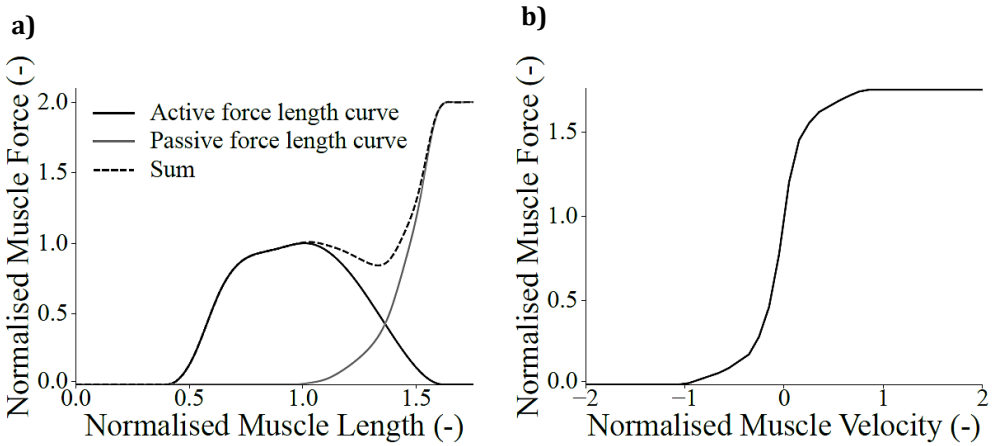

Figure 16. Normalized force relationships: a) Active, $f(L^M)$, and passive, $f_p(L^M)$, normalized muscle fibre force-length relationships; b) Normalized muscle fibre force-velocity relationship, $f(V^M)$ (image from [97]).

From Muscle Force to Joint Torque

Musculoskeletal modelling and simulation require accurate estimations of musculotendon kinematics, including musculotendon length (L^{mt}) and three-dimensional moment arms (r) to accurately predict musculotendon forces (F^{mt}) and joint moments [9].

Once all muscles' force acting on the joint of interest have been computed, these forces have to be projected on the joint using the moment arm. This parameter is often computed numerically through the "tendon excursion method" [98] using equation 3.4:

$$r_\theta = \frac{dl}{d\theta} \quad \text{(Eq. 3.4)}$$

where r_θ is the MA, dl the MTU length displacement and $d\theta$ the joint's displacement.

Therefore, the joints' torque can be computed through the following summatory (Eq. 3.5):

$$\tau = \sum_m r_{\theta,m} \cdot F_m^{MTU} \quad \text{(Eq. 3.5)}$$

where τ is the joint torque, $r_{\theta,m}$ the MA for the muscle m and F_m^{MTU} the force of that same muscle.

3.2. Human-Machine Interface for Real-Time Exoskeleton Control

Regarding the previously stated paradigm, as an alternative to current research on HMI, a new class of methodologies can be explored for developing new HMIs that can effectively assist impaired subjects in motor tasks in real-time. As a new approach, NMS modelling allows the biomechanical model to estimate the user's intention through EMG, i.e., surrogate of neural drive to muscles.

This method is based on EMG-driven modelling, where the human body's kinematics and dynamics can be represented by mathematical relations, thus allowing the computation of a large set of biomechanical outputs such as joint torques [99], muscle forces [100], joint contact forces [101], and joint stiffnesses [102] with a better set of sensors than classic methods such as ID. This large set of mechanical outputs is fundamental for a better understanding of the wearable's impact on the wearer, thus offering better control. It also offers the advantage to be personalized [103] through calibration

and scaling, which is of first importance for patients with multiple and different impairments and motor deficits. Moreover, this method is not bound to any task and does not need any further algorithm to switch between states to adapt to other tasks, as it was the main limitation of other pre-computed torque and position patterns. Finally, this HMI solution can easily be adapted to other exoskeletons or body parts as only the substitution of the model to a new one is needed.

3.2.1. Group Advances on Developing an EMG-Driven Human-Machine Interface

To benefit from both EMG-driven model's ability to account for differences in an individual's muscle recruitment strategy and ID-based method's ability to account for the right joint moments, Sartori *et al.* [43,100] developed a hybrid NMS model, combining EMG-driven modelling with static optimization methods. The model measured EMG to track experimental joint moments. Its static optimization component made possible that experimental joint torques were tracked, EMG measurements were minimally adjusted, and squared excitations were low. However, this model was too elaborated, requiring a lot of computational time, which made it unmatchable with the real-time assistance requirements.

With this limitation in mind, Durandau *et al.* [6,10,75,78,97,104] adapted the offline EMG-driven model from Sartori *et al.* to work in real-time by changing the OpenSim IK algorithm to a multithreaded algorithm and simultaneously running multiple IK computations on different threads. The model, represented in Figure 17, which will be fully discussed further, also used B-spline functions per MTU for faster and efficient estimation of the muscle-tendon length and MA using nominal length values generated via OpenSim, and a cubic B-spline algorithm [9], respectively. These advances could bring EMG-driven modelling close to real-time performance, i.e. computation time below the EMD (≅ 50 ms) and were capable of torque extrapolation and prediction.

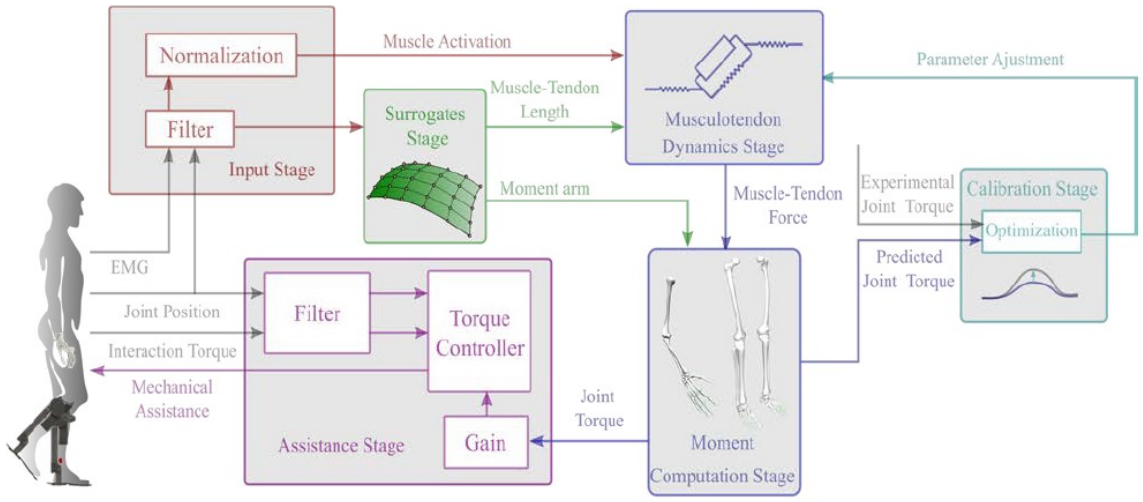

Figure 17. Schematic representation of the HMI developed by Durandau *et al.* (image from [6]).

Given some limitations concerning the EMG acquiring system, Aalten *et al.* [87] optimized the models of Sartori *et al.* and Durandau *et al.* to better work in real-time on a hybrid model combining ID and FD. The adjusted algorithms overcame some torque errors in the open-loop EMG-based NMS modelling due to the intrinsic limitations of the EMG measurements (such as cross-talk, movement artefacts and the weak association between EMG amplitude and MUAP) and some other imperfections.

3.3. Key-problematic and Key-directions

The current neurorehabilitation strategy for stroke and SCI patients is focused on the intensive repetition of movements and exercises. This approach is based on the rationale that intensive

task repetition mediates learning and neural plasticity through a process of sensory motor integration [105]. Besides the system developed by the research group, there is no other referenced WRO on the market, either in the rehabilitation domain, such as Lokomat®, or in the assistive one, such as Rewalk™, that operates as a function of a patient's residual muscle force-generating capacity. Therefore, these recent studies from the group may underpin a central element hampering the ability of current robotic exoskeletons to impact neurorehabilitation in these patients.

This rehabilitation processes can effectively benefit from the assistance of an exoskeleton, mainly in the early stages, because it is capable of sharing the effort of the intensive training with the patient by providing an external assistive joint torque [75]. However, the main problematic relies on this reality, i.e., exoskeletons only give motor assistance through the application of joint moments, not taking into account the changes and the rehabilitation of each separate muscle. Due to that fact, when an external torque is applied to a joint, it seems logical that the assistance will be intrinsically distributed to all muscles acting on it. However, this torque might not be the optimal condition for the rehabilitation of a specific muscle that might have been perturbated due to stroke or SCI. Moreover, compounding the challenge, physiological and neurological differences between individuals can cause divergent responses to the same device, and responses can change considerably during adaptation. Taking into account this paradigm, the group's EMG-driven model strategy still operates on a joint level and does not focus the given assistance on a muscular level. Additionally, the model operates in open-loop, not adapting its behaviour during the assistance and ignoring any changing patterns of the subjects' body along all rehabilitation phases.

Methods for automatically discovering, customizing, and continuously adapting assistance could overcome the stated challenges, allowing robotic exoskeletons to achieve their true potential. Assistance strategies designed to keep the human "in-the-loop" can therefore be used as inspiration. Models from [7,8,45,46] intended to optimize the human-exoskeleton performance by measuring metabolic variables with a respiratory system. Their main goal was to dynamically adjust the controlling laws during the use of an exoskeleton so it would minimize the subject effort and, consequently, its metabolic costs. These methods have the capacity to adjust the exoskeleton's behaviour online in response to measured changes in human coordination patterns, which allow the human and device to co-adapt and potentially result in an improved human-robot interaction and better rehabilitation.

In this sense, applying NMS modelling with a human-in-the-loop-inspired optimization approach could give a better understanding of the NMS mechanics involved in the human body, enabling clinicians to discover which muscle or group of muscles have been causing abnormal gait patterns, helping to optimize the specific assistance level and, consequently, to improve the outcomes of a muscle-specific treatment.

Chapter 4. Muscle-in-the-loop Optimization

This fourth chapter intends to address the approach and methodologies that were held concerning the stated key-problematic. Firstly, the study strategy and directions will be explored, followed by the model's pipeline. Finally, the software used and the implemented algorithm will be described.

4.1. Study Strategy

With the described key-problematic in mind, it is aimed to optimize and enhance the group's EMG-driven HMI in order to truly make a connection between each individual neural drive and the robotic exoskeleton so it can give effective muscle-specific neurorehabilitation. Specifically, we expect to be able to target a specific muscle, implement a dynamic optimization algorithm to compute and adjust the Support Ratio (SR) of each muscle online, and, consequently, predict the assistive torque to give an effective muscular rehabilitation.

4.1.1. Joint, Muscle Set, and DOFs

During the present work, we will focus on the ankle joint and consider the movement of the foot on the sagittal plane, i.e., the one-DOF dorsi-plantarflexion movement. The most important muscular groups acting on the ankle joint are detailed in Table 1. In this sense, we will observe mainly on the *triceps surae* and the *tibialis anterior* (TA), responsible for the dorsi-plantarflexion movement.

The *triceps surae* consists of the *soleus* (SOL), *gastrocnemius medialis* (GM) and *gastrocnemius lateralis* (GL). Since GM and GL share the same two main functions, plantarflexion, and knee flexion, and both insert into the Achilles tendon, they are very often regarded as the same muscle (*gastrocnemius*) such that they are named the "twin muscles". However, there is some indirect evidence that GM and GL may produce different ankle torques [106]. SOL is also responsible for plantar-flexion of the foot and stabilizes the leg on the ankle during standing position, contributing to balance maintenance. On the other hand, TA dorsiflexes and inverts the foot, contributes to balance on resisting backward tipping of the body, as well as it also helps to support the medial longitudinal arch of the foot [65].

4.1.2. Muscle Level Optimization and Rehabilitation Strategy

When enrolling an external ankle joint torque, the exoskeleton will intrinsically be acting on all muscles that contribute to that joint movement. By optimizing the assistive torque considering the changes that occur in a specific muscle, we may be able to induce a positive modulation of the neuromuscular activity of that muscle. Ideally, the exoskeleton behaviour will adapt to the changing pattern of the targeted muscle's activity over time and supplant part of its role in a certain motor task while having a minimum impact on the other muscles' activity.

In the present work, we will be adapting the EMG-driven model described in Figure 17 in order to optimize the assistive torque, computed according to (Eq. 4.2), applied by the exoskeleton online depending on the muscles' activity. Specifically, the optimization algorithm intended to minimize the objective function that defines the SR of the four studied muscles (Eq. 4.1):

$$f(SR_{SOL}, SR_{GM}, SR_{GL}, SR_{TA}) = C_o \left|(1\text{-}\delta) \cdot \overline{EMG}_o^{(REF)} - \overline{EMG}_o^{(n)}\right| + C_s \sum_{no} \left(\left|\overline{EMG}_{no}^{(REF)} - \overline{EMG}_{no}^{(n)}\right|\right) \qquad \text{(Eq. 4.1)}$$

whose variables are described as followed:

- SR_{SOL}: Support Ratio of Soleus;
- SR_{GM}: Support Ratio of Gastrocnemius Medialis;
- SR_{GL}: Support Ratio of Gastrocnemius Lateralis;

- SR_{TA}: Support Ratio of Tibialis Anterior;
- no: Muscle index of the non-optimized muscles list;
- o: Optimized muscle (SOL, GM, GL, or TA);
- C_o: Muscle-specific contribution weight of the optimized muscle;
- C_s: Sum's Muscle-specific contribution weight for the non-optimized muscles;
- δ: Muscle-specific Target Reduction Factor;
- $\overline{EMG}^{(n)}$: Mean of the post-processed EMG signal of each muscle at the iteration n;
- $\overline{EMG}^{(REF)}$: Mean of the post-processed reference EMG signal of each muscle.

Considering that the optimized muscle is the SOL, the algorithm shall minimize two terms. Namely, the minimization of the absolute difference between the mean of the reference SOL's post-processed EMG, multiplied by a Muscle-specific Target Reduction Factor, and the mean of the SOL's post-processed EMG of the current iteration ensures that the muscle activity of SOL is reduced by a defined factor δ. On the other hand, the minimization of the sum of the absolute differences of the other muscles' EMG mean between the reference and the current iteration ensures that the optimization process has a minimum effect on their muscular effort.

For the optimization to take place in real-time, the model must update the SR of all the studied muscles each iteration so it can change the exoskeleton's control laws. However, this task may be highly challenging since obtaining a mathematical model of the $\overline{EMG}$ to compute the objective function for a certain set of SRs may require a large set of data and lengthy evaluation periods, which would be incompatible with real-time assistance and adjustment to the user's body dynamics. As a matter of fact, the human body can be compared to a "black-box", where it is impossible, or very difficult, to predict and modulate its internal processes and how it will react to a certain disturbance or the application of an external torque. In this sense, it is known that the applied SR is in a way related to the muscles' activity such that $\overline{EMG}(SR)$. However, this is an empirical relation that is not known *a priori*, *i.e.*, it is only possible to compute a set of $\overline{EMG}$s after a certain set of SRs had been applied in the control laws of the exoskeleton. Additionally, the human body has also time-varying dynamics that make optimization difficult, including slow components of adaptation and strong history dependence, reflecting complex neurocognitive factors [8]. Therefore, by closing the loop between the robotic exoskeleton's controller and the user, we must be able to measure the latter one's response to a certain given assistive torque and adjust the SR online to better correspond to the user's dynamics and our main optimization goal, as shown in Figure 18. For that, we will make use of the EMG signals from SOL, GM, GL, and TA, NMS variables derived from the EMG-driven model (Figure 17), and GRF, which will be used to analyse events of the gait cycle and control the updating loop period, *i.e.,* the loop will restart when a defined number of steps have been observed.

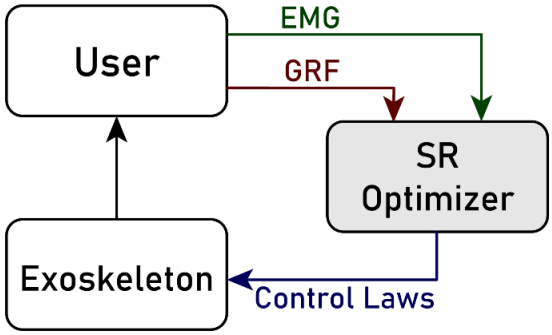

Figure 18. Closed loop between the robotic exoskeleton and the user

Nevertheless, the evolution strategy, *i.e.*, how the SRs set is updated over time in this study, is quite challenging to implement since optimization procedures based on measurements of human motor performance typically requires lengthy evaluation periods and contains substantial noise. Initial

efforts in this domain have evaluated the ability to optimize a single gait or device parameter using line search [7] or gradient descent [46], however, these methods were found to be inefficient, also being sensitive to drift and noise. Moreover, they still scale poorly, requiring many more evaluations for each parameter to be optimized.

Regarding these limitations, an evolutionary stochastic algorithm will be implemented to generate new candidates of SRs that will update the control laws of the next iteration. Starting from an initial set of SR candidates, the EMG signal of the four muscles will be then measured and processed during a whole gait cycle, or a defined number of gait cycles. After that, the EMG signals' mean will be computed, and the objective function evaluated so a decision concerning the SRs set can be made. The next set of SRs will then be defined and the exoskeleton controlling laws updated, restarting the loop represented in Figure 19.

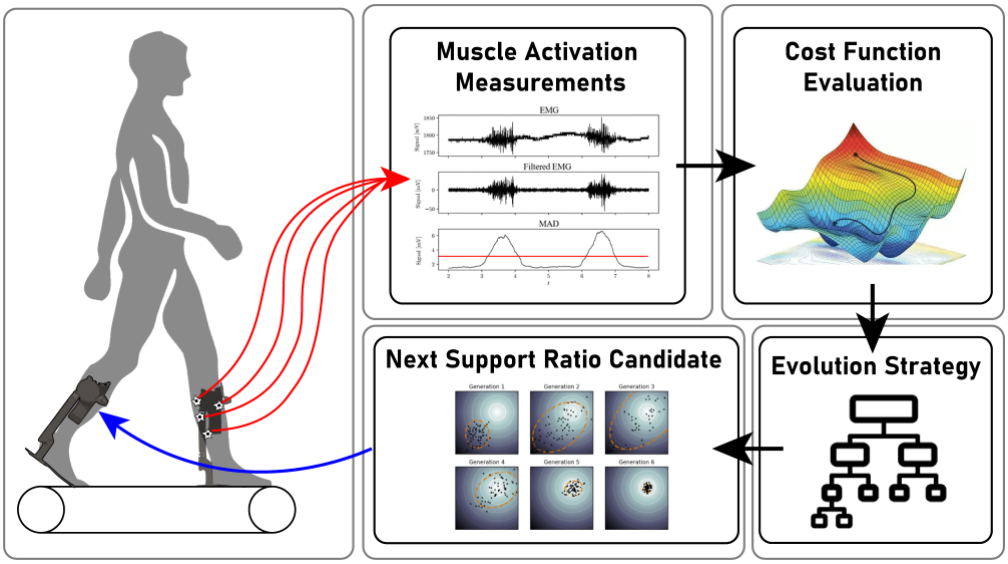

Figure 19. Muscle-in-the-loop strategy scheme

4.1.3. Online Optimization

Regarding the challenges stated before, a Covariance Matrix Adaptation Evolutionary Strategy (CMA-ES) [107] will be used for finding the optimal set of SR, which minimize (Eq. 4.1) while walking with assistance. CMA-ES is a stochastic algorithm that does not explicitly use derivative terms and is often used for non-linear, non-convex optimization problems. The method is well-suited for a human-in-the-loop optimization approach since it addresses noisy measurements, expensive objective function evaluations, objective functions with unknown structures, and complex, subject-dependent human learning and adaptation processes [107].

It was not the purpose of this study to exhaustively test different potential optimization algorithms, however, CMA-ES has been referenced as the most effective strategy for this type of stochastic and empirical-based study [8]. CMA-ES first evaluates a group of candidate parameter sets that form the population of one first generation. Candidate parameter sets are randomly selected according to a multivariate normal distribution of the parameters, characterized by a mean, a covariance matrix and a standard deviation. The mean of the distribution represents the current estimate of the optimal parameter values. After evaluating the current generation, the parameter sets are ranked in terms of performance/fitness and a rank-weighted average of the best sets becomes the mean of the next generation. The change in means is used to update the covariance matrix of the next generation, while additional multi-generational terms refine the covariance matrix and standard deviation to improve computational efficiency. This process is repeated from generation to generation as a natural selection-based algorithm. The mean of the final calculated generation is then provided as

the best estimate of the optimal parameter values. Herewith, an overview of the algorithm and rationale for its choice in this work is provided.

As already explained, optimizing EMG-driven assistance from human muscle activity measurements is quite challenging in multiple ways. First, human data is generally noisy, owing to complicated human physiological and biochemical processes. CMA-ES is stochastic, which makes it less sensitive to noise than derivative-based methods such as gradient descent or 'hill-climbing' methods. Another challenge is that the evaluation of candidate conditions is quite expensive in terms of time and human effort since the measurement and evaluation of the muscle activity requires some time for the subject to interact with the device and adapt to its assistance. Often, multivariate optimization methods require a large number of function evaluations per step, and this number increases with the dimensionality of the control parameter space. As a matter of fact, CMA-ES might only need a few evaluations per generation for converging [8].

A third challenge, as stated before, is that the nature of the relationship between the exoskeleton and the controlling parameters is not known in advance and may include complex nonlinearities and local minima. CMA-ES is stochastic and includes mechanisms to grow or shrink the standard deviation of the randomly selected parameter values depending on the evolution of the mean over time. These features make CMA-ES more robust against thresholds, discontinuities and local minima.

Lastly, humans exhibit complex, individualized learning and adaptation processes when using a WRO. This puts gradient-based and quadratic approximation methods at a disadvantage, since calculating the gradient or Hessian requires substantial time, during which the human is changing. The computed gradient or quadratic will therefore often be inaccurate, resulting in poor subsequent guesses at the optimal parameter values or requiring additional evaluations to recalculate the model of the space. CMA-ES is, therefore, less sensitive to these problems owing to it using only the rank order of the parameter sets, and not the objective function values or their partial derivatives.

4.2. Enhanced Human-Machine-Interface Pipeline

With the described strategy in mind, an additional logical box for the optimization stage will be added to an adapted pipeline of Durandau *et al.* (Figure 17), as shown in Figure 20.

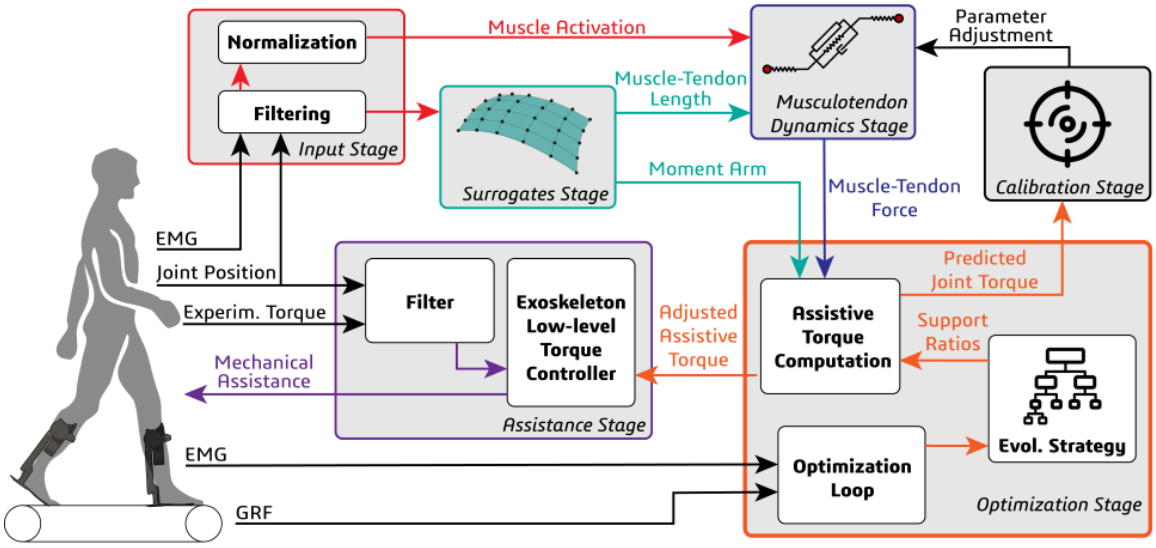

Figure 20. Schematic pipeline of the enhanced HMI, with the representation of the Optimization Stage

In this model, two different signals are recorded from the human body. EMG signals and joint positions are first delivered into an input stage (Figure 20, red box) where they are filtered to remove artefacts and noises. The EMGs are further processed by normalization against the maximum

voluntary contractions recorded offline. The filtered joint positions are then sent to a surrogates stage (Figure 20, green box), where muscle-tendon lengths and MAs of the muscles are computed using a cubic B-splines algorithm [9]. The obtained muscle activations after normalization of the EMGs and the muscle-tendon lengths are sent to a musculotendon dynamics stage (Figure 20, blue box) where muscle-tendon forces (MTF) are computed. This stage is based on the Hill-type muscle model and on previous works from Lloyd *et al*. [44] and Sartori *et al*. [100]. MTFs, MAs, EMG signals and GRF signals are then sent to the optimization stage (Figure 20, orange box) where joint torques are iteratively computed and adjusted for each step to better correspond to the optimal SR set. The computed joint torques are then sent to an assistance stage (Figure 20, purple box), where these are delivered to the user through the robotic exoskeleton's low-level torque controller.

The NMS model needs to be personalized to every specific user to obtain precise joint torque predictions. In this sense, an offline calibration stage is used (Figure 20, black box) to determine different muscle parameters such as maximal isometric force, tendon slack length, optimal fibre length, and EMG-to-activation shape factor. An optimization procedure is used to minimize the error between predicted joint torques (before muscle-in-the-loop optimization) and experimental joint torques by changing these parameters. This calibration stage only takes place on the first time the user operates the models.

4.3. Software and Libraries

The software used to implement the muscle-in-the-loop optimization and run the EMG-driven model to control the exoskeleton assistance in real-time is described below.

SimTK, SimBody and OpenSim

Simbios, the NIH Center for physics-based Simulation of Biological Structures at Stanford University, has developed an open-source biosimulation software called SimTK, which contains different programming tools. Simbody [108] is an open-source, object-oriented C++ Application Programming Interface (API) of SimTK, which allows performing simulations of multibody systems. Applications using Simbody have been implemented in areas of biomedical research, such as studying the motion of biomolecular machines built from amino and nucleic acid, pathological gait in musculoskeletal models of humans, design of biologically inspired robots and avatars.

An open-source multibody simulation environment called OpenSim has also been developed and maintained on SimTK by a growing group of participants to accelerate the development and sharing of simulation technology and to better integrate dynamic simulations into the field of movement science. OpenSim, therefore, allows users to develop, analyse, and visualize models of the musculoskeletal system, and to generate dynamic simulations of movement. In this software, a musculoskeletal model consists of rigid body segments connected by joints. Muscles span these joints and generate forces that, consequently, produce motion. Once a musculoskeletal model is created, OpenSim enables users to create custom studies, including investigating the effects of musculoskeletal geometry, joint kinematics, and muscle-tendon properties on the forces and joint moments the muscles can produce [80]. During the development of the present work, OpenSim 3.3 was used to implement the plugin, being the developed software updated later to work on OpenSim 4.1.

CEINMS offline and CEINMS-RT

The Calibrated EMG-Informed Neuromusculoskeletal Modelling Toolbox (CEINMS) is an OpenSim toolbox to explore the effect of different neural control solution algorithms using consistent musculoskeletal geometry. It allows the estimation of the human lower extremity muscle and joint dynamics by implementing all the transformations that take place from the onset of muscle excitation to the generation of muscle forces and resulting joint moments [109].

CEINMS can also be applied to state-of-art neurorehabilitation technologies using wearable robots and EMG-driven HMIs. The very first step into this purpose relies on using additional software resources to make use of CEINMS in real-time (CEINMS-RT), mainly by using MTU Splines for faster

computation of L^{mt} and MA, OpenSim biomechanical models and real-time IK and ID that could be applied to those models. Additionally, modules that enable TCP/IP direct connections should also be implemented for communicating with external devices, such as motion capture cameras, EMG amplifiers, and actuators' low-level controllers, so that the data is transmitted with a minimum delay [10].

Data can be measured in real-time or read from a file. The former method is used, understandably, when doing experiments with subjects. Data are measured and processed by CEINMS-RT's plugins and are immediately sent to the NMS model. The latter method can be used to test the real-time model without the need of having an experiment each time the data and the HMI is tested. Data can be recorded when doing an experiment and saved into a file. When running the software, the saved data can then be read from the file frame by frame as if the actual measurements were being done in real-time.

Pagmo 2.17.0

Pagmo [110] is a C++ scientific library for parallel optimization. It is built around the idea of providing a unified interface to optimization algorithms and problems, and to make their deployment in massively parallel environments easy. This library can be used to solve constrained, unconstrained, single objective, multiple objective, continuous and integer optimization problems, stochastic and deterministic problems, as well as to perform research on novel algorithms and paradigms and easily compare them to state-of-the-art implementations of established ones.

To use pagmo, at least three classes are needed, an optimization problem, an algorithm, and a population. In order to define an optimization problem in pagmo, the user must first define a class (or a struct) whose methods describe the properties of the problem and allow to compute the objective function, the constraints, beyond others. In pagmo, such class is referred to as a user-defined problem (UDP). Once defined and instantiated, a UDP can then be used to construct an instance of this class, *pagmo::problem*, which provides a generic interface to optimization problems. On the other hand, the Algorithm class offers a common interface to all types of algorithms, such as CMA-ES, or Corana's Simulated Annealing (SA), that can be applied to find a solution to a generic mathematical programming problem as represented by the *pagmo::problem* class. Finally, the Population class represents a population of individuals, *i.e.*, potential candidate solutions to a given problem. In pagmo an individual is determined by a unique ID, used to track it across generations and migrations, a chromosome (a decision vector itself), and the fitness of the chromosome as evaluated by a *pagmo::problem*. A special mechanism is implemented to track the best individual that has ever been part of the population. Such an individual is called the champion and its decision vector and fitness vector are always automatically kept updated.

4.4. Muscle-specific Support Ratio Optimization Plugin

The online muscle-in-the-loop optimization plugin (Figure 21) was written in ANSI C++ as an extension of the EMG-driven model ran in CEINMS-RT. This model consists of one core class with an NMS model containing its properties and data. The NMS model's properties include subject-specific parameters such as muscle's optimal fibre length, tendon slack length, maximum isometric force, beyond others, that are set during initialization. The NMS model's data is received and set in real-time from different plugins and methods during the execution of CEINMS-RT, as previously described. The optimization plugin then receives the post-processed EMGs, MTFs and MAs from CEINMS-RT and GRF directly from the force plate of the treadmill and performs the real-time computation of the assistive torque, while iteratively adjusting the SR so it finds the optimal set. The implemented methods will be fully detailed and described below. The code implementation of the plugin can be found in Supplementary Content 5. The developed software had been subjected to a BSD license, which will allow the open-source development, imposing minimal restrictions on its use and distribution, along with the public release of CEINMS-RT.

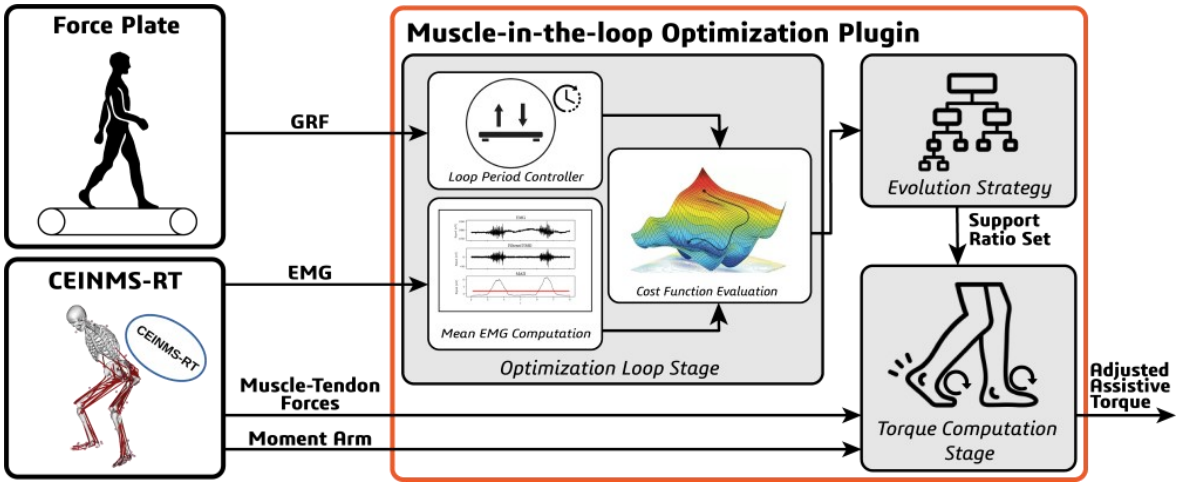

Figure 21. Schematic of the Muscle-specific Support Ratio Optimization Plugin

4.4.1. Parameters Definition and Passing

For the execution of the plugin, it is important to externally input and define some parameters and variables into the plugin, such as which muscles and DOFs will be considered, which muscles will be optimized, the parameters for the objective function C_{SOL}, C_S, and δ, the parameters for the algorithm used for the optimization, the number of gait cycles for the evaluation of each SR candidate during optimization and for getting the reference EMG, and, finally, the optimization criteria stating if the optimization will consider whether the EMG or the MTF to minimize.

To define and pass these parameters into the plugin and the model, an Extensible Markup Language (XML) file was created. Moreover, an XML Schema Definition (XSD) file was also inserted into the software to describe how the XML elements should be read and defined in the program. By running a command to build a tree and root the elements, an *.hxx* and a *.cxx* files are automatically generated from the XSD file, which defines how to get the parameters from the XML file. To facilitate the definition of the variables into the plugin, an XML Reader class was therefore implemented. This class has a variety of functions that get the elements from the XML file as described in the *.hxx* and a *.cxx* files and, when called by the plugin, return the requested variable.

Many muscles are biarticular, *i.e.,* are connected and apply muscle forces in two different joints. The biarticularity of these muscles increases the complexity of NMS modelling, thus increasing computation time. In this matter, the set of DOFs shall be reduced to the only ones the required or the purpose of this study by specifying them on the *DOFsOptimized* element of the XML file.

4.4.2. Initialization

During the start-up of CEINMS-RT, the muscle-in-the-loop optimization plugin is called and initialized. During this initialization, in the *init()* method, the NMS model core class is set up by reading the muscles list, DOFs and calibration parameters from a configuration file. Then, the variables and parameters previously defined in the XML file are loaded into the plugin to state the optimization criterion, weighting parameters of the objective function, and the muscles and DOFs lists used in the plugin. After that, the indexes of the muscles stated in the configuration file and that will be used are saved into vectors so that the order of the vectors regarding the muscles' information maintain the same order. Then, the baseline of the SR vector is created concerning the muscles-to-optimize's position in the vector, and the boundaries vectors for the optimization algorithm are initialized. Finally, some important parameters are set into the UDPs of the right and left legs, namely, the objective function's parameters, the muscles indexes on vector, the SR boundaries, a SRandEmg object's pointer, and a condition variable's pointer, which will be fully described below. As of last, the loggers are initialized, so the output of the variables such as used DOFs, time, step number, EMG mean,

SR, and the correspondent fitness are written into specific files, and the communication client is created to obtain the GRF (or gait cycle percentage) and to send the computed torque to the WRO.

In order to execute the plugin within the EMD, *i.e.*, the delay time compatible with real-time assistance, the torque computation and optimization processes for each leg take place in three different threads: the torque, optimization, and algorithm threads, as schematized in Figure 22.

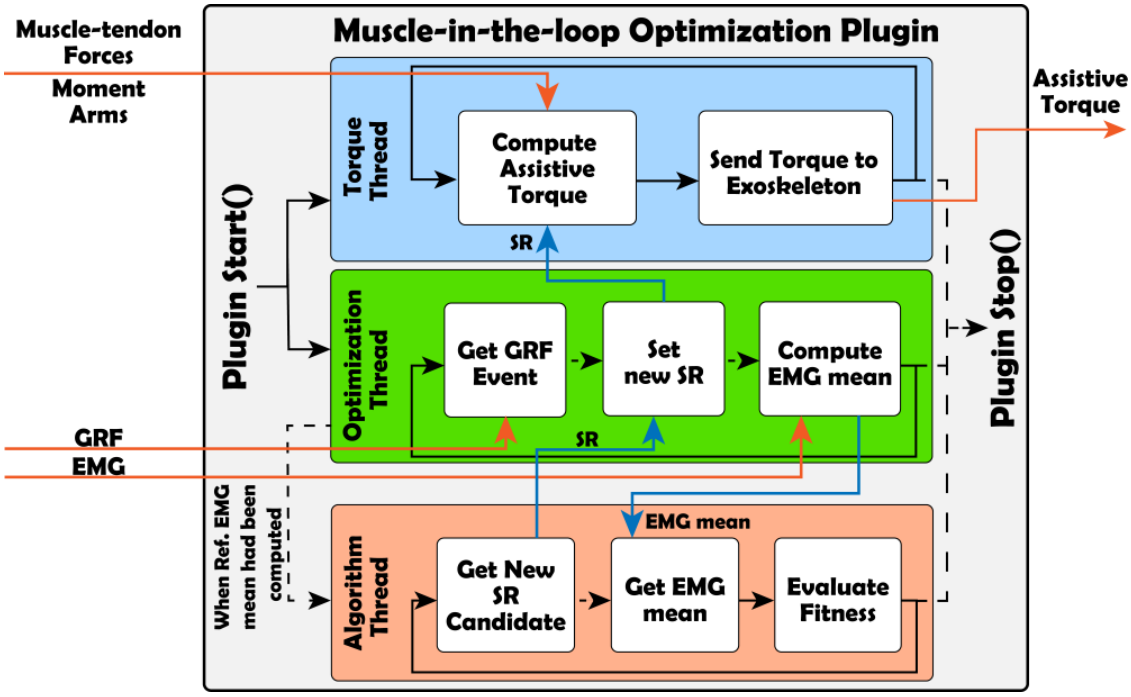

Figure 22. Schematic of the Plugin's Threads and Processes. A solid line pointer means that it is a direct process, whereas a dashed one means that the process has to wait until it gets the data it needs or that the process needs a trigger to occur.

After initialization, the plugin is effectively started by the method *start()*, where the two worker threads are created and started. The algorithm thread is also created in *start()*, but stays on hold until the EMG reference is computed by the optimization thread, which then triggers the algorithm thread to start. The torque thread receives MTFs and MAs from CEINMS-RT and the SRs from the optimization thread and is responsible for computing the assistive torque and sending it online to the exoskeleton. On the other hand, the optimization thread receives the gait cycle percentage obtained from the GRFs values of the force plate and post-processed EMG signals from CEINMS-RT and iteratively adjusts the SR for each muscle in order to test and find the optimal solution. Finally, when the algorithm thread starts its execution, it is responsible to run the optimization algorithm, iteratively getting new candidates of SR, and, when the respectively EMG mean had been computed, evaluate the fitness, *i.e.*, the objective function value of that SR.

In a general view, these three threads run on the scope of two main conceptual loops, which have different roles. The model loop incorporates the execution of the torque thread whereas the optimization loop incorporates both optimization and algorithm threads, which operate in co-dependency, *i.e.*, both need the other's processed data to continue its role. A full explanation concerning these two loops is given below.

4.4.3. Model Loop

The model loop is run in real-time and continuously in the torque thread. During each cycle, as stated before, the plugin receives MTF and MA of each muscle from CEINMS-RT and the updated SR set from the optimization loop. After validating that the received data is new data, the MTF of each muscle is then multiplied by the respective SR and set into the NMS model as updated-like MTFs, as well as the

received MA. The model subsequently computes the assistive torque for each leg online and according to (Eq. 4.2), which is an adaptation of (Eq. 3.5):

$$\tau = \sum_{m} SR_m \cdot r_{\theta,m} \cdot F_m^{MTU} \qquad \text{(Eq. 4.2)}$$

where SR_m is the SR defined by the optimization algorithm for the muscle m.

After getting the updated assistive torque from the NMS model, it is then sent to the exoskeleton's low-level controller using an Ethernet for Control Automation Technology (EtherCAT) communication protocol. For that, a TwinCAT 3 (Beckhoff Automation GmbH & Co. KG, Germany) library was linked to the project and a new client was initialized and used on loop to send the computed assistive torque in hard real-time using the Automation Device Specification (ADS) protocol.

4.4.4. Optimization Loop

The ideologic optimization loop (Figure 23) is run also continuously and in real-time within the optimization and the algorithm co-dependent threads. During a certain number of first steps, whose value was previously defined in the XML file, the algorithm thread is on hold while the optimization thread is running in loop executing the necessary commands to compute the reference $\overline{EMG}$ while the exoskeleton is on minimal impedance mode, *i.e.*, while the SR is null and, consequently, the exoskeleton gives no assistance. Firstly, a condition to validate if there is new EMG (or MTF, if that was the optimization criterion chosen on the XML file) data delivered by CEINMS-RT occurs and, in case of a positive result, the new EMG (or MTF) data is appended to a vector whose final population refers to the EMG data of a whole gait cycle. Then, a new conditional method takes place to verify if a step was observed, *i.e.*, when a periodic gait cycle had been concluded. In case of a step event, the $\overline{EMG}$ of each muscle is computed and added to another vector whose final population is the $\overline{EMG}$ set of the first defined number of steps. When the whole first set of $\overline{EMG}$ have been computed and added to the vector, the reference EMG, $\overline{EMG}^{(REF)}$, and its standard deviation for each muscle are computed from that vector. This procedure allows, further than getting the reference EMG for the objective function, to inform about the variability of the EMG without any assistance, such that it can be admitted afterwards when validating the muscle-in-the-loop optimization. After that moment, the algorithm thread becomes active and the actual optimization process begins.

As referred before, Pagmo 2 was linked and used for the implementation of the optimization, which would search for the optimal controlling laws. Therewith, a UDP class was created and added to the software in order to declare and define the optimization problem, *i.e.*, the objective function, the boundaries, and the methods to acquire the decision vector, in this case, the $\overline{EMG}$ corresponding to the applied SR. In this sense, on the algorithm thread, a *pagmo::problem* object is created from the UDP and the *pagmo::algorithm* is instantiated. In the implemented model two algorithms, beyond others that were not tested, can be used, being these the Corana's Simulated Annealing [111] and CMA-ES [107]. The former one is reliable in finding the global optimum (as opposed to a local optimum) because of its ability to make uphill moves, however, it is a costly algorithm and not as suitable for stochastic optimization since it evaluates each candidate separately. On the other hand, CMA-ES is a population-based algorithm where the mean of each new generation represents the best estimate of the optimal control parameter values, and the shape and size of the distribution are chosen to increase the likelihood of further improvement in subsequent generations. Therefore, after the stopping criteria had been reached, *i.e.*, after a defined number of generations had been evaluated, the mean of the final one is admitted to be the optimized set of SR. This optimization strategy is relatively tolerant to both measurement noise and human adaptation because neither the objective function values nor their derivatives are used directly, and each generation is evaluated independently [8,87].

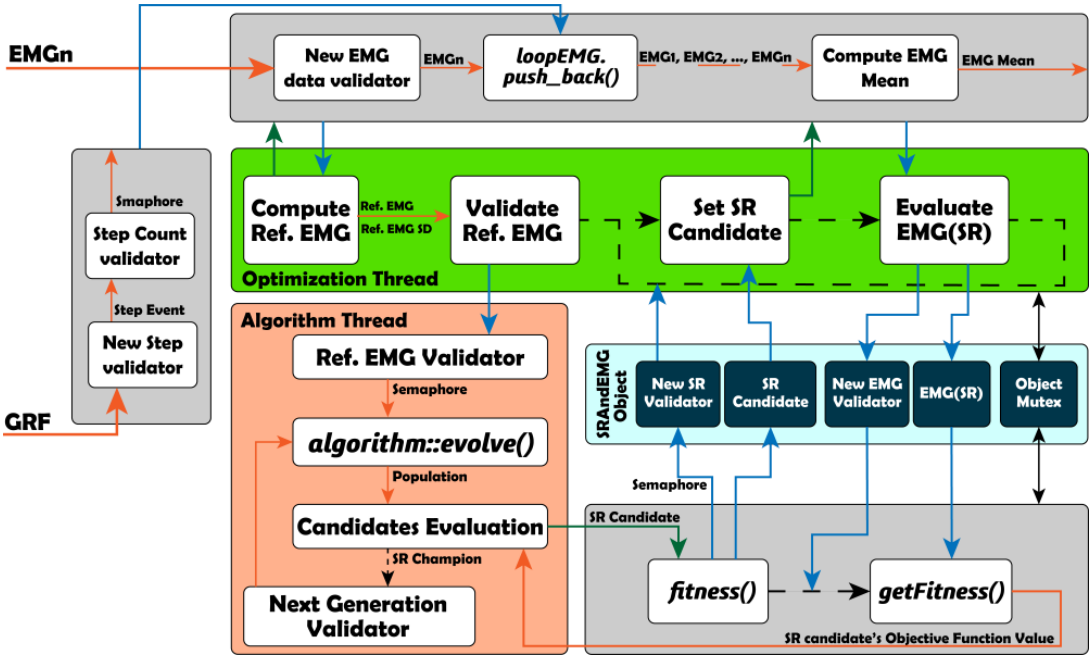

Figure 23. Schematic of the Optimization Loop. A solid orange pointer means that it is a direct process, whereas a dashed black means that the process has to wait until it gets is triggered. Blue pointers mean the reading of a variable and the green ones the calling of a method or function.

After instantiating the algorithm, a population is then generated and the *algorithm::evolve()* is called over it, which will randomly assign new SR candidates within the boundaries previously defined in the UDP for the first generation of candidates. For the evaluation of each SR candidate, the algorithm will intrinsically call the UDP's *fitness()* method in order to obtain its fitness, *i.e.*, it's correspondent objective function value. Since the decision vector, $\overline{EMG}$, which correspond to the applied SR, such that $\overline{EMG}(SR)$, is not known *a priori*, we first apply the SR candidate, given by the algorithm itself as argument of the UDP's *fitness()*, to the controlling laws of the exoskeleton, make the method wait until the user reacts to the change in assistance and the $\overline{EMG}$ is computed by the optimization thread and, only then, compute the respective SR fitness. For that, a personalized *SrAndEmg* class was created so that the SR candidate and its corresponding $\overline{EMG}$ can be dynamically set, gotten, and therefore passed between the two co-dependent threads and classes by using the same *std::mutex* and C++ pointers to the object's variables and a *std::condition_variable*'s memory addresses. Besides the SR, the $\overline{EMG}$, and the public set and get methods and functions, this class also declares two *std::booleans* to state the presence of new data concerning the SR and $\overline{EMG}$, and two *std::mutex*, one for the object's variables, which is implemented on the public set and get methods, and the other for the object itself, so that the co-dependent threads cannot access the object mutually at the same time.

Regarding the described idea, after calling the *algorithm::evolve()* method, the optimization thread waits until the algorithm had through the first SR candidate and the algorithm thread had set it on the *SrAndEmg* object. When the optimization thread is notified that there is a new SR candidate available in the object and that the algorithm thread is now on pause waiting for the correspondent $\overline{EMG}$, it gets the SR from the object, updates it on the controlling laws of the exoskeleton, and execute the previously described commands for computing the respective $\overline{EMG}$. As soon as this process is concluded, the optimization thread sets the new $\overline{EMG}$ on the *SrAndEmg* object and notifies the algorithm thread that the new variable was made available. The algorithm thread then gets the new value from the object and proceed to the computation of the SR candidate's fitness, which is then returned to the algorithm itself, so a new SR candidate can be thrown, restarting the described cycle.

When the optimization had been concluded and an optimal SR set found, the last one is then set to the model and the algorithm thread is set on pause while the optimization thread is kept running for recording purposes only.

Chapter 5. Validation Experimental Studies

The present chapter presents and describes the experimental pilot studies for validating the developed optimization model. Specifically, the materials and methods implemented in the present work will be fully detailed, followed by the studies design and the obtained results and its discussion.

5.1. Materials and Methods

To assure voluntary and continuous torque control, exoskeleton commands are computed as a direct function of the estimated subject's biological torque. Therewith, the proposed HMI uses a person-specific neuromechanical model of the human leg to simulate in real-time all transformations that take place from the EMG onset to joint torque generation. This is a data-driven model-based, sensor-fusion procedure that effectively fuses a higher-dimensional multimodal set of wearable sensor signals, *i.e.*, 8 leg EMGs and 4 knee-ankle joint angular positions across both legs, into a set of 2-dimensional ankle plantar-dorsi flexion torque profiles. These biological torque estimates are subsequently subjected to an optimization procedure and then fed into a low-level controller based on a disturbance observer to effectively translate model-based optimized torque estimates into exoskeleton motor commands while following the voluntary motion of the user.

5.1.1. Model Personalization

A generic musculoskeletal geometry model is scaled linearly to each individual using the open-source software OpenSim, GRF, and 3D motion capture data of body landmarks (bony areas) recorded during a static standing pose. During this procedure, the muscle-tendon bone-wrapping and origin insertion points, as well as the centre of mass values and positions of the anatomical segments, are linearly adjusted to match a human body's anthropometry.

The human model used during this experiment contained the following joints: left and right plantar dorsiflexion and knee flexion-extension and the following 14 muscles tendon units: left and right SOL, TA, GM, GL, Peroneus Longus, Brevis and Tertius. The following tasks were used for the calibration of the model: static pose for 10 seconds, 60 seconds of treadmill walking at 1.8 km/h and 2.8 km/h, 10 calf rises and 10 front foot rises.

This scaled model was then used to create a multidimensional B-Spline function per MTU as described before for the computation of the subject's specific L^{mt} and MA. Four parameters were calibrated for each muscle in the model including: the EMG shape factor, the tendon slack length, the optimal fibre length, and the maximal isometric muscle force, MVC. This calibration is based on a two-step procedure [97]. First, a previously presented pre-tuning procedure is employed to identify initial values for the optimal fibre length and the tendon slack length. After these initial values had been found, all the four described muscle parameters are optimized to enable the subject-specific model to fuse recorded EMGs and joint angles into joint torque profiles over a range of locomotion trials. This is based on a SA procedure that minimizes the error between the estimated torque by the model and the experimental torque derived via inverse dynamics.

5.1.2. Robotic Exoskeleton

During the present study, the modules for the ankle right and left joints of the rigid Symbitron Wearable Exoskeleton 2 (WE2, Figure 24.)) [112], each one with a weight of around 5 kg, were used to assist plantar-dorsiflexion during locomotion tasks. Each of the exoskeleton's ankle modules presents two degrees of freedom, which consists of active plantar flexion and dorsiflexion, and passive inversion and eversion. The active degree of freedom is actuated with a rotary series elastic actuator (SEA), which transmits the desired interaction forces via a push-pull rod from its distal location to the ankle joint. The SEA consists of a motor (Tiger Motor U8-10(Pro), T-Motor, Nancheng, China) that is connected to a harmonic drive (LCSG20, Leader Drive, Jiangsu, China) with a gear ratio of 1:100. The

harmonic drive is connected to the output of the motor with a custom rotary spring with stiffness of 1534 Nm/rad. The actuator can deliver a controlled peak torque of 100 Nm and has a maximum output speed of 5 rad/s. The motor is controlled via an Everest Net drive (Ingenia, Barcelona, Spain), which communicates with the control computer via EtherCAT. The motor position is measured via a rotational encoder (16 b MHM, IC Haus, Bodenheim, Germany). Additionally, the actuator measures the spring deflection and joint position with two encoders (20 b Aksim, RLS (Renishaw), Kemnda, Slovenia) which are transmitted to the control computer via the Everest Net drive. The control computer, a NUC (Intel, Santa Clara, USA) that executes the controller in TwinCAT 3 (Beckhoff Automation, Verl, Germany) in real-time with a sampling frequency of 1 kHz, and is located in the exoskeleton's backpack, which weighs around 10 kg. Additionally, the backpack also contains two batteries, supplying the computer and actuators with power.

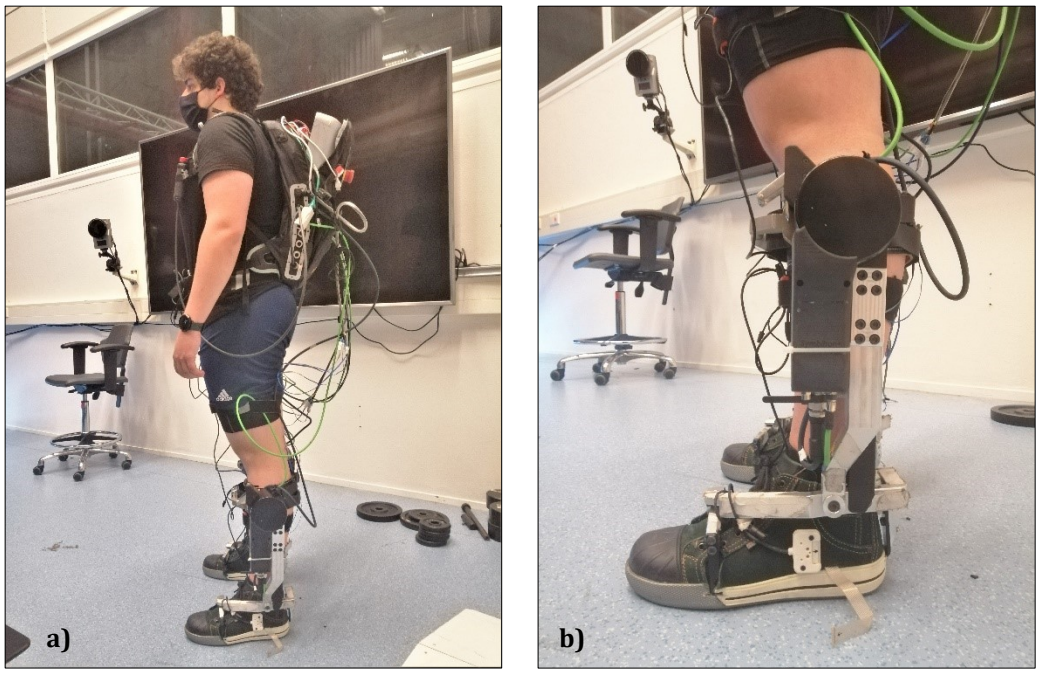

Figure 24. Symbitron Wearable Exoskeleton 2 with the ankle modules: a) Full body view; b) Ankle module view

5.1.3. Data Collection

During the experiments of the present work, some biological and kinematic data were collected, processed, and delivered to OpenSim, CEINMS-RT, and the optimization plugin in order to compute the assistive torque to be delivered to the subject by the exoskeleton.

Motion capture's 3D markers data were recorded using a motion camera system (Oqus, Qualisys, Sweden) and GRF were measured directly on the treadmill (M-Gait, MotekForce Link, The Netherlands) to personalize the model using the methods previously described. GRF were also used to predict the gait cycle percentage online, which allowed the control of the optimization loop. EMGs from right and left GM, GL, SOL, and TA were recorded from the subjects, amplified, and filtered directly by the surface electrodes using proprietary signal detection and an acquisition system (AxonMaster 13E500, Ottobock, Germany). Filtered EMGs were then normalized using pre-recorded maximal voluntary contractions (MVC) to compute muscle excitation. The tasks used for getting the MVC were static co-contraction as well as dynamic calf rise and toe rise. The muscle excitations were then used to drive a set of a virtual model's MTUs.

To measure the knee joint angle, an Inertial Measurement Units (IMU) suit was used (Link, Xsens, the Netherlands), the ankle joint angle was directly available from the joint encoder of the exoskeleton. The knee angles are required for the simulated Gastrocnemius muscles that span the ankle and knee joints. To update the kinematic state of the virtual muscle-tendon units, the muscle-

tendon length is computed from joint angles in real-time using a B-spline algorithm [9]. B-spline coefficients for each muscle-tendon unit are consequently computed using values from the muscle analysis tool of OpenSim where the full range of motion of each joint is sparsely explored. The MA is obtained via the partial derivative relative to joint angles using the same B-spline algorithm, which will be then updated in the optimization plugin.

During the experiments, the following processed data was recorded into file so it would be made available for future analysis: time, step number, EMG, SR, muscle activation, MTF, MA, L^{mt}, beyond others.

5.2. Experimental Design and Procedures

The experimental pilot studies were conducted as the first approach to validate and evaluate the effectiveness of the developed optimization scheme and its parameters by looking into the EMG, torque, and muscle forces profiles along with the exoskeleton's assistance. A single naïve participant (male, 23 years old, with no instance of musculoskeletal injury or motor-control impairment, shoe size of 44, body mass of 88 kg, 182 cm height) performed all the experimental tests, which took place on different days.

During the experimental tasks, the EMG-driven framework (Figure 20), and the TwinCAT software were operated on a desktop computer (Intel Xeon 2.80GHz (32 cores), 128 Gb Ram, Windows 10) with the PCI EtherCAT slave card installed on it. This computer was connected to the WE2 computer via an Ethernet cable.

Before the pilots could be started, a first protocol was carried out with the purpose of personalizing the NMS model to the individual using the approach priorly detailed. After calibration, the exoskeleton was adjusted to fit the subject's body and he walked for around 20 minutes with the exoskeleton in minimal impedance mode, *i.e.* with zero-torque assistance, and with different levels of static assistance so he could get used to the device. This last training was important to eliminate learning effects during the experiments and so that the subject could get acclimated to confidently walk with the exoskeleton.

The firsts *in-vivo* experimental tests were conducted in order to simply evaluate if the implemented software was able to run in real-time, debug and correct some minor issues on the software and hardware, and adjust the optimization parameters. Therefore, the pitot studies only took place some weeks after the calibration and adaptation procedures, not harming, however, the learned adaptation and capacity of the subject to walk with the exoskeleton. As soon as all the software and hardware requirements had been fulfilled, the recorded pilots were carried out following the parameters described in Table 2.

All tests were performed by the subject on the treadmill with zero inclination and at a constant speed of 2.5 km/h. The optimization parameters on each pilot were adjusted concerning the initial plan and set previously according to the results of the former studies so that some events, relationships, or hypotheses could be further studied. CMA-ES was used in all optimization pilots, resorting to 4 or 6 generations. Both SOL and GL were studied as optimized muscles, depending on the pilot test, so that a possible relationship between these two agonists muscles could be found and discussed. Moreover, further from the first pilot, all the other pilots observed a higher weight on the objective function of the optimized muscles (1.5) towards the non-optimized (1). Also, beyond Pilot 1, at the end of each of one of the other tests, the subject experienced a zero-torque assistance so that his physical condition at the end of the task could be compared to the initial state before the experiment had begun. Additionally, as for Pilots 4 and 5, it is noteworthy that, although the SR candidate set had been applied on the control laws during the whole loop, only the last 5 steps were considered to the computation of the mean of the EMG of that loop, which would be used on the evaluation of the objective function correspondent to that candidate. This would consider an initial adaptation time of the muscles to the new implemented SR. Finally, the tests named "SOL20" and "GL30", correspond to tests that were carried out without the optimization, *i.e.*, in the beginning, the subject walked on a zero-

torque assistance mode and, at a certain point of time, a static SR of 20% and 30% were set on the model to the SOL and GL, respectively, whereas the SR of the other muscles remained null.

Table 2. Experimental pilot tests parameters. For each test, the algorithm and number of generations, the Muscle-specific target reduction factor, the number of SR candidates per generation, the number of steps for computing the EMG reference, the number of steps for evaluating each SR candidate and the objective function's specific weights are detailed.

Test	Algorithm	Optimized muscles	δ	Nr. of candidates per Gen.	Nr. Steps for reference	Nr. of steps for each SR	C_o	C_s
Pilot 1	CMA-ES 6 Gens.	SOL Right SOL Left	0.15	16	15	5	1	1
Pilot 2	CMA-ES 4 Gens.	SOL Right SOL Left	0.15	6	15	10	1.5	1
Pilot 3	CMA-ES 4 Gens.	SOL Right SOL Left	0.2	6	50	50	1.5	1
Pilot 4	CMA-ES 6 Gens.	SOL Right SOL Left	0.2	15	50	10, but only the last 5 were considered	1.5	1
Pilot 5	CMA-ES 6 Gens.	GL Right GL Left	0.2	15	50	10, but only the last 5 were considered	1.5	1
SOL20	-	-	0.2	-	15	-	-	-
GL30	-	-	0.3	-	50	-	-	-

5.3. Data Processing and Analysis

The data extracted from the experimental tests allowed the study of the model's performance concerning the set of parameters described in Table 2. In the Results section, only a short parallel relation between the applied SR and the EMG tendency is presented. The detailed experimental graphical results can be further consulted in Supplementary Content 6. For each one of the experimental tests, only the foot that showed the most plausible results were presented and analysed. The experimental EMG mean outliers, i.e., the data elements that were more than 1.5 interquartile ranges above the upper quartile or below the lower quartile, were detected and replaced by a linear interpolation of neighbouring, non-outlier value.

For each recorded experiment, the detailed experimental results in Supplementary Content 6. for the right or left ankle, depending on the test, are presented using three figures, whose graphs present four different phases, being: 1) Reference acquisition; 2) Optimization; 3) Validation; and 4) Zero-torque assistance, separated by black dashed vertical lines. The first figure for each experiment shows the behaviour of the SR and the EMG mean, also represented in Figure 25 to Figure 29, as well as the objective function across the whole walking task. The first graph of this figure presents the SR evolution as a relation to the number of steps. During the firsts steps, the SR is set to null so that the exoskeleton is in a zero-assistance state so that the reference EMG mean and standard deviation could be computed. This can be related to the null horizontal lines in the graph during the firsts steps. After that, the optimization begins, and the SR is set online by the plugin regarding the values given by the Pagmo algorithm. This phase is represented in the graph by the cluttered lines that, within some generations and for some of the experiments, become individually more stabilised around the optimal value as the objective function evaluation, represented in the fourth graph, ideally decreases. When the stopping criteria had been met, the best SR is set to the model so that the exoskeleton starts being controlled by the optimal static laws, which can be seen by the constant horizontal lines. At the end of the task, apart from Pilot 1, the exoskeleton returns to a zero-assistance state, so that a comparison between the beginning and the end of the experiment can be made for every single test. This is represented in the graph by all the individual SR returning to the horizontal axis. As for the second

graph of the first figure, the raw EMG mean of the four muscles normalized to the computed reference are expressed in relation to the number of steps. Since these data is not that perceptible, a smoothing filter (third-order Savitzky-Golay) was applied and represented in the third graph, corresponding also to the second graph of Figure 25 to Figure 29, allowing to study the EMG overall time tendency along with the task phases. It is noteworthy that, only during the validation phase it is possible to measure the effective variation in the muscles' EMG when compared to the reference since it is the one that presents the theoretic optimal static SR set. This variation is given in percentage and computed during that phase in terms of the mean of those EMG values and its respective standard deviation interval. During the optimization and zero-torque phases, it is not plausible to relate a standard deviation to the EMG variation since both moments are expected to have some kind of evolution in the EMG.

On the other hand, the second figure's graphs allow a better understanding of the EMG evolution relatively the number of steps. For all the studied muscles, the graphs represent the computed Reference EMG mean and its standard deviation (dark red line and light red shadow, respectively), the raw EMG mean for each evaluation loop (black dots), and the tendency off EMG mean (smoothed EMG, blue line). Therefore, it is possible to study if the EMG effectively observes a reduction due to the exoskeleton assistance or if an observed decline on the EMG of a specific cycle was just an intrinsic behaviour of the muscle to maintain body balance (or for another purpose), that may be also observed during the Reference Acquisition phase and mirrored in the computed standard deviation. By last, the third figure only shows the SR evolution for all the muscles separately over the step count.

5.4. Results

Starting from Pilot 1, Figure 25 presents the results for the left ankle, demonstrating that GL experienced an escalation in the EMG of 12 ± 9 %, TA of 32 ± 7 %, SOL of 53 ± 3 %, and GM of 97 ±6 % after the optimization.

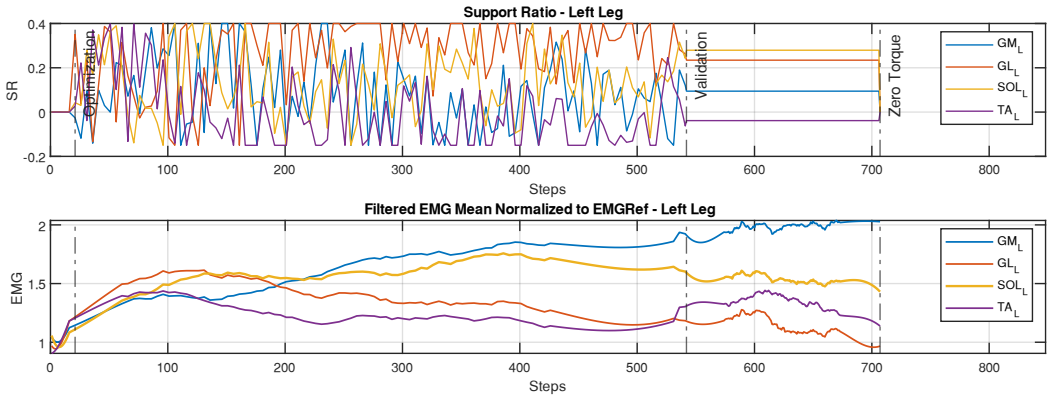

Figure 25. Pilot 1, left ankle results: Parallel relation between SR and EMG.

Figure 26 shows the behaviour of the muscle effort for Pilot 2. In this case, the second graph explicitly shows that, throughout the optimization, both GL and SOL have decreased in terms of muscular effort, converging to an almost stationary value during the validation phase, *i.e.* a reduction of 71 ± 2 % and 53 ± 4 %, respectively, when comparing to the EMG reference, and both returning to higher values after the zero-torque assistance. The objective function value, represented in the fourth graph of Supplementary Figure 6.2.1, indicates the performance of the optimization's algorithm by its continuous reduction during the optimization phase, normalization on the validation phase and consecutive increasing when zero-torque is applied. Another indicator is that both GM and TA did not observe much variation, maintaining its EMG within the standard deviation during the whole experiment, as demonstrated in Supplementary Figure 6.2.2. Although it seems that GL and SOL suffered a substantial reduction, mostly taking into account the fact that δ was only 15%, Supplementary Figure 6.2.2 shows that both muscles' EMG gets lower just about the reference

standard deviation during the optimization, for instance, around 35 % and 15 %, respectively, comparing to the lower boundary of the standard deviation.

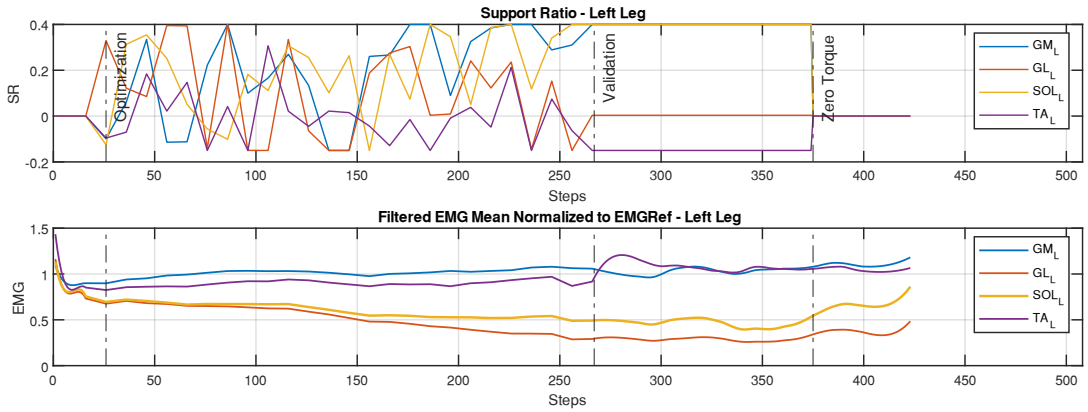

Figure 26. Pilot 2, left ankle results: Parallel relation between SR and EMG.

Regarding Pilot 3, Figure 27 shows that SOL had a steady reduction across the optimization phase while GM and TA rounded the reference value and GL, after a moment where it noticed a reduction, returned to its reference value. Nevertheless, when entering the validation phase with the supposed optimal set of SRs, although SOL got an EMG reduction of 37 ± 8 %, all the other muscles also suffered a decrease in its EMG, with the biggest impact on GL, with 26 ± 13 % reduction, which presented almost as much reduction as SOL in this phase. These findings are also supported by the graphs of Supplementary Figure 6.3.2, where the standard deviation is taken into consideration.

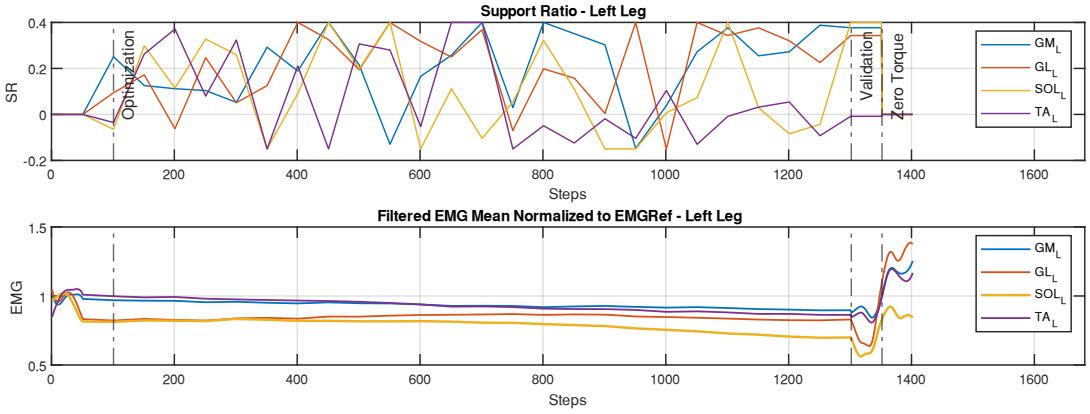

Figure 27. Pilot 3, left ankle results: Parallel relation between SR and EMG.

The second graph of Figure 28, related to Pilot 4, explicitly shows that, during the optimization phase, both GL and SOL EMG have decreased, converging to an almost stationary value during the validation phase, i.e. a reduction of 32 ± 5 % and 61 ± 3 %, respectively, when comparing to the reference EMG mean. On the other hand, GM and TA were subjected to a muscular increase in EMG of 39 ± 7 % and 30 ± 7 %, respectively. The objective function value, represented in the fourth graph of Supplementary Figure 6.4.1., indicates the behaviour of the optimization's algorithm by its homogenous reduction during the optimization phase, normalization on the validation phase and consequently increasing during zero-torque assistance.

Results from Pilot 5, which considered GL as optimized muscle instead of SOL, are represented in Figure 29. In this case, as optimization took place, GL's EMG constantly decreased, converging to a reduction of about 29 % even during the optimization phase. As for the validation phase, GL reduction was capable of reaching 41 ± 10 %, rapidly increasing to values similar to the reference during the zero-torque phase, as shown in the second graph. On the other hand, GM and TA did not suffer much effect during all the experiments, being contained within the reference standard deviation for almost

the whole task, as shown in Supplementary Figure 6.5.2. Finally, SOL did suffer a little increase in the EMG, of about 17 %, during the optimization, followed by a decrease down to similar reference values on the validation phase (8 ± 14 %), and by a new growth up to around 56 % after switching to zero-torque mode.

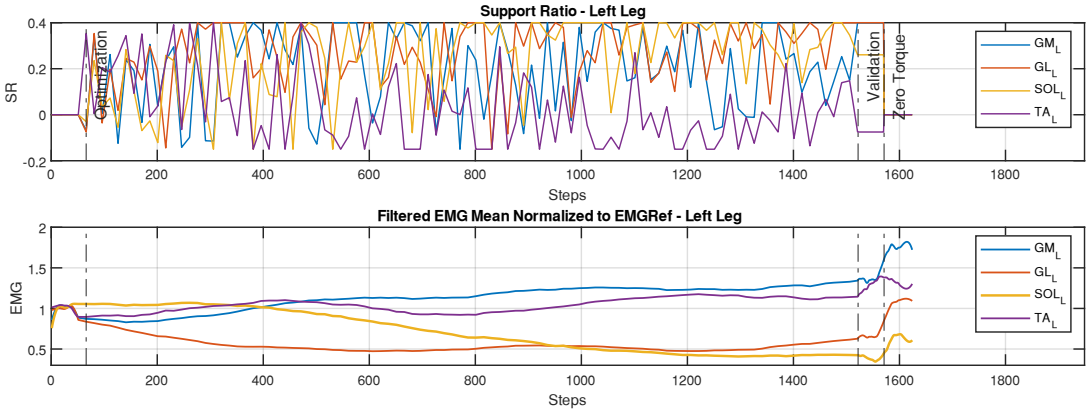

Figure 28. Pilot 4, left ankle results: Parallel relation between SR and EMG.

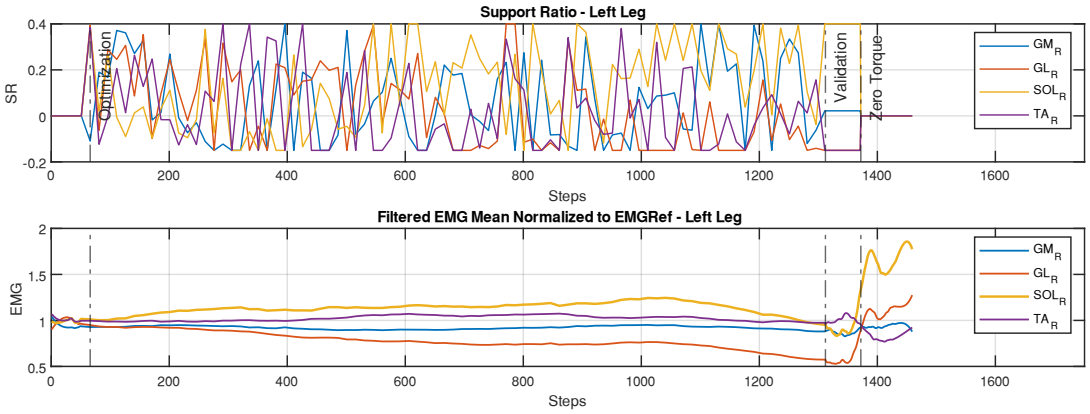

Figure 29. Pilot 5, right ankle results: Parallel relation between SR and EMG.

Finally, as for SOL20 and GL30 experimental tests, the preliminary results of both (see Supplementary Content 6.) show that, after applying an impulse, *i.e.*, a new level of assistance, by the exoskeleton to the subject's legs, the agonist muscles need at least 40 to 60 steps to converge to a new level of effort. In fact, SOL20 presented a reduction of around 25 % for SOL after 40 steps and GL30 observed a reduction of 35 % for GL after 60 steps whereas the other muscles maintained quite the same effort over the step counting. Additionally, it is noteworthy that, in SOL20, both GM and GL had an even higher reduction than SOL, of around 30 % both.

5.5. Discussion

The developed muscle-in-the-loop optimization, integrated in the form of a plugin into a NMS model enabled the execution of five validation pilots and two additional tests. Starting with Pilot 1, although the number of candidates per generation and the number of generations were relatively high, all four muscles suffered an increase in effort, since all the EMG observed a growth as related to the EMG reference, when it was expected that the SOL would have observed a reduction of 15% whereas the other muscles should have remained stable with a null variation. For instance, these firsts results made it wonder what the problem with the optimization model would be and the hypothesis that maybe the muscles did not have enough cycles to adapt to each new assistance emerged, meaning that the 5 steps per SR evaluation were not sufficient for the optimization to work, actually increasing

muscular effort. This outcome either implies much more steps, and consequently much more time, or fewer candidates per generation, with reduced efficiency, for the optimization to converge. Moreover, it was also assumed that the optimized muscles have too little weight on the objective function when it was intended for them to have a bigger impact on the SR set evaluation.

As for Pilot 2, the number of steps for the evaluation of each SR candidate was therefore increased (5 to 10) and the weight of the optimized muscles set to 1.5, so it would have a more notorious influence concerning the non-optimized muscles. The number of candidates per generation (16 to 6) and the number of generations were also reduced (6 to 4) so that the optimization would not take much time. In this case, both GL and SOL have decreased in terms of muscular effort throughout the optimization, converging to an almost stationary value during the validation phase, and both returning to higher values after the zero-torque assistance. Moreover, the objective function analysis demonstrated the feasibility of the optimization's algorithm. Another positive indicator is that both GM and TA did not observe much variation, maintaining its EMG within the standard deviation during the whole experiment. The substantial EMG reduction on SOL and GL could be explained by the large variability of the EMG data during the measuring of the reference EMG due to, perchance, the adaptation of the subjects' muscles to the additional constraints of the exoskeleton in zero-torque mode. The most remarkable dilemma of this pilot effective relied on the reduction of the GL's EMG, which accompanied the SOL behaviour when it was not intended. Although both agonist muscles share the same functions in multiple motor tasks, the algorithm should be theoretically able to extract and isolate both muscles' effort in the data processing. This limitation may indicate that there should have been some bad placement of the EMG sensors that promoted cross-talking, or that both muscles reduction was intrinsically commanded by the CNS to maintain body balance, for instance. This bad placement may also be confirmed by the differences in the theoretically optimal SR between test, proving that the optimization did not converge to the same results every time.

Regarding the limitations with the muscle delay on adapting to the new constrained or assistive conditions, for Pilot 3, the number of steps for computing the reference (15 to 50) and the number of steps for the evaluations of each SR (10 to 50) were increased so it could take into account the changes on the muscle effort into account. Also, δ was set to 20 % so a more pronounced reduction could be studied. The behaviour of all four muscles seemed to be what was intended, with SOL having a steady reduction across the optimization phase while GM and TA rounded the reference value and GL, after a moment where it noticed a reduction, returned to its reference value. Nevertheless, when entering the validation phase with the supposed optimal set of SRs, although SOL got the intended decline in effort, all the other muscles also suffered a decrease in its EMG, with the biggest impact on GL, which presented almost as much reduction as SOL in this phase. This consequence might be explained by the fact that the number of candidates per generation and the number of generations were not enough, preventing the optimization to converge to the optimal set.

A novel outcome and an interesting point of view comes with the final zero-torque mode in Pilot 3, where all the non-optimized muscles suffered a growth in effort to superior values when compared to the reference EMG whereas SOL was the only one that presented values within the standard deviation interval. These noticeable results may imply that, along with the optimization procedure, SOL was the only muscle that did not suffer from fatigue, which is one of the stated imperative effects for the muscle-specific rehabilitation and suggesting that SOL had received adequate assistance.

Alternatively, Pilot 4 took into consideration the non-converging limitation from Pilot 3 and the limitations with the muscle delay on adapting to the new conditions. Therewith, the number of candidates per generation (6 to 15) and the number of generations (4 to 6) were increased in detriment of the number of steps for the evaluation of each candidate set (50 to 10), so that the experiment will not take much more time. As for the evaluation of each SR candidate, only the last 5 of the 10 steps were considered for computing the EMG mean so that the muscles would have the first 5 ignored steps for adapting to the new assistance level. During the optimization phase, both GL and SOL's EMG have decreased, converging to an almost stationary value during the validation phase. On

the other hand, GM and TA were subjected to a higher muscular effort, which would not be problematic in case both muscles present a healthy prognostic. Moreover, the outcomes for the zero-torque phase corroborated the hypothesis stated before that SOL received adequate muscle-specific assistance regarding the fact that it was the only muscle that presented low EMG values when compared with the reference. The objective function value indicated, again, the feasibility of the optimization's algorithm by its homogenous reduction during the optimization phase, normalization on the validation phase and consequently increasing during zero-torque assistance.

Pilot 4 presented also another relevant event concerning the already stated dilemma of the non-intended reduction on GL's EMG. As a matter of fact, it is possible to notice that, as soon as the optimization phase starts, *i.e.*, when the exoskeleton is shifted from a minimal impedance mode to an assistive mode, GL instantaneously suffered a significant reduction in muscular effort, whose EMG value remained almost constant until the end of the validation phase. One possible explanation relies on the fact that the heavy actuators are placed on the lateral side of each leg with no further support than the floor and the leg itself. In this situation, the device is generating an additional lateral momentum, with the centre of curvature on the ground, that may have been unconsciously supplemented by an additional effort of the lateral leg muscles to preserve the body balance. Therefore, while measuring the EMG for the reference, a circumstance when the exoskeleton is not providing any assistance, GL might have been implementing much more effort than usual for counteracting the external momentum, therefore contaminating the computation of an accurate reference EMG. When the exoskeleton started giving assistance by applying external torques, it may have started supporting the additional forces and supplementing the GL additional effort, consequently reducing GL's EMG.

Taking this GL impasse into further study, Pilot 5 considered GL as optimized muscle instead of SOL. In this case, as optimization took place, GL's EMG constantly decreased during the optimization phase, reaching a pleasant reduction during the validation phase, and rapidly increasing to values similar to the reference during the zero-torque phase. The SOL's EMG growth during zero-torque mode may be explained by the fatigue accumulated during the prolongated optimization phase of around 1300 steps, when SOL suffered a higher demand on effort. These outcomes may be the firsts study suggestions of the impact of the placement of the actuators on the lateral muscles of the leg. In fact, it was proven that, when the optimization is focused on the most demanded muscles, due to the added momentum, it is possible to optimize the assistance to those specific muscles, while having a minimal impact on the other muscles.

As for SOL20 and TA30 experimental tests, both made part of small parallel studies which came out from Pilot 1 and 2 results and intended to analyse the response of the studied muscles to an "impulse", *i.e.*, study how many steps were required for the muscle to adapt to a sudden static assistance. The fact that the muscles need at least 40 to 60 steps to converge to a new level of effort suggests that the muscles need at least this number of steps to adapt to the new assistance, which highly contrasts with the number of steps set in most of the executed pilots. This parallel study, open doors for future research work, which may allow the enhancement of the optimization model developed in the present work.

As a final noteworthy remark, it is important to mention that both the used NMS model, for driving the exoskeleton and the optimization plugin, and the Symbitron+ WE2 exoskeleton are still elements endangered to deep research and were not fully validated yet. Therefore, it is not possible to ensure that the variables computed by CEINMS-RT, such as L^{mt}, MA, and F^{mt}, given as input to the plugin, as well as the torque delivered by the exoskeleton to the user present a high level of accuracy. In this case, it is plausible, and accepted as a constraint, that these elements, which were integrated into the pilots, might have affected the experiments and the validity of their results.

Chapter 6. Conclusion

6.1. Achieved Goals and Impact in Science

The work developed throughout this dissertation allowed the establishment of a paradigm shift in the way exoskeletons for physical rehabilitation, mainly for muscle-specific neurorehabilitation, are controlled. That was possible, first of all, by implementing a neuromechanical model in detriment of a position or impedance-controlled HMI, which allow the patient to voluntarily control the robotic device while inducing a positive modulation of their neuromuscular activity, and, secondly, by designing and implementing an optimization model that adapts the assistance in real-time in order to focus and improve the training for one specific impaired muscle, or group of muscles, instead of applying the attention on the macroscopic complex of the joint. This model was therefore named muscle-in-the-loop optimization.

This muscle-in-the-loop optimization was developed in the form of a plugin and was integrated on a neuromechanical model-based interface for driving a bilateral active ankle exoskeleton on a normal walking task, which allowed to study the different parameters of the optimization model. Experimental pilot tests confirmed the feasibility of the model in real-time and validated the hypothesis that the optimization could reduce the muscular effort of a specific muscle while having a minimal impact on the other agonist and antagonist muscles. Results of the most significant pilots achieved EMG reductions up to 61 ± 3 % in SOL and 41 ± 10 % in GL. Moreover, results also demonstrated the effectiveness of the optimization's specific reduction on rehabilitation by looking into muscle fatigue, directly related to the EMG variation, and consequently to muscle effort, of all the muscles after each experiment. Additionally, a hypothesis, which may be further studied in the future, came up concerning the additional muscular effort of the lateral leg muscles due to the added momentum generated by the additional weight of the exoskeleton's actuators, which are generally placed in the lateral sides of the body. Finally, a parallel preliminary study emerged from some pilots, which opened doors to future research concerning muscle adaptation when subjected to an impulse, or a new assistive condition, over time.

Taking into account the obtained results, it was therefore possible to resolve the initially stated hypothesis. As for what concerns to the first research question, "Is the optimization model able to run on the EMG-driven HMI developed by Durandau *et al.* and send the computed assistive torque to the WE2 exoskeleton in real-time?", it was confirmed, even priorly to the recorded experimental tests, that the developed plugin was able to receive the NMS variables online as input from CEINMS-RT, *i.e.*, the EMG-driven model, run the optimization, compute the assistive torque, and deliver it in real-time as input to the exoskeleton low-level controller so it would be converted into real joint external torque. Regarding the second stated hypothesis, "Can the optimized assistive torque reduce the effort of a specific muscle while having a minimal impact on the other muscles that act on the ankle joint?", it was partially validated by the pilots 3, 4, and 5. Although there is an open dilemma, which requires further research, concerning the relation between SOL and GL linked reductions, it has been proven that it is possible to force a reduction of one specific muscle or group of muscles without much influence on the other muscles that act on the same joint. Finally, as for the third question, "For each Support Ratio candidate, is it possible to evaluate its optimality within 1, 3, or 5 gait cycles?", it was demonstrated on pilot 1 that 5 steps per SR evaluation were not enough for the optimization to work, even increasing the muscles' effort. In fact, this limitation presented itself as a major drawback since it will imply much more time for the optimization to converge with the same accuracy.

The research developed in the scope of the present dissertation presents itself as a new way of looking into neurorehabilitation solutions, where the main goal is to improve the patients' independent mobility. The EMG-driven interface allows the subject to naturally control a robotic orthosis without depending on pre-defined patterns. Additionally, the developed muscle-specific rehabilitation strategy sets off new horizons in the treatment of individual impaired muscles in

incomplete SCI and post-stroke patients, contributing to the continuous enhancement of their quality of life. Looking forward to the improvement of the implemented plugin, all the code that was written during the present work, as well as its documentation, will be made available for open-source development under a BSD license, imposing minimal restrictions on its use and distribution, along with the public release of CEINMS-RT.

6.2. Limitations and Directions for Future Research

Facing the fact that the present study was, to the best of the author's knowledge, the first attempt to develop a muscle-specific optimization for neurorehabilitation with exoskeletons, it was therefore taken as an evolutionary process, during which several ideas and hypotheses started to come over in consort with the limitations that were being instantiated. Taking into consideration the identified problems, it is then possible to suggest new approaches and resolutions that may lead to interesting future work in research.

First of all, one important limitation lied in the COVID-19-related restrictions, which imposed the closure of the laboratories and hindered the access to its resources, such as the 3D-motion cameras, the treadmills, the desktop computer, and the exoskeleton, and hampered the in-person experiments. These constraints limited the time and resources that were made available along with the take-off of the experimental part of the present study. Additionally, another obstacle lied on the exoskeleton itself, mainly in the actuators and board's bad electromagnetic isolation and in the deficient cable connections, which presented several anomalies, consequently delaying the experiments. A different challenge relied on the additional momentum, as already stated, due to the lateral position and heaviness of the actuators. As a matter of fact, the WE exoskeleton is still a research prototype in the scope of the *Symbitron+* project, still presenting various drawbacks. Therefore, future research will lead to the improvement and correction of the detected imperfections before new experiments can take place, or even proceed with the experiments with another exoskeleton that supports the developed HMI's requirements.

Another limitation is focused on the great amount of time that the optimization takes and on the level of assistance (and applied torque) that sometimes counteracted the muscle's will, which may result in discomfort to any healthy or pathologic patient. Future research will study the muscle adaptation over time to new assistive conditions and the impact of the different plugin's parameters with the aim of optimizing the model, so it takes less time with minimal discomfort for the patient. Further studies may also imply the testing of other optimization algorithms, rather than CMA-ES, and even new proposals for the objective function. With these steps in mind, the research group already had approval from the Natural Sciences and Engineering Sciences Ethics Committee of the University of Twente (reference number 2021.84) for leading the additional enhancement and validation studies on different subjects, which will allow a more rigorous statistical analysis of the suggested framework. Moreover, additional studies will look at each individual muscle forces reduction along with the optimization in order to fully validate the muscle-in-the-loop optimization approach.

As for what the experimental procedures concern, some unconscious practices might have led to design and results inaccuracy. First of all, it is important to point out that, since all the experiments were conducted by the same subject, it is possible that the learning effects, *i.e.*, the fact that he had been getting used and getting comfortable with the exoskeleton over time, may have yield differences in EMG reduction even if the same support ratio was used. Additionally, the accuracy of the results may also have been affected by the quality level of the model calibration, the accuracy of the MVC tasks, the intrinsic problems of surface EMG sensors, and the NMS model itself. The usage of surface EMG includes the difficulty of having the same level of EMG between recording sessions due to placement and replacement of EMG sensors, changes in skin condition, movement artefacts, and so on. These problems could be solved in the future by switching to textile HD-EMG with automatic muscle detection and real-time decomposition, where the actual neural drive from the SC could be used to drive the NMS model and the optimization.

Another limitation relies on the software requirements and lab equipment used during these first experiments and that hamper the opportunity of getting out of the lab to the street with the exoskeleton. Firstly, the fixed desktop computer that ran CEINMS-RT, TwinCAT, and the optimization plugin, which required a great computational effort and therefore could not be substituted by the exoskeleton integrated computer, was connected to the exoskeleton with ethernet and HDMI cables for data and video transfer. Future suggestions may pass by connecting both devices, *i.e.,* the desktop computer and the exoskeleton's computer, wirelessly so both can communicate without any attachment. Additionally, GRF were measured using the treadmill with the only purpose of getting the gait cycle percentage. Future work might suggest using an integrated set of oscillators or gyroscopes to measure the body's segments positions or orientation and trigger the new step validator.

One important limitation, which not directly relies on the developed plugin but on the neuromechanical model interface that drives the exoskeleton, is the calibration process, which may include too much constraint for disabled patients. For instance, wheelchair-bounded SCI patients cannot easily walk on a force plate. A bypass solution would be to get informed of the muscle parameters directly by using imaging techniques (ultrasound and MRI) to better constrain the muscle model parameters using experimentally recorded tendon length, fibre length, pennation angle and physiological cross-section area. Furthermore, since the used HMI is based on an EMG-driven modelling approach, accessing healthy EMGs might be difficult when working with paretic patients such as complete SCI patients, who may not have EMG signals anymore, or stroke patients that have some muscles that do not present EMG signals or are perturbed by non-voluntary EMG signals (i.e., spasticity). This could be solved by using synergies between agonist muscles instead of experimentally recorded EMGs, where muscle activations are represented by the recombination of a small set of basic signals or primitives that would drive the NMS model and the optimization.

Finally, exoskeletons are still bulky with heavy components and poor ergonomics, which difficult the long-term usage by patients. Soft exosuits are able to transfer some of the load of the actuators from the user's limb to the user's back and are generally lighter, presenting themselves as a long-term substitute. However, these devices still present limitations with ergonomics, as forces meant for only one joint can be distributed to the whole body, and with providing a good level of assistance capacity due to the poor actuation capacity.

References

[1] Giovacchini F, Vannetti F, Fantozzi M, Cempini M, Cortese M, Parri A, et al. A light-weight active orthosis for hip movement assistance. Rob. Auton. Syst., vol. 73, Elsevier; 2015, p. 123–34. https://doi.org/10.1016/j.robot.2014.08.015.

[2] World Health Organization. The top 10 causes of death. 2018.

[3] World Health Organization. The atlas of heart disease and stroke / Judith Mackay and George Mensah ; with Shanthi Mendis and Kurt Greenland 2004.

[4] World Health Organization. Spinal cord injury 2013. https://www.who.int/news-room/fact-sheets/detail/spinal-cord-injury (accessed November 16, 2020).

[5] Delgado A, Han S. Stroke Recovery: Rehabilitation, Recovery, and Complications 2018. https://www.healthline.com/health/stroke/recovery#outlook6 (accessed November 16, 2020).

[6] Durandau G. Towards the next Generation in Human-machine-interfacing: Controlling Wearable Robots via Neuromusculoskeletal Modelling. University of Twente, 2020. https://doi.org/10.3990/1.9789464211221.

[7] Felt W, Selinger JC, Donelan JM, Remy CD. "Body-in-the-loop": Optimizing device parameters using measures of instantaneous energetic cost. PLoS One 2015. https://doi.org/10.1371/journal.pone.0135342.

[8] Zhang J, Fiers P, Witte KA, Jackson RW, Poggensee KL, Atkeson CG, et al. Human-in-the-loop optimization of exoskeleton assistance during walking. Science (80-) 2017;356:1280–3. https://doi.org/10.1126/science.aal5054.

[9] Sartori M, Reggiani M, van den Bogert AJ, Lloyd DG. Estimation of musculotendon kinematics in large musculoskeletal models using multidimensional B-splines. J Biomech 2012;45:595–601. https://doi.org/10.1016/j.jbiomech.2011.10.040.

[10] Durandau G, Rampeltshammer W, Van Der Kooij H, Sartori M. Toward Muscle-Driven Control of Wearable Robots: A Real-Time Framework for the Estimation of Neuromuscular States during Human-Exoskeleton Locomotion Tasks. Proc. IEEE RAS EMBS Int. Conf. Biomed. Robot. Biomechatronics, 2018. https://doi.org/10.1109/BIOROB.2018.8487723.

[11] Schiele A, Van Der Helm FCT. Kinematic design to improve ergonomics in human machine interaction. IEEE Trans Neural Syst Rehabil Eng 2006;14:456–69. https://doi.org/10.1109/TNSRE.2006.881565.

[12] Stienen AHA, Hekman EEG, van der Helm FCT, van der Kooij H. Self-aligning exoskeleton axes through decoupling of joint rotations and translations. IEEE Trans Robot 2009;25:628–33. https://doi.org/10.1109/TRO.2009.2019147.

[13] Chen B, Zi B, Qin L, Pan Q. State-of-the-art research in robotic hip exoskeletons: A general review. J Orthop Transl 2020;20:4–13. https://doi.org/10.1016/j.jot.2019.09.006.

[14] Chen B, Ma H, Qin LY, Gao F, Chan KM, Law SW, et al. Recent developments and challenges of lower extremity exoskeletons. J Orthop Transl 2016;5:26–37. https://doi.org/10.1016/j.jot.2015.09.007.

[15] Riener R, Lünenburger L, Jezernik S, Anderschitz M, Colombo G, Dietz V. Patient-cooperative strategies for robot-aided treadmill training: First experimental results. IEEE Trans Neural Syst Rehabil Eng 2005;13:380–94. https://doi.org/10.1109/TNSRE.2005.848628.

[16] Hadjidj A, Souil M, Bouabdallah A, Challal Y, Owen H. Wireless sensor networks for rehabilitation applications: Challenges and opportunities. J Netw Comput Appl 2013;36:1–15. https://doi.org/10.1016/j.jnca.2012.10.002.

[17] Kooij H, Asseldonk E, Oort G, Veneman J. LOPES | Department of Biomechanical Engineering n.d. https://www.utwente.nl/en/et/be/research/projects/lopes/ (accessed May 10, 2020).

[18] Veneman JF, Kruidhof R, Hekman EEG, Ekkelenkamp R, Van Asseldonk EHF, Van Der Kooij H. Design and evaluation of the LOPES exoskeleton robot for interactive gait rehabilitation. IEEE Trans Neural Syst Rehabil Eng 2007;15:379–86. https://doi.org/10.1109/TNSRE.2007.903919.

[19] Lokomat® - Hocoma n.d. https://www.hocoma.com/solutions/lokomat/ (accessed May 10, 2020).

[20] Alcobendas-Maestro M, Esclarín-Ruz A, Casado-López RM, Muñoz-González A, Pérez-Mateos G, González-Valdizán E, et al. Lokomat Robotic-Assisted Versus Overground Training Within 3 to 6 Months of Incomplete Spinal Cord Lesion. Neurorehabil Neural Repair 2012;26:1058–63. https://doi.org/10.1177/1545968312448232.

[21] Vaney C, Gattlen B, Lugon-Moulin V, Meichtry A, Hausammann R, Foinant D, et al. Robotic-assisted step training (Lokomat) not superior to equal intensity of over-ground rehabilitation in patients with multiple sclerosis. Neurorehabil Neural Repair 2012;26:212–21. https://doi.org/10.1177/1545968311425923.

[22] Atashzar SF, Shahbazi M, Patel R V. Haptics-enabled Interactive NeuroRehabilitation Mechatronics: Classification, Functionality, Challenges and Ongoing Research. Mechatronics 2019;57:1–19. https://doi.org/10.1016/j.mechatronics.2018.03.002.

[23] Calabrò RS, Russo M, Naro A, Milardi D, Balletta T, Leo A, et al. Who May Benefit From Armeo Power Treatment? A Neurophysiological Approach to Predict Neurorehabilitation Outcomes. PM R 2016;8:971–8. https://doi.org/10.1016/j.pmrj.2016.02.004.

[24] Armeo®Power - Hocoma n.d. https://www.hocoma.com/solutions/armeo-power/# (accessed May 10, 2020).

[25] Viteckova S, Kutilek P, Jirina M. Wearable lower limb robotics: A review. Biocybern Biomed Eng 2013;33:96–105. https://doi.org/10.1016/j.bbe.2013.03.005.

[26] ReWalk™ Personal 6.0 - ReWalk – More Than Walking n.d. https://rewalk.com/rewalk-personal-3/ (accessed May 18, 2020).

[27] ReWalk: Robotic Exoskeletons for Spinal Cord Injury | CADTH.ca n.d. https://www.cadth.ca/dv/ieht/rewalk-

robotic-exoskeletons-for-spinal-cord-injury (accessed May 18, 2020).
[28] Esquenazi A, Talaty M, Packel A, Saulino M. The Rewalk powered exoskeleton to restore ambulatory function to individuals with thoracic-level motor-complete spinal cord injury. Am J Phys Med Rehabil 2012;91:911–21. https://doi.org/10.1097/PHM.0b013e318269d9a3.
[29] Prosthetic Knee – Reboocon Bionics n.d. http://www.rbionics.com/products/prosthetic-knee/ (accessed May 18, 2020).
[30] Zoss AB, Kazerooni H, Chu A. Biomechanical design of the Berkeley Lower Extremity Exoskeleton (BLEEX). IEEE/ASME Trans Mechatronics 2006;11:128–38. https://doi.org/10.1109/TMECH.2006.871087.
[31] Wehner M, Quinlivan B, Aubin PM, Martinez-Villalpando E, Baumann M, Stirling L, et al. A lightweight soft exosuit for gait assistance. Proc. - IEEE Int. Conf. Robot. Autom., 2013, p. 3362–9. https://doi.org/10.1109/ICRA.2013.6631046.
[32] Soft Exosuits | Harvard Biodesign Lab n.d. https://biodesign.seas.harvard.edu/soft-exosuits (accessed May 9, 2020).
[33] Dahmen C, Hölzel C, Wöllecke F, Constantinescu C. Approach of Optimized Planning Process for Exoskeleton Centered Workplace Design. Procedia CIRP, vol. 72, Elsevier B.V.; 2018, p. 1277–82. https://doi.org/10.1016/j.procir.2018.03.185.
[34] Kadota K, Akai M, Kawashima K, Kagawa T. Development of power-assist robot arm using pneumatic rubber muscles with a balloon sensor. Proc. - IEEE Int. Work. Robot Hum. Interact. Commun., 2009, p. 546–51. https://doi.org/10.1109/ROMAN.2009.5326335.
[35] de Looze MP, Bosch T, Krause F, Stadler KS, O'Sullivan LW. Exoskeletons for industrial application and their potential effects on physical work load. Ergonomics 2016;59:671–81. https://doi.org/10.1080/00140139.2015.1081988.
[36] Yang T, Xie D, Li Z, Zhu H. Recent advances in wearable tactile sensors: Materials, sensing mechanisms, and device performance. Mater Sci Eng R Reports 2017;115:1–37. https://doi.org/10.1016/j.mser.2017.02.001.
[37] Leardini A, Belvedere C, Nardini F, Sancisi N, Conconi M, Parenti-Castelli V. Kinematic models of lower limb joints for musculo-skeletal modelling and optimization in gait analysis. J Biomech 2017;62:77–86. https://doi.org/10.1016/j.jbiomech.2017.04.029.
[38] Angerame MR, Holst DC, Jennings JM, Komistek RD, Dennis DA. Total Knee Arthroplasty Kinematics. J Arthroplasty 2019;34:2502–10. https://doi.org/10.1016/j.arth.2019.05.037.
[39] Õunpuu S, Davis RB, DeLuca PA. Joint kinetics: Methods, interpretation and treatment decision-making in children with cerebral palsy and myelomeningocele. Gait Posture 1996;4:62–78. https://doi.org/10.1016/0966-6362(95)01044-0.
[40] Zhao G, Ahmad Sharbafi M, Vlutters M, van Asseldonk E, Seyfarth A. Bio-Inspired Balance Control Assistance Can Reduce Metabolic Energy Consumption in Human Walking. IEEE Trans Neural Syst Rehabil Eng 2019;27:1760–9. https://doi.org/10.1109/TNSRE.2019.2929544.
[41] Leal Junior AG, de Andrade RM, Filho AB. Series Elastic Actuator: Design, Analysis and Comparison. Recent Adv. Robot. Syst., InTech; 2016. https://doi.org/10.5772/63573.
[42] Lapatki BG, Van Dijk JP, Jonas IE, Zwarts MJ, Stegeman DF. A thin, flexible multielectrode grid for high-density surface EMG. J Appl Physiol 2004;96:327–36. https://doi.org/10.1152/japplphysiol.00521.2003.
[43] Sartori M, Farina D, Lloyd DG. Hybrid neuromusculoskeletal modeling to best track joint moments using a balance between muscle excitations derived from electromyograms and optimization. J Biomech 2014;47:3613–21. https://doi.org/10.1016/j.jbiomech.2014.10.009.
[44] Lloyd DG, Besier TF. An EMG-driven musculoskeletal model to estimate muscle forces and knee joint moments in vivo. J Biomech 2003;36:765–76. https://doi.org/10.1016/S0021-9290(03)00010-1.
[45] Jackson RW, Collins SH. Heuristic-Based Ankle Exoskeleton Control for Co-Adaptive Assistance of Human Locomotion. IEEE Trans Neural Syst Rehabil Eng 2019;27:2059–69. https://doi.org/10.1109/TNSRE.2019.2936383.
[46] Koller JR, Gates DH, Ferris DP, Remy CD. "Body-in-the-loop" optimization of assistive robotic devices: A validation study. Robot. Sci. Syst., 2016. https://doi.org/10.15607/rss.2016.xii.007.
[47] Karadsheh M. Gait Cycle - Foot & Ankle - Orthobullets 2020. https://www.orthobullets.com/foot-and-ankle/7001/gait-cycle (accessed November 29, 2020).
[48] Dawe EJC, Davis J. (vi) Anatomy and biomechanics of the foot and ankle. Orthop Trauma 2011;25:279–86. https://doi.org/10.1016/j.mporth.2011.02.004.
[49] Saladin K, Sullivan S, Gan C. Human Anatomy. 5th edition. McGraw-Hill Education; 2017.
[50] Karol G. The effect of design variations on stresses in total ankle arthroplasty. University of Pittsburgh, 2002.
[51] Michael JM, Golshani A, Gargac S, Goswami T. Biomechanics of the ankle joint and clinical outcomes of total ankle replacement. J Mech Behav Biomed Mater 2008;1:276–94. https://doi.org/10.1016/j.jmbbm.2008.01.005.
[52] Saladin K. Anatomy and Physiology: The Unity & Form of Function. 3rd edition. Mc Graw-Hill; 2004.
[53] Rodrigues D de O. Biomechanics of the Total Ankle Arthroplasty : Stress Analysis and Bone Remodeling 2013.
[54] Ankle Musculature, Part 1: Posterior Muscles | CrossFit 2020. https://www.crossfit.com/essentials/ankle-musculature-part-1-posterior-muscles (accessed November 28, 2020).
[55] Ankle Musculature, Part 2: Anterior and Lateral Muscles | CrossFit 2020. https://www.crossfit.com/essentials/ankle-musculature-part-2-anterior-and-lateral-muscles (accessed November 28, 2020).
[56] Coelho D. Estudo numérico e experimental da articulação do tornozelo. University of Aveito, 2014.
[57] Hall S. Basic Biomechanics. Sixth Edit. New York: McGraw-Hill; 2012.

[58] Mann RA. Biomechanics of the Ankle. Jt. Surg. Up to Date, Tokyo: Springer Japan; 1989, p. 73–81. https://doi.org/10.1007/978-4-431-68096-3_8.
[59] Lundberg A, Svensson OK, Nemeth G, Selvik G. The axis of rotation of the ankle joint. J Bone Jt Surg - Ser B 1989;71:94–9. https://doi.org/10.1302/0301-620x.71b1.2915016.
[60] Hintermann B. Anatomic and Biomechanical Characteristics of the Ankle Joint and Total Ankle Arthroplasty. Total Ankle Arthroplast., Springer-Verlag; 2005, p. 25–42. https://doi.org/10.1007/3-211-27254-2_4.
[61] Completo A, Fonseca F. Fundamentos de Biomecânica Músculo-esquelética e ortopédica. Publindústria, Edições Técnicas; 2011.
[62] Amatya S, Lafmejani AS, Poddar S, Sridar S, Sugar T, Polygerinos P. Design, development, and control of a fabric-based soft ankle module to mimic human ankle stiffness. IEEE Int. Conf. Rehabil. Robot., vol. 2019- June, IEEE Computer Society; 2019, p. 886–91. https://doi.org/10.1109/ICORR.2019.8779495.
[63] Brockett CL, Chapman GJ. Biomechanics of the ankle. Orthop Trauma 2016;30:232–8. https://doi.org/10.1016/j.mporth.2016.04.015.
[64] Burdett RG. Forces predicted at the ankle during running. Med Sci Sports Exerc 1982;14:308–16. https://doi.org/10.1249/00005768-198204000-00010.
[65] Saladin KS. Anatomy & Physiology The Unity of Form and Function. 6th ed. New York: McGraw-Hill; 2012.
[66] Purves D, Augustine GJ, Fitzpatrick D, Hall WC, LaMantia A-S, Mooney RD, et al. Neuroscience. 6th ed. Sinauer Associates (Oxford University Press); 2017.
[67] Madigan NN, Windebank AJ. Spinal cord injury. Princ. Tissue Eng. 5th ed., Elsevier; 2020, p. 1047–91. https://doi.org/10.1016/B978-0-12-818422-6.00060-5.
[68] Pereira A. Development of a Hill-Type Muscle Model With Fatigue for the Calculation of the Redundant Muscle Forces using Multibody Dynamics. Instituto Superior Técnico, 2009.
[69] Dietz V. Proprioception and locomotor disorders. Nat Rev Neurosci 2002. https://doi.org/10.1038/nrn939.
[70] Bickenbach J. International Perspectives on Spinal Cord Injury. 2013.
[71] Papa S, Mauri E, Rossi F, Perale G, Veglianese P. Introduction to spinal cord injury as clinical pathology. Spinal Cord Inj. Repair Strateg., Elsevier; 2020, p. 1–12. https://doi.org/10.1016/B978-0-08-102807-0.00001-6.
[72] National Spinal Cord Injury Statistical Center. Spinal Cord Injury Facts and Figures at a Glance. 2020.
[73] Verstraeten S, Mark RE, Dieleman J, van Rijsbergen M, de Kort P, Sitskoorn MM. Motor Impairment Three Months Post Stroke Implies A Corresponding Cognitive Deficit. J Stroke Cerebrovasc Dis 2020;29:105119. https://doi.org/10.1016/j.jstrokecerebrovasdis.2020.105119.
[74] Cohen JW, Ivanova TD, Brouwer B, Miller KJ, Bryant D, Garland SJ. Do Performance Measures of Strength, Balance, and Mobility Predict Quality of Life and Community Reintegration After Stroke? Arch Phys Med Rehabil 2018;99:713–9. https://doi.org/10.1016/j.apmr.2017.12.007.
[75] Durandau G, Farina D, Asín-Prieto G, Dimbwadyo-Terrer I, Lerma-Lara S, Pons JL, et al. Voluntary control of wearable robotic exoskeletons by patients with paresis via neuromechanical modeling. J Neuroeng Rehabil 2019. https://doi.org/10.1186/s12984-019-0559-z.
[76] Winby CR, Lloyd DG, Besier TF, Kirk TB. Muscle and external load contribution to knee joint contact loads during normal gait. J Biomech 2009;42:2294–300. https://doi.org/10.1016/j.jbiomech.2009.06.019.
[77] Fleischer C, Hommel G. A human-exoskeleton interface utilizing electromyography. IEEE Trans Robot 2008;24:872–82. https://doi.org/10.1109/TRO.2008.926860.
[78] Durandau G, Sartori M, Bortole M, Moreno JC, Pons JL, Farina D. EMG-driven models of human-machine interaction in individuals wearing the H2 exoskeleton. IFAC-PapersOnLine 2016;49:200–3. https://doi.org/10.1016/j.ifacol.2016.12.214.
[79] Buchanan TS, Lloyd DG, Manal K, Besier TF. Estimation of muscle forces and joint moments using a forward-inverse dynamics model. Med. Sci. Sports Exerc., vol. 37, Med Sci Sports Exerc; 2005, p. 1911–6. https://doi.org/10.1249/01.mss.0000176684.24008.6f.
[80] Delp SL, Anderson FC, Arnold AS, Loan P, Habib A, John CT, et al. OpenSim: Open-source software to create and analyze dynamic simulations of movement. IEEE Trans Biomed Eng 2007;54:1940–50. https://doi.org/10.1109/TBME.2007.901024.
[81] Hahn ME. Feasibility of estimating isokinetic knee torque using a neural network model. J Biomech 2007;40:1107–14. https://doi.org/10.1016/j.jbiomech.2006.04.014.
[82] Durandau G, Farina D, Sartori M. Robust Real-Time Musculoskeletal Modeling Driven by Electromyograms. IEEE Trans Biomed Eng 2018. https://doi.org/10.1109/TBME.2017.2704085.
[83] Rasmussen J, Vondrak V, Damsgaard M, de Zee M, Christensen ST. The AnyBody project - Computer analysis of the human body. Comput. Anal. Hum. Body. Biomech. Man , 2002.
[84] Murai A, Kurosaki K, Yamane K, Nakamura Y. Musculoskeletal-see-through mirror: Computational modeling and algorithm for whole-body muscle activity visualization in real time. Prog Biophys Mol Biol 2010. https://doi.org/10.1016/j.pbiomolbio.2010.09.006.
[85] Farina D, Yoshida K, Stieglitz T, Koch KP. Multichannel thin-film electrode for intramuscular electromyographic recordings. J Appl Physiol 2008;104:821–7. https://doi.org/10.1152/japplphysiol.00788.2007.
[86] Lulic-Kuryllo T, Negro F, Jiang N, Dickerson CR. Standard bipolar surface EMG estimations mischaracterize pectoralis major activity in commonly performed tasks. J Electromyogr Kinesiol 2020:102509. https://doi.org/10.1016/j.jelekin.2020.102509.
[87] Aalten T van. Online optimization of EMG using a hybrid model approach. University of Twente, 2021.
[88] Farina D, Vujaklija I, Sartori M, Kapelner T, Negro F, Jiang N, et al. Man/machine interface based on the discharge timings of spinal motor neurons after targeted muscle reinnervation. Nat Biomed Eng 2017;1.

https://doi.org/10.1038/s41551-016-0025.
[89] Sartori M, Yavuz U, Farina D. In Vivo Neuromechanics: Decoding Causal Motor Neuron Behavior with Resulting Musculoskeletal Function. Sci Rep 2017;7. https://doi.org/10.1038/s41598-017-13766-6.
[90] Farina D, Sartori M. Surface Electromyography for MAN-Machine Interfacing in Rehabilitation Technologies. Surf. Electromyogr. Physiol. Eng. Appl., Hoboken, New Jersey: John Wiley & Sons, Inc.; 2016, p. 540–60. https://doi.org/10.1002/9781119082934.ch20.
[91] Aoi S, Funato T. Neuromusculoskeletal models based on the muscle synergy hypothesis for the investigation of adaptive motor control in locomotion via sensory-motor coordination. Neurosci Res 2016;104:88–95. https://doi.org/10.1016/j.neures.2015.11.005.
[92] Ekeberg Ö, Pearson K. Computer simulation of stepping in the hind legs of the cat: An examination of mechanisms regulating the stance-to-swing transition. J Neurophysiol 2005;94:4256–68. https://doi.org/10.1152/jn.00065.2005.
[93] Ogihara N, Yamazaki N. Generation of human bipedal locomotion by a bio-mimetic neuro-musculo-skeletal model. Biol Cybern 2001;84:1–11. https://doi.org/10.1007/PL00007977.
[94] Yamaguchi GT. Dynamic Modeling of Musculoskeletal Motion. Springer US; 2001. https://doi.org/10.1007/978-0-387-28750-8.
[95] Hill A. The heat of shortening and the dynamic constants of muscle. Proc R Soc London Ser B - Biol Sci 1938;126:136–95. https://doi.org/10.1098/rspb.1938.0050.
[96] Haeufle DFB, Günther M, Bayer A, Schmitt S. Hill-type muscle model with serial damping and eccentric force-velocity relation. J Biomech 2014;47:1531–6. https://doi.org/10.1016/j.jbiomech.2014.02.009.
[97] Durandau G, Rampeltshammer W, van der Kooij H, Sartori M. Neuromechanical model-based control of bi-lateral ankle exoskeletons: biological joint torque and electromyogram reduction across walking conditions 2021.
[98] Sherman MA, Seth A, Delp SL. What is a moment arm? Calculating muscle effectiveness in biomechanical models using generalized coordinates. Proc. ASME Des. Eng. Tech. Conf., vol. 7 B, American Society of Mechanical Engineers; 2013. https://doi.org/10.1115/DETC2013-13633.
[99] Runge CF, Shupert CL, Horak FB, Zajac FE. Ankle and hip postural strategies defined by joint torques. Gait Posture 1999. https://doi.org/10.1016/S0966-6362(99)00032-6.
[100] Sartori M, Reggiani M, Farina D, Lloyd DG. EMG-Driven Forward-Dynamic Estimation of Muscle Force and Joint Moment about Multiple Degrees of Freedom in the Human Lower Extremity. PLoS One 2012;7:52618. https://doi.org/10.1371/journal.pone.0052618.
[101] Gerus P, Sartori M, Besier TF, Fregly BJ, Delp SL, Banks SA, et al. Subject-specific knee joint geometry improves predictions of medial tibiofemoral contact forces. J Biomech 2013;46:2778–86. https://doi.org/10.1016/j.jbiomech.2013.09.005.
[102] Sartori M, Maculan M, Pizzolato C, Reggiani M, Farina D. Modeling and simulating the neuromuscular mechanisms regulating ankle and knee joint stiffness during human locomotion. J Neurophysiol 2015;114:2509–27. https://doi.org/10.1152/jn.00989.2014.
[103] Sartori M, Llyod DG, Farina D. Neural data-driven musculoskeletal modeling for personalized neurorehabilitation technologies. IEEE Trans Biomed Eng 2016. https://doi.org/10.1109/TBME.2016.2538296.
[104] Durandau G, Sartori M, Bortole M, Moreno JC, Pons JL, Farina D. Real-time modeling for lower limb exoskeletons. Biosyst. Biorobotics, 2017. https://doi.org/10.1007/978-3-319-46532-6_21.
[105] Miljković N, Milovanović I, Dragin A, Konstantinović L, Popović DB. Muscle synergies with Walkaround® postural support vs cane/therapist assistance. NeuroRehabilitation 2013. https://doi.org/10.3233/NRE-130982.
[106] Hug F, Del Vecchio A, Avrillon S, Farina D, Tucker KJ. Muscles from the same muscle group do not necessarily share common drive: evidence from the human triceps surae. J Appl Physiol 2020. https://doi.org/10.1152/japplphysiol.00635.2020.
[107] Hansen N. The CMA Evolution Strategy: A Comparing Review. Towar. a New Evol. Comput., 2007. https://doi.org/10.1007/3-540-32494-1_4.
[108] Sherman M, Eastman P. SimTK: Simbody: Multibody Physics API: Project Home n.d. https://simtk.org/projects/simbody/ (accessed April 12, 2021).
[109] Pizzolato C, Lloyd DG, Sartori M, Ceseracciu E, Besier TF, Fregly BJ, et al. CEINMS: A toolbox to investigate the influence of different neural control solutions on the prediction of muscle excitation and joint moments during dynamic motor tasks. J Biomech 2015;48:3929–36. https://doi.org/10.1016/j.jbiomech.2015.09.021.
[110] Biscani F, Izzo D. A parallel global multiobjective framework for optimization: pagmo. J Open Source Softw 2020. https://doi.org/10.21105/joss.02338.
[111] Corana A, Marchesi M, Martini C, Ridella S. Minimizing Multimodal Functions of Continuous Variables with the "Simulated Annealing" Algorithm. ACM Trans Math Softw 1987. https://doi.org/10.1145/29380.29864.
[112] Meijneke C, Wang S, Sluiter V, van der Kooij H. Introducing a modular, personalized exoskeleton for ankle and knee support of individuals with a spinal cord injury. Biosyst. Biorobotics, 2017. https://doi.org/10.1007/978-3-319-46532-6_28.
[113] Anatomical terminology: Planes, directions & regions | Kenhub n.d. https://www.kenhub.com/en/library/anatomy/anatomical-terminology (accessed November 28, 2020).